Relating generalized and specific modeling in population dynamical systems

Relating generalized and specific modeling in population dynamical systems

Contents

Chapter 1

Introduction

Without a doubt, our environment is a highly complex system. Interestingly, in the past century many important insights have been gained from quite simple mathematical models. Although these abstract models neglect biological details and focus rather on the most fundamental processes the observed dynamics can be very complicated (May and Oster, 1976). The typically qualitative results of simple models may help to understand the consequences of the incorporated processes. In this way simple generic models are useful to investigate the basic mechanisms behind ecological interactions.

One of the most dominant aspects of ecology is the dynamics of populations and the interactions between them. In the past century an abundant number of simple models has been proposed and analyzed to explore these dynamics. The majority of the proposed models are specific in the sense that the mechanisms under consideration are represented by fully parameterized functions. In principle, these models allow a detailed analysis of the system dynamics. However, the properties of such *specific models* are often very sensitive to the exact mathematical formulation of the processes. A detailed derivation from field or lab experiments is in general difficult while a derivation from theoretical reasoning can hardly capture the complex nature behind these processes. This problem appears not only in ecology but in many fields of science where complex systems are under consideration. The formulation of *generalized models* avoids instead to parameterize each processes under consideration. Recently, the analysis of generalized models has been improved by a framework that allows for extensive insights on the local stability properties of the system. Moreover, it can be used to gain information about the presence of global dynamics (Gross and Feudel, 2006). As we will see, this approach has opened new vistas to old debates within the community of applied and theoretical ecology. Before we discuss actual topics of ecology and the pros and cons of the different modeling approaches, let us briefly rehash the histor-

ical development of modern theoretical population dynamics and some basics of dynamical system theory.

In 1798 Thomas Malthus proposed an exponential growth of populations in his *Essay on the Principle of Population*. But Malthus was concerned about the impact of limited resources. Basically, he reasoned that resources remain constant or only increase linearly. Thus, the growth must cease when the demand for resources exceeds the supply. It was Verhulst (1838) who formulated these principles in terms of the *logistic growth* where the per capita growth rate is given by a constant term minus a term that is proportional to the existing population. The latter term expresses the *intra-specific competition* for resources. This formulation leads for small populations to an initial exponential growth which saturates with increasing abundance of the population. Interestingly, this drastic simplification of nature describes the growth of many single-species populations very well (i.e. Gause (1934); Perni et al. (2005)).

The first model which describes predator-prey interactions between different populations was proposed by Lotka (1925) (and independently soon afterwards by Volterra (1928)). Following the chemical principle of mass action, he proposed that the predation and the growth of the predator depend bi-linear on the abundances of the prey and predators. Further, he assumed constant rates for the growth of prey and mortality of the predator. The simple model was originally used to explain an increased amount of predator fishes in the Adriatic sea during the first world war. Solutions of this model are neutrally stable limit cycles. If the linear growth term is substituted by a logistic growth the system evolves into a stable focus. Although the logistic growth is often used in predator-prey systems, its validity to capture the effect of limited resources on a multiple species system is rather questionable (e.g. Kooi et al. (1998)).

A next major milestone was the introduction of predator functional response describing the predation rate as a nonlinear function of the abundance of prey. It was argued by Solomon (1949) and Holling (1959) that the predation rate should not be linear since predators can only handle a limited amount of prey per unit of time. Many variations of the Lotka-Volterra model have been analyzed for several different functional responses (e.g. Rosenzweig and MacArthur (1963); Truscott and Brindley (1994); Wolkowicz et al. (2003)). Often, these models show transitions from stationary to oscillatory behavior when the amount of resources, i.e. the related parameter is increased. These oscillations can lead temporarily to very low prey populations. Thus, stochastic extinction of the prey population becomes likely to occur (Cunningham and Nisbet, 1983; Pascual and Caswell, 1997). In that sense, these models predict a devastating effect of enrichment, the extinction of both populations. This counterintuitive effect of increasing resources is called Rosenzweig's Paradox of enrichment (Rosenzweig, 1971). In contrast to the commonness of this effect

in theoretical models, only some experiments show the paradox of enrichment but others do not (e.g. Morin and Lawler (1995)).

In theoretical ecology several model modification have been proposed that do not show this paradoxical effect. Arditi and Ginsburg (1989) showed that the paradox of enrichment is absent when the functional response depends on the ration between prey and predator abundances. However, ratio-dependent models show other unrealistic effects instead. Predators still interfere at low predator densities and rarity even allows them to capture high amounts of prey even when prey density is extremely low (Hanski 1991, Abrams 1994). Using a generalized model, Gross et al. (2004) have shown the usage of quantitatively similar alternatives to common functional responses can even lead to stabilizing effects of enrichment.

Apart from stationary or periodic behavior chaotic dynamics can be found in many population models, even in the simplest models like the logistic map (May and Oster, 1976). While population cycles can be observed in many wild populations, most prominently the snowhare-lynx populations in Canada and lemmings population in north Europe (e.g. Elton (1924)) but also reoccurring pests of forest insects (e.g. Berryman (1996)), chaotic dynamics are rarely evidenced in nature (Hastings et al., 1993). Similar to the paradox of enrichment the debate whether chaotic dynamics are likely to appear is often hold on modeling details. For instance, Ruxton and Rohani (1998) observed that for some models the chaotic dynamics disappear when the models are slightly changed. Using the generalized modeling approach Gross et al. (2005) showed that food chains with more than 3 trophic levels are in general chaotic.

The examples of the paradox of enrichment and the chaotic dynamics demonstrate that generalized models can reveal generic system properties concerning stability effects and complex dynamics. These results are derived from a bifurcation analysis of generalized models. But also in the analysis of specific models bifurcation theory plays a central role (Bazykin, 1998).

Bifurcations are qualitative transitions of the long term dynamics of the system, like the transition from stationary to oscillatory behavior. In the field of ecology several bifurcations have shown to be important. For instance, the existence boundaries of populations are often tangent or transcritical bifurcations (e.g. Kooijman et al. (2004)). Further, a Hopf bifurcation (Hopf, 1942) is involved in the paradox of enrichment and can be observed experiments on living populations (Fussmann et al., 2000) and homoclinic bifurcation are assumed to play an important role in the dynamics of insect pests (Gragnani et al., 1998) and plankton blooms (Scheffer et al., 1997). Because these bifurcations also play a central role in in the presented work, we provide in the following a short description and some illustrating figures. More detailed information can be found in (Guckenheimer and Holmes, 2002; Kuznetsov, 2004).

First we consider Bifurcations of steady states as shown in Fig. 1.1. In a tangent bifurcation two steady states merge together and disappear, as it is illustrated in Fig. 1.1(a) in case of a stable and an unstable steady state. This bifurcation scenario is also called saddle-node bifurcation. Beyond the bifurcation point p_{cr} the system approaches another attractor. This means that the original state of the system is in general hardly re-obtained once the critical parameter value has passed. Due to certain conditions a degenerated form of the saddle-node bifurcation is often encountered in predator-prey models. Figure 1.1(b) shows a transcritical bifurcation where two steady states exchange stability. This bifurcation is often related to a deterministic extinction of a species when an equilibrium state exchanges stability with a solution where one or more populations are zero.

(a) An unstable steady state (saddle) and a stable steady state (node) merge and disappear in a saddle-node bifurcation at p_{cr}

(b) An unstable equilibrium and a stable steady state exchange stability in a transcritical bifurcation at p_{cr}
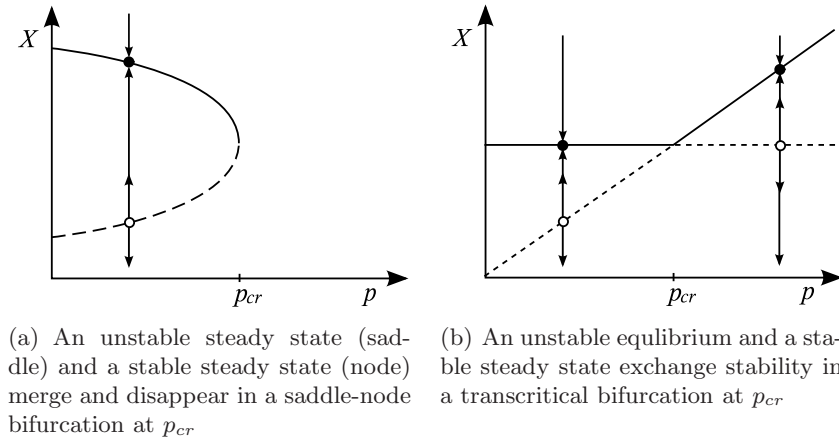
Figure 1.1: Examples of steady state bifurcations.

Bifurcations of steady states and limit cycles are shown in Fig. 1.2 and Fig. 1.3. Figure 1.3 shows two types of Hopf bifurcations. While a stable steady state becomes unstable, either a stable limit cycle emerges (supercritical Hopf bifurcation, Fig. 1.2(a)) or an unstable limit cycle disappears (sub-critical Hopf bifurcation, Fig. 1.2(b)).

Another possibility for limit cycles to (dis)appear are homoclinic bifurcations as shown in Fig. 1.3. In a homoclinic saddle bifurcation a limit cycle turns into a homoclinic connection as shown in Fig. 1.3(a). On a homoclinic connection the system evolves forward and backward in time towards the same steady state. Consequently, such a homoclinic loop takes an infinite amount of time, i.e. has an infinite period. The cycle disappears beyond the bifurcation. It is also possible that a stable and an unstable steady state with a heteroclinic connection merge in a homoclinic saddle-node bifurcation as shown in Fig.1.3(b). Thereby the heteroclinic connection becomes a homo-

(a) A stable steady state becomes unstable and a stable limit cycle emerges in a super-critical Hopf bifurcation at p_{cr}.

(b) A stable steady state becomes unstable and an unstable limit cycle disappears in a sub-critical Hopf bifurcation at p_{cr}..
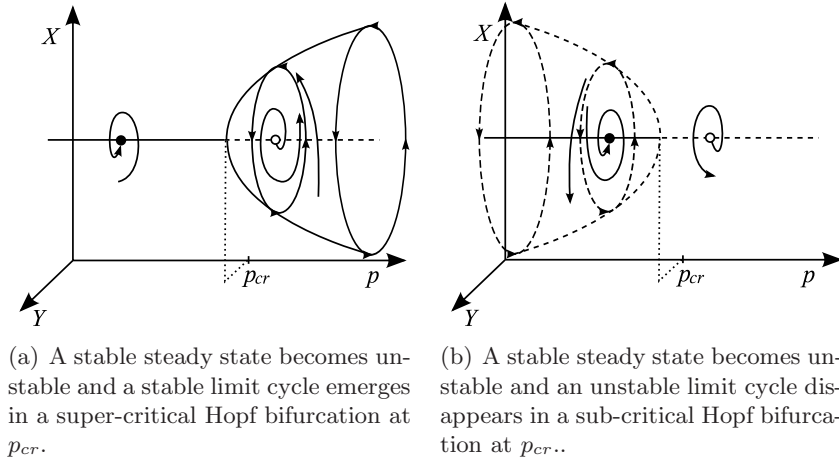
Figure 1.2: Hopf bifurcations.

clinic connetion in the bifurcation point which turns into a limit cycle beyond the critical parameter value. Homoclinic bifurcations play also an important role in the emergence of chaotic dynamics (Kuznetsov, 2004).

(a) A limit cycle disappears after it intersects with an unstable steady state (saddle) in a homoclinic bifurcation at p_{cr}.

(b) An unstable steady state and a stable steady state with a heteroclinic connection merge in a homoclinic saddle-node bifurcation at p_{cr} and a limit cycle appears.
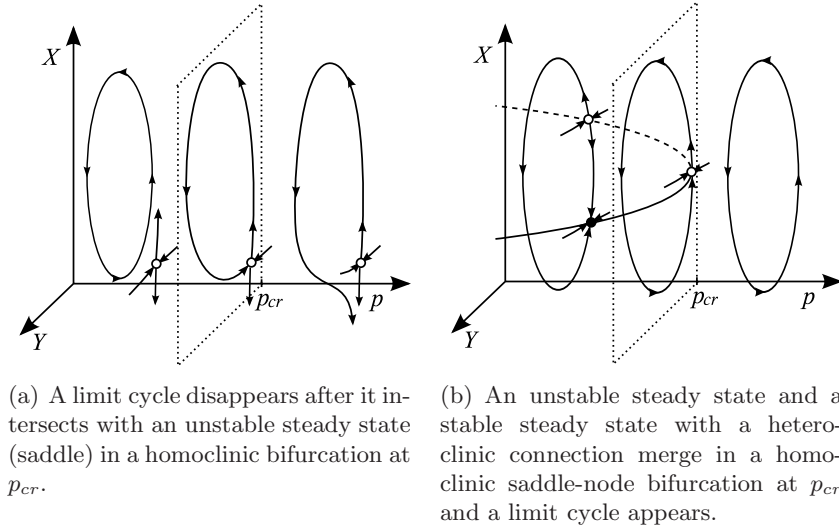
Figure 1.3: Homoclinic bifurcations.

For the analysis of specific models the computation of these bifurcations can be done numerically using continuation methods as in powerful software packages like AUTO (Doedel et al., 1997; Doedel and Oldeman, 2009), CONTENT (Kuznetsov and Levitin, 1996) and MATCONT (Dhooge et al., 2003). These programs allow to follow the stationary or periodic solutions by vary-

ing one parameter in order to find the bifurcation points. Once a bifurcation point is detected, it is possible to follow the bifurcation point while another parameter is varied. In this way bifurcation curves are obtained which can lead to even more complicated bifurcation situations.

The application of these techniques to generalized models is not possible since the generalized formulations allows not even a computation of a steady state. Therefore, in the field of generalized modeling classical methods are of advantage and allow for the computation of tangent and Hopf bifurcations (Gross and Feudel, 2004). Thereby, the problem that the steady state is in general unknown is overcome by a renormalization procedure. In principle, the analytical bifurcation condition can be used to derive three-dimensional bifurcation diagrams. Basically, a three-dimensional representation is of advantage for two reasons. First, such a visualization reveals much more information about the influence of a parameter on the stability. For instance, increasing the distance to destabilizing bifurcations could be interpreted as stabilization. However, a parameter variation that increases the distance to a bifurcation surface with respect to one parameter could decrease the distance to the bifurcation surface with respect to another parameter. Such a *weak stabilization* can not be recognized from a one-dimensional bifurcation diagram (Van Voorn et al., 2008). Second, a three-dimensional visualization helps to quickly locate more complicated bifurcation situations at the intersections of the computed bifurcation surfaces. These bifurcations can indicate the presence of additional bifurcations, like homoclinic bifurcations and chaotic dynamics (Kuznetsov, 2004). Most importantly, an advantage of the localization of bifurcations in generalized models is, that the analysis is independent of biological or mathematical details. Consequently, the results hold for whole classes of specific models.

In order to capitalize on these advantages a method for the computation of the bifurcation surfaces from implicit test functions is needed. Especially for the localization of the more complicated bifurcation situations, a faithful representation of the bifurcation surfaces is crucial. Therefore, a central point of the presented thesis is the implementation of a technique that cope with these demands.

The properties of generalized models depend on the model structure, i.e. the variables and the considered gain and loss processes of these variables and on which variables the processes depend on. In (Gross, 2004a) predator-prey models have been analyzed in a very general form. In the following we will introduce two modern branches of ecology, *stoichiometric ecology* and *ecological epidemiology* that change the functional dependency and the structure of predator prey systems respectively. The former considers the chemical composition of the populations and the flow of nutrients between the populations (Sterner and Elser, 2002; Moe et al., 2005). These aspects change the depen-

dencies of the processes that are restricted by stoichiometric constraints. The latter considers the effects of diseases spreading among the interacting populations. This can be modeled by changing the structure of food chain models Venturino (1995, 2002a). Both model types have not yet been analyzed in a generalized form.

Although Lotka (1925) devoted much attention to stoichiometric aspects of the energy transformation, the topic received not much attention in the community of theoretical ecologists. However, in the past two decades there was a renewed interest on this topic and an increasing number of experimental and theoretical studies in ecological stoichiometry Moe et al. (2005). It shows that stoichiometric constraints can greatly affect population dynamics (e.g.Huxel (1999); Loladze and Kuang (2000); Sterner and Elser (2002); Kooijman et al. (2004)).

Primarily, two processes are effected by stoichiometric constraints. First, the growth of the first trophic level, the *primary production* is limited by the availability of nutrients like carbon, phosphorus or nitrogen. However, as soon as the primary producer is in a predator-prey relation, the predator gets the essential nutrients from the consumed prey and the nutrients become partly stored in the higher trophic level. Therefore the primary production depends in general also on the predator population.

Second, the conversion efficiency depends on the nutrient content of the prey. Most food chain models assume that the conversion efficiency is constant. This is reasonable as long as the predator and prey populations have a fixed stoichiometric composition. However, it has been shown that primary producers often have a rather variable nutrient content (Sterner and Elser, 2002). Consequently, such a variable *food quality* must lead to a variable conversion efficiency.

The effects of stoichiometric constraints depend again on the specific modeling approaches. Loladze and Kuang (2000) for instance considered carbon and phosphorus as limiting nutrients with a variable ratio within the producer. For an intermediate total phosphorus concentration they observed the paradox of enrichment but the oscillations disappear after a homoclinic bifurcation and the system approaches another equilibrium. At low phosphorus concentration the paradox of enrichment completely disappears. Instead, they observe a destabilizing effect due to increasing phosphorus they call the paradox of nutrient enrichment. Kooijman et al. (2004) investigate a model with a variable carbon concentration in the prey that results from reserves. In this model also a homoclinic bifurcation is found but in contrast to the model by Loladze and Kuang (2000) both populations go extinct beyond the bifurcation. In conclusion, stoichiometric constraints show a great influence on the dynamics but a unifying modeling approach has not been found yet. Therefore, the presented thesis aims to identify generic model properties by the analysis of a generalized

stoichiometric model. The results of this analysis are compared to previous results of specific stoichiometric models in order to find common effects and to understand the differences from a generalized point of view.

Ecological epidemiology focuses on the interplay of disease and population dynamics. Theoretical epidemic models have been developed parallel to predator-prey models and have many similarities. Like the Lotka-Volterra model in population dynamics Kermack and Mckendrick (1927) proposed a model for disease that is based on the principles of mass-action. It separates a population into susceptibles, infected and removed or recovered individuals (SIR). The *incidence function* that describes the infection rate was assumed to be be proportional to the abundance of susceptibles and infected while the infected recovered or died with a constant per capita rate. Similar to the functional response in population dynamics several functional forms of the incidence function have been proposed in the history of theoretical epidemiology (McCallum et al., 2001). A spreading diseases can affect ecological dynamics in many ways. Anderson et al. (1986) proposed two modified Lotka-Volterra models, one with infected prey and one with infected predators. They assumed that the infection may increase mortality, decrease reproductivity, infected prey becomes more vulnerable to predation and infected predators may be less effective in predation. It shows that infections tend to destabilize the predator-prey community. Up to now there are numerous theoretical studies of eco-epidemic models with infected prey. On one hand many field studies have shown that predators take a disproportionate large number of prey infected by parasites (Hethcote et al., 2004). On the other hand there are also examples where the predator can recognize an infection and avoid the infected prey (Roy and Chattopadhyay, 2005). Most eco-epidemic models predict that diseases tend to destabilize the predator-prey system (Anderson et al., 1986; Dobson, 1988; Hadeler and Freedman, 1989; Xiao and Bosch, 2003) but also stabilizing effects have been observed (Hilker and Schmitz, 2008). Compared to models with infected prey the influence of infected predators is rarely investigated. Nevertheless diseases spreading in a predator populations can have a major influence on population dynamics. An accidentally human-introduced disease has dramatically reduced the number of wolfs on the Isle Royal, USA from 1980 to 1982 and has led to an increased moose population (Wilmers et al., 2006). In biological control programs diseases are introduced for example to reduce non-native cat populations on islands but most often with no or minor success (Mills and Getz, 1996). In conclusion, the poor success of control programs and contradicting results of modeling shows that the interplay of disease and population dynamics are not yet well understood.

A main point of the presented thesis is to understand how diseases in predator populations can effect the dynamics of the predator-prey interactions from a general perspective. While some specific models show that diseases in

the predator population can lead to oscillations (Anderson et al., 1986; Xiao and Bosch, 2003; Haque and Venturino, 2007), we focus on the generation of more complex dynamics. The generalized analysis is used to propose a specific model that allows for a more detailed analysis of the emergence of such complex dynamics.

In summary, the presented thesis introduces an innovative technique for the computation of bifurcation surfaces. This technique is applied in combination with the approach of generalized modeling to identify generic effects of stoichiometric constraints and diseases on predator-prey interactions. A main focus of the thesis is, however, the comparison of specific and generalized models. Thereby new methods are invented to combine specific and generalized bifurcation diagrams. It shows that both modeling approaches can take benefit from each other.

In Chapter 2 a technique for the computation of bifurcation surfaces is introduced. The basic method was first used in Stiefs (2005) and has been further developed and improved. Using an adaptive triangulation method this technique allows to visualize the test functions of bifurcations in three-dimensional diagrams. To be specific, the algorithm computes a closed mesh of triangles with vertices on the bifurcation surface. To allow for a detailed representation of the bifurcation surface by the mesh the size of the triangles is adapted to the local surface curvature. In order to visualize the three-dimensional structure of the surfaces level lines on these on the mesh are plotted instead of the mesh structure. This technique is a fast and efficient method for the computation of bifurcation surfaces and the localization of complicated bifurcation situations. The capabilities of these method are then demonstrated in Chapter 3 and 4.

A generalized stoichiometric producer grazer model is analyzed in Chapter 3. We focus the analysis of on the effects of a variable food quality and of primary productions that depend additionally on the predator abundances. Thereby, we find a generic paradoxical effect of intra-specific competition. The findings are demonstrated on several specific models which encounter different mechanisms behind the stoichiometric constraints. For instance, this comparison shows that the paradox of competition incorporates Rosenzweig's paradox of enrichment and the paradox of nutrient enrichment as well. Moreover we demonstrate how bifurcation scenarios of specific models obtained by continuation methods can be mapped into bifurcation diagrams obtained by the triangulation technique of Chapter 2. The combined bifurcation diagrams illustrate the relations of specific and generalized model parameters.

In Chapter 4 a generalized eco-epidemic predator-prey model with a disease spreading upon the predator population is analyzed. Thereby we concentrate our analysis on the generalized functional response and the generalized incidence function as the most debated processes. We use the approach from

Chapter 2 to locate complicated bifurcation situations that give information about complex dynamics. We show that diseases in predator populations can generate chaotic dynamics in predator-prey populations. This implication is demonstrated for a specific example model. The generalized analysis is used to find a parameter regions of complex dynamics. It is shown that the chaotic parameter regions can be widespread and the specific model allows for an exemplary investigation of the routes into chaos with numerical techniques.

Finally, we discuss the results in a comprehensive way in Chapter 5 and give an outlook for further investigations.

Chapter 2

Computation and Visualization of Bifurcation Surfaces*

2.1 Abstract

The localization of critical parameter sets called bifurcations is often a central task of the analysis of a nonlinear dynamical system. Bifurcations of codimension 1 that can be directly observed in nature and experiments form surfaces in three dimensional parameter spaces. In this chapter we propose an algorithm that combines adaptive triangulation with the theory of complex systems to compute and visualize such bifurcation surfaces in a very efficient way. The visualization can enhance the qualitative understanding of a system. Moreover, it can help to quickly locate more complex bifurcation situations corresponding to bifurcations of higher codimension at the intersections of bifurcation surfaces. Together with the approach of generalized models the proposed algorithm enables us to gain extensive insights in the local and global dynamics not only in one special system but in whole classes of systems.

2.2 Introduction

The long-term behavior of dynamical systems plays a crucial role in many areas of science. If the parameters of the system are varied, sudden qualitative transitions can be observed as critical points in parameter space are crossed. These points are called bifurcation points. The nature and location of bifurcations

---

*This Chapter is a modified version of a published manuscript (Stiefs et al., 2008). Some notations are changed in order to be consistent with the other chapters. The example section is not included, since chapter 3 and 4 provide examples for an application of the method.

is of interest in many systems corresponding to applications from different fields of science. For instance the formation of Rayleigh-Bénard convection cells in hydrodynamics (Swinney and Busse, 1981), the onset of Belousov-Zhabotinsky oscillations in chemistry (Zaikin and Zhabotinsky, 1970; Agladze and Krinsky, 1982) or the breakdown of the thermohaline ocean circulation in climate dynamics (Titz et al., 2002; Dijkstra, 2005) appear as bifurcations in models. The investigation of bifurcations in applied research focuses mostly on codimension-1 bifurcations, which can be directly observed in experiments (Guckenheimer and Holmes, 1983). In order to find bifurcations of higher codimension, in general at least two parameters have to be set to the correct value. Therefore, bifurcations of higher codimension are rarely seen in experiments. Moreover the computation of higher codimension bifurcations cause numerical difficulties in many models. Hence, an extensive search for higher codimension bifurcations is not carried out in most applied studies.

From an applied point of view the investigation of codimension-2 bifurcations is interesting, since these bifurcations can reveal the presence of global codimension-1 bifurcations–such as the homoclinic bifurcations–which are otherwise difficult to detect. The recent advances in the investigation of bifurcations of higher codimension are a source of many such insights (Kuznetsov, 2004). While this source of knowledge is often neglected in applied studies, the investigation of bifurcations of higher codimension suffers from a lack of examples from applications (Guckenheimer and Holmes, 1983). In this way a gap between applied and fundamental research emerges, that prevents an efficient cross-fertilization.

A new approach that can help to bridge this gap between mathematical investigations and real world systems is the investigation of generalized models. Generalized models describe the local dynamics close to steady states without restricting the model to a specific form, i.e. without specifying the mathematical functions describing the dynamics of the system (Gross et al., 2004; Gross and Feudel, 2006). The computation of local bifurcations of steady-states in a class of generalized models is often much simpler than in a specific conventional model. A bifurcation that is found in a single generalized model can be found in every generic model of the same class. In this way the investigation of generalized models can provide examples of bifurcations of higher codimension in whole classes of models. From an applied point of view, it provides an easy way to utilize the existing knowledge on the implications of bifurcations of higher codimension on the dynamics.

For generalized models, the application of computer algebra assisted classical methods (Guckenheimer et al., 1997; Gross and Feudel, 2004) for computing bifurcations is advantageous. These methods are based on testfunctions for specific eigenvalue constellations corresponding to specific types of bifurcations (Seydel, 1991).

Classical methods yield implicit functions describing the manifolds in parameter space on which the bifurcation points are located. For codimension-1 bifurcations these manifolds are hypersurfaces. In order to utilize these advantages, an efficient tool for the visualization of implicitly described bifurcation hypersurfaces is needed. A properly adapted algorithm for curvature dependent triangulation of implicit functions can provide such a tool.

Generalized modeling, computer algebra assisted bifurcation analysis and adaptive triangulation are certainly interesting on their own. However, here we show that in combination they form a powerful approach to compute and visualize bifurcation surfaces in parameter space. This visualization yields also the relationship between the different bifurcations and identifies higher codimension bifurcations as intersections of surfaces. This way the proposed algorithm can help to bridge the present gap between applied and fundamental research in the area of bifurcation theory.

First, in Sec. 2.3 we briefly review how generalized models are constructed and how implicit test functions can be derived from bifurcation theory. In Sec. 2.4 we explain how these implicit functions can be combined with an algorithm of triangulation in order to visualize the bifurcations in parameter space. In chapter 3 and 4 we show how the proposed method efficiently reveals certain bifurcations of higher codimension and thereby provides qualitative insights in the local and global dynamics of large classes of systems.

2.3 Generalized Models and Computation of Bifurcations

The state of many real world systems can be described by a low dimensional set of state variables $X_1, \ldots, X_N$, the dynamics of which are given by a set of ordinary differential equations

$$\dot{X}_i = F_i(X_1, \ldots, X_N, p_1, \ldots, p_M), \quad i = 1 \ldots N \qquad (2.1)$$

where $F_i(X_1, \ldots, X_N, p_1, \ldots, p_M)$ are in general nonlinear functions. For a large number of systems it is a priori clear which quantities are the state variables. Moreover, it is generally known by which processes the state variables interact. However, the exact functional forms by which these processes can be described in the model are often unknown. In practice, the functions in the model are often chosen as a compromise between empirical data, theoretical reasoning and the need to keep the equations simple. It is therefore often unclear if the dynamics that is observed in a model is a genuine feature of the system or an artifact introduced by assumptions made in the modeling process (e.g. (Ruxton and Rohani, 1998)).

One way to analyze models without an explicit functional form is provided by the method of generalized models (Gross and Feudel, 2006). Since it will play an essential role in Chapter 3 and 4, let us briefly review the central idea of this approach.

Let us consider the example of a system in which every dynamical variable is subject to a gain term $G_i(X_1, \ldots, X_N)$ and a loss term $L_i(X_1, \ldots, X_N)$. So that our general model is

$$F_i = G_i(X_1, \ldots, X_N) - L_i(X_1, \ldots, X_N) \tag{2.2}$$

Note that the parameters $(p_1, \ldots, p_M)$ do not appear explicitly, since the explicit functional form of the interactions G_i and L_i is not specified.

Since our goal is to study the stability of a nontrivial steady state, we assume that at least one steady state $\boldsymbol{X}^* = X_1^*, \ldots, X_N^*$ exists, which is true for many systems. Due to the fact that a computation of $\boldsymbol{X}^*$ is impossible with the chosen degree of generality we apply a normalization procedure with the aim to remove the unknown steady state from the equations. For the sake of simplicity we assume that all entries of the steady state are positive. We define normalized state variables $x_i = X_i/X_i^*$, the normalized gain terms $g_i(x) = G_i(X_1^* x_1, \ldots, X_N^* x_N)/G_i(\boldsymbol{X}^*)$ as well as the normalized loss terms $l_i(x) = L_i(X_1^* x_1, \ldots, X_N^* x_N)/L_i(\boldsymbol{X}^*)$. Note, that by definition $x_i^* = g_i(\boldsymbol{x}^*) = l_i(\boldsymbol{x}^*) = 1$. Substituting these terms, our model can be written as

$$\dot{x}_i = (G_i(\boldsymbol{X}^*)/X_i^*)g_i(\boldsymbol{x}) - (L_i(\boldsymbol{X}^*)/X_i^*)l_i(\boldsymbol{x}). \tag{2.3}$$

Considering the steady state this yields

$$(G_i(\boldsymbol{X}^*)/X_i^*) = (L_i(\boldsymbol{X}^*)/X_i^*). \tag{2.4}$$

We can therefore write our normalized model as

$$\dot{x}_i = \alpha_i(g_i(\boldsymbol{x}) - l_i(\boldsymbol{x})) \tag{2.5}$$

where $\alpha_i := G_i(\boldsymbol{X}^*)/X_i^* = L_i(\boldsymbol{X}^*)/X_i^*$ are scale parameters which denote the timescales - the characteristic exchange rate for each variable.

The normalization enables us to compute the Jacobian in the steady state. We can write the Jacobian of the system as

$$\mathbf{J}_{i,j} = \alpha_i(\gamma_{i,j} - \delta_{i,j}). \tag{2.6}$$

where we have defined

$$\gamma_{i,j} := \left. \frac{\partial g_i(x_1, \ldots, x_N)}{\partial x_j} \right|_{x=x^*} \tag{2.7}$$

and

$$\delta_{i,j} := \left.\frac{\partial l_i(x_1,\ldots,x_N)}{\partial x_j}\right|_{x=x^*} \tag{2.8}$$

While the interpretation of $\gamma_{i,j}$ and $\delta_{i,j}$ describe the required information on the mathematical form of the gain and loss terms, we will see in Chapter 3 and 4 that the parameters generally have a well defined meaning in the context of the application.

2.3.1 Testfunctions for bifurcations of steady states

Our aim is to study the stability properties of the steady state. Thus, only two bifurcation situations are of interest: (i) the loss of stability due to a bifurcation of tangent type where a real eigenvalue crosses the imaginary axis or (ii) a bifurcation of Hopf type where a pair of complex conjugate eigenvalues crosses the imaginary axis.

If a tangent bifurcation type occurs, at least one eigenvalue of the Jacobian **J** becomes zero. Therefore, the determinant of **J** is a test function for this bifurcation situation.

Hopf bifurcations are characterized by the existence of a purely imaginary complex conjugate pair of eigenvalues. We use the method of resultants to obtain a testfunction (Guckenheimer et al., 1997). Since at least one symmetric pair of eigenvalues has to exist

$$\lambda_a = -\lambda_b. \tag{2.9}$$

The eigenvalues $\lambda_1,\ldots,\lambda_N$ of the Jacobian **J** are the roots of the Jacobian's characteristic polynomial

$$P(\lambda) = |\mathbf{J} - \lambda\mathbf{I}| = \sum_{n=0}^{N} c_n\lambda^n = 0. \tag{2.10}$$

Using condition (2.9) Eq. (2.10) can be divided (after some transformations) into two polynomials of half order

$$\sum_{n=0}^{N/2} c_{2n}\chi^n = 0, \tag{2.11}$$

$$\sum_{n=0}^{N/2} c_{2n+1}\chi^n = 0 \tag{2.12}$$

where $\chi = \lambda_a{}^2$ is the Hopf number and N/2 has to be rounded up or down to an integer as required.

In general two polynomials have a common root if the resultant vanishes (Gelfand et al., 1994). The resultant R of Eq.(2.11) and Eq.(2.12) can be written as a Hurwitz determinant of size $(N-1) \times (N-1)$. If we assume that N is odd we have

$$R_N := \begin{vmatrix} c_1 & c_0 & 0 & \ldots & 0 \\ c_3 & c_2 & c_1 & \ldots & 0 \\ \vdots & \vdots & \vdots & \ddots & \vdots \\ c_N & c_{N-1} & c_{N-2} & \ldots & c_0 \\ 0 & 0 & c_N & \ldots & c_2 \\ 0 & 0 & 0 & \ldots & c_2 \\ \vdots & \vdots & \vdots & \ddots & \vdots \\ 0 & 0 & 0 & \ldots & c_{N-1} \end{vmatrix}. \tag{2.13}$$

With the condition $R_N = 0$ we have found a sufficient test function for symmetric eigenvalues. The Hopf number χ gives us the information whether the eigenvalues are real ($\chi > 0$), purely imaginary ($\chi < 0$), zero ($\chi = 0$) or a more complex situation (χ undefined). In the case $\chi = 0$ we have a double zero eigenvalue which corresponds to a codimension-2 Takens-Bogdanov bifurcation (TB). In a Takens-Bogdanov bifurcation a Hopf bifurcation meets a tangent bifurcation. While the Hopf bifurcation vanishes in the TB bifurcation, a branch of homoclinic bifurcations emerges. For more details see (Gross and Feudel, 2004).

2.4   Visualization

The testfunctions, described above, yield an implicit description of the codimension-1 bifurcation hypersurfaces. Since it is in general not feasible to solve these functions explicitly we have to search for other means for the purpose of visualization. In the following we focus on the visualization in a three dimensional parameter space, in which the bifurcation hypersurfaces appear as surfaces. We propose an algorithm, that constructs the bifurcation surfaces from a set of bifurcation points, which have been computed numerically.

In order to efficiently obtain a faithful representation of the bifurcation surface, the density of these points has to be higher in regions of higher curvature. Moreover, the algorithm has to be able to distinguish between different - possibly intersecting - bifurcation surfaces.

2.4.1   Adaptive Triangulation

A triangulation is the approximation of a surface by a set of triangles. We apply a simplification of a method introduced by Karkanis and Stewart (2001)

and extend it using the insights of the previous section. The algorithm consists of two main parts. The first is the *growing phase*, in which a mesh of triangles is computed that covers a large part of the surface. The second is the *filling phase*, in which the remaining holes in this partial coverage are filled.

2.4.2 The seed triangle

Denoting the three parameters as x, y and z, we start by finding one root $\mathbf{p}_1 = (x_1, y_1, z_1)$ of the testfunction, by a Newton-Raphson method (e.g. Kelley (2003)). Suppose $\mathbf{p}_1$ is a vertex of the *seed triangle*, then we search for two other points as two additional vertices that define a triangle of appropriate size and shape. We find another two roots $\mathbf{p}_{2\,\text{initial}}$ and $\mathbf{p}_{3\,\text{initial}}$ close to $\mathbf{p}_1$. $\mathbf{p}_{2\,\text{initial}}$ and $\mathbf{p}_{3\,\text{initial}}$ are within a radius of d_{initial} around $\mathbf{p}_1$ wherein the surface can be sufficiently approximated by a plane. We find the next vertex $\mathbf{p}_2$ using a point in the direction of $\mathbf{p}_{2\,\text{initial}}$ with the distance d_{initial} to $\mathbf{p}_1$ as initial conditions for the Newton-Raphson method. The initial condition for the third vertex $\mathbf{p}_3$ is a point in the plane that is spanned by $\mathbf{p}_1$, $\mathbf{p}_{2\,\text{initial}}$ and $\mathbf{p}_{3\,\text{initial}}$, orthogonal to the line between $\mathbf{p}_1$ and $\mathbf{p}_2$, with a distance of d_{initial} to $\mathbf{p}_1$ as well. We get an almost isosceles seed triangle that approximates the bifurcation surface close to $\mathbf{p}_1$ sufficiently to our demands.

2.4.3 Growing phase

Starting from the seed triangle adjoining triangles can be added successively. The size of the adjoining triangles has to be chosen according to certain, possibly conflicting requirements. On the one hand the algorithm has to adapt the size of the triangles to the local surface curvature in order to obtain a higher resolution in regions of higher complexity and vice versa. On the other hand it has to maintain a minimal and a maximal resolution. At first we adapt the size of the triangle to the curvature of the surface.

We construct an interim triangle by mirroring $\mathbf{p}_1$ at the straight line through $\mathbf{p}_2$ and $\mathbf{p}_3$ and to find a point $\mathbf{p}_{4\,\text{initial}}$ on the surface as shown in Fig.2.1. Thus $\mathbf{p}_{4\,\text{initial}}$ defines together with $\mathbf{p}_2$ and $\mathbf{p}_3$ the interim triangle. The angle ϕ between the normals of the new triangle and the parent is used to approximate the local radius of curvature. Following Karkanis and Stewart (2001) we define the radius of curvature as

$$R = \frac{d}{2sin\left(\frac{\phi}{2}\right)} \tag{2.14}$$

where d the distance of the centers of both triangles (cf. Fig. 2.1). We choose a desired ratio $\rho = R/d$ to compute a curvature adapted distance $d_{\text{adapt}} = R/\rho$. Finally we use again the Newton-Raphson method to find a bifurcation point
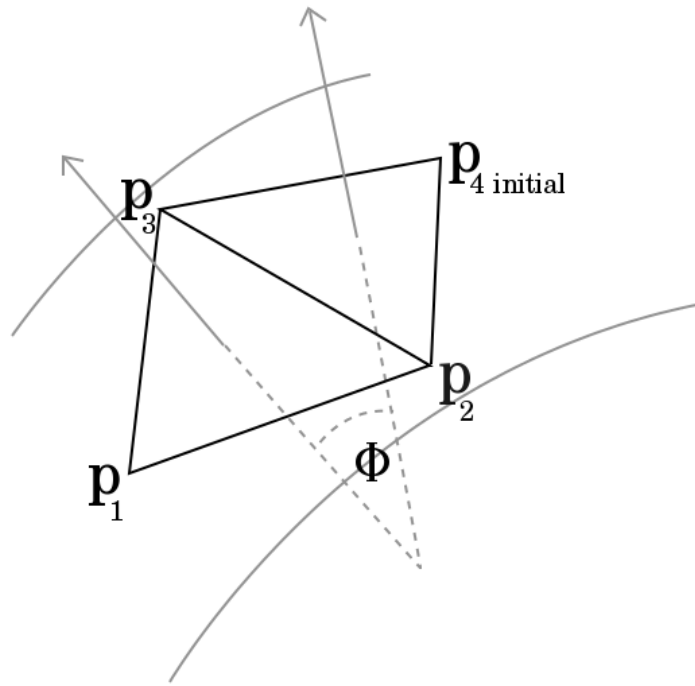
Figure 2.1: Seed triangle with one adjacent triangle.

$\mathbf{p}_4$ at the distance d_{adapt} from the straight line through $\mathbf{p}_2$ and $\mathbf{p}_3$ in the direction of $\mathbf{p}_{4\,\text{initial}}$. The bifurcation points $\mathbf{p}_2, \mathbf{p}_3$ and $\mathbf{p}_4$ then are the vertices of the adapted triangle. As mentioned above the adjacent triangles have to satisfy additional requirements. In order to maintain a minimal resolution we define a maximum d_{max}. To restrict the number of computed bifurcation points we also define a minimum d_{min}. If d_{adapt} is larger than d_{max} or smaller than d_{min} we set it to d_{max} or d_{min} respectively to find $\mathbf{p}_4$. To check the quality of the adapted triangle we also define a maximum angel ϕ_{max}. We decrease the distance d, if the angle between the normals of the triangles is greater than ϕ_{max} .

Proceeding as described above the algorithm adds to every triangle up to two adjacent triangles. In order to prevent overlapping triangles, we reject a triangle if its center is closer to the center of an opposite triangle than one and a half times the largest edge of both. To allow for self intersections of bifurcation surfaces, we allow an intersection of triangles if the angle between the normals of the triangles is bigger than $2\phi_{\text{max}}$. Another possibility which has to be taken into account is that our system may possess more than one bifurcation surface. To prevent transitions ϕ_{max} has to be small enough. For instance, if two surfaces intersect at an angle $\hat{\phi}$, we have to choose ϕ_{max} much smaller than $\hat{\phi}$. Concerning Hopf bifurcations the Hopf number χ offers a tool to distinguish between different surfaces, even if the angle of intersection is very small. Along one Hopf bifurcation surface χ varies smoothly. On a different Hopf bifurcation surface the Hopf number is in general different since another pair of purely imaginary eigenvalues is involved. We can therefore check the continuity of χ between the new bifurcation point and the parent to make sure that the new point belongs to the same surface.

Since the bifurcation surfaces are in general not closed, we have to restrict the parameter space according to a volume of interest V. We choose minimal and maximal values for each variable to define a cuboid which includes V. Triangles with vertices outside of the cuboid are rejected.

Apart from this restriction it is possible, that we find borders of the bifurcation surface within our cuboid. One example is a Hopf bifurcation surface that ends in a Takens-Bogdanov bifurcation as described in Sec. 2.3. If we cross the Takens-Bogdanov bifurcation, the new point still can be settled down on the surface described by the test function. But in this case the Hopf number χ is positive and the symmetry condition is satisfied by a pair of purely real eigenvalues that is not related to a bifurcation situation. To place the new point directly onto the border of the Hopf bifurcation surface we compute the root of the χ-function using the coordinates of the new point as initial conditions. Then we use the resulting point again to find the root of our test function. Repeating this procedure we find iteratively our new point directly on the border of the Hopf bifurcation surface. In this way we can not only

prevent a jump from one Hopf bifurcation surface to another one by checking the sign of χ, but we also approximate the border of the Hopf bifurcation surface.

Following the procedure described above we can successively add triangles to our mesh until no further triangle is possible. After the growing phase the complete surface, in the prescribed region of parameter space, is covered by a mesh of triangles as seen in the upper diagram in Fig. 2.2.

2.4.4   Focus

Sometimes the bifurcation surfaces are quite smooth but in some regions they possess a more complicated structure. If the radius of curvature changes too rapidly the algorithm fails to adapt the size of the triangles and the structure is poorly approximated in this region. In these regions it is useful to increase the minimal resolution in order to obtain a more accurate approximation of the bifurcation surface. We realize this by so-called focus points. In a certain radius $\hat{r}$ around these focus points we reduce the maximal size of the triangles. The new maximal triangle size $\hat{d}_{\max}$ is then given as

$$\hat{d}_{\max} = \begin{cases} \left(c + \frac{(1-c)r}{\hat{r}}\right) d_{\max} & r < \hat{r} \\ d_{\max} & r \geq \hat{r} \end{cases}, \tag{2.15}$$

where r is the distance to the closest focus point and c is a constant between 0 and 1. By definition $\hat{d}_{\max}$ decreases linearly with r from $d_{\max}$ to a lower value $cd_{\max}$, where c is a constant between 0 and 1. In Fig. 2.2 we see a triangulation of an example surface after the growing phase. The upper diagram shows that two centers of a higher resolution exit. The lower diagram shows that the surface looks like a landscape with a hill and a plane. One center of high resolution is on top of the hill and the other one in the plane. This example shows both resolution control mechanisms, the size adaption due to the radius of curvature (left) and due to a focus point (right).

While in Fig. 2.2 the focus point is not advantageous, this additional resolution control is essential for the computation of rather complicated bifurcation situations.

2.4.5   Filling phase

While the growing phase covers a large fraction of the surface with connected traces of triangles, space between the traces remain. While we fill this gap, we have to take care that we do not fill space that lies outside the bifurcation surface, e.g. beyond a Takens-Bogdanov bifurcation. In the following we start by describing the filling phase for surfaces without boundaries and then go on to explain how boundaries are handled.
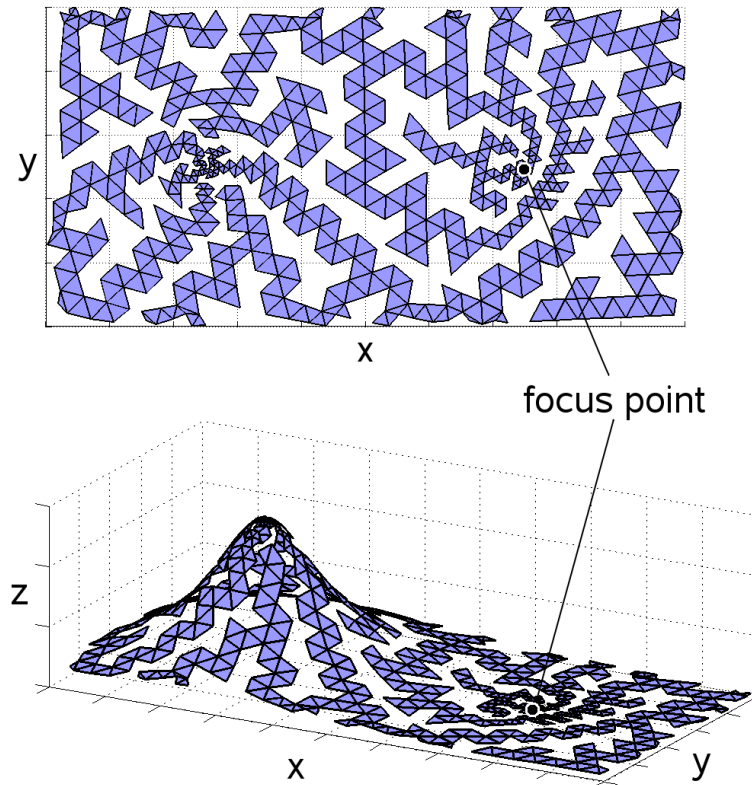
Figure 2.2: Example surface after the growing phase computed with one focus point. The size of the triangles adapts to the local curvature and the proximity to the focus point.

The first task we have to perform in the filling phase is to identify the gap. We can acquire the gap between the traces by starting at a vertex $\mathbf{p}_1$ and following the vertices at the boundary clockwise. In this way we construct a sequence of all N vertices.

Once we have defined a gap we start to separate the gap into subgaps. To each point of the gap we associate the normal $\mathbf{n}_k$ of an adjacent triangle and the closest neighbor. Similar to Karkanis and Stewart (2001) we define all points as neighbors of $\mathbf{p}_k$ which are located between the two half planes which are spanned by the normal $\mathbf{n}_k$ and the two vectors from $\mathbf{p}_k$ to $\mathbf{p}_{k-1}$ and $\mathbf{p}_{k+1}$ shown in Fig. 2.3(a). The closest neighbor of $\mathbf{p}_k$ is the neighbor with the smallest Euclidean distance. If we find two points, which are the closest neighbors to each other they form a so-called *bridge*. We divide the gap at the first bridge we find into two subgaps by connecting the two vertices. If a subgap consists of only three vertices, we add it as a triangle to the mesh we obtained from the growing phase. We proceed with the subgaps as described above until no bridges are left. Afterwards we divide the remaining subgaps at the point with the smallest distance to its closest neighbor. In the end of this procedure the hole gap is completely filled up with triangles.

2.4.6   Borders in the filling phase

If the bifurcation surfaces are not closed but possess some boundaries due to margins of the parameter region under consideration, or due to a codimension-2 bifurcation e.g. a Takens Bogdanov bifurcation then we have gaps which are not supposed to be filled up. In order to prevent bridges connecting these borders, we use similar criteria for the bridges and all connections we make to divide the gaps, as used in the growing phase.

First, the connections the algorithm produces by the division of gaps should not be much larger than $d_{\max}$ to preserve a minimal resolution. In order to prevent long connections at the margins of the parameter region we look for closest neighbors in a radius of $3d_{\max}$. In order to prevent triangles with edges longer than $2d_{\max}$, we choose the maximal connection length as $1.8d_{\max}$. If a connection is longer, we compute an additional point on the surface close to the middle of the bridge and take this additional point into account. This criterion may also prevent the filling of an area where the bifurcation condition is not satisfied. This is particularly true in case of a Hopf bifurcation if the Hopf number χ is positive at this point. As described above the algorithm would automatically try to find a bifurcation point at the border of the Hopf bifurcation surface. If the computation of the new bifurcation point fails the division is denied.

Second, the angles between the resulting triangles and the triangles of the mesh should not be larger than $\phi_{\max}$. This criterion keeps the triangulation
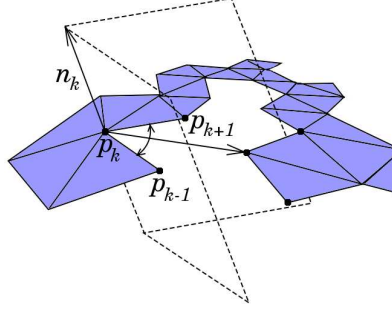
(a) The space of possible neighbors of $\mathbf{p}_k$ is within the two half planes spanned by the normal $\mathbf{n}_k$ associated to $\mathbf{p}_k$ and the two vectors from $\mathbf{p}_k$ to $\mathbf{p}_{k-1}$ and $\mathbf{p}_{k+1}$.
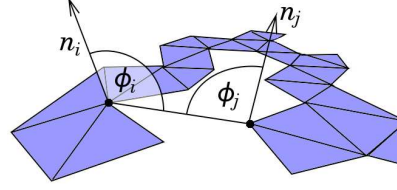
(b) The difference between the angles ϕ_i and ϕ_j to 90 degrees has to be less than $\phi_{\max}$
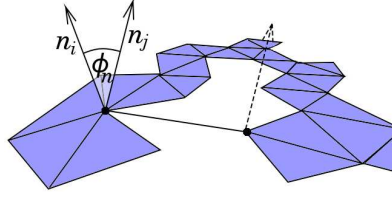
(c) The angle ϕ_n between the normals of the connected points has to be less than $\phi_{\max}$
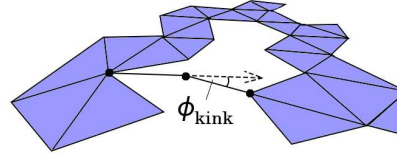
(d) If an additional point in the middle of the bridge is necessary the angle ϕ_{kink} has to be less then $\phi_{\max}$

Figure 2.3: A connection in the filling phase is called bridge and has to satisfy different conditions.

smooth and may prevent the covering of a more complex region of the surface. Let ϕ_i and ϕ_j denote the angles between the connection and the normals $\mathbf{n}_i$ and $\mathbf{n}_j$ associated to the connected vertices as shown in Fig.2.3(b). Further, we denote ϕ_{n} as the angle between the two normals $\mathbf{n}_i$ and $\mathbf{n}_j$ (see Fig.2.3(c)). If the difference from ϕ_i and ϕ_j to 90 degrees is larger than $\phi_{\max}$ or ϕ_{n} is larger than $\phi_{\max}$, we compute an additional point between as well. As illustrated in Fig.2.3(d) a new point in the connection will in general cause a kink. If the angle of the kink in the connection is bigger than $\phi_{\max}$, the division is denied. If we can not compute the new point, because probably the bifurcation does not exist close to it, the division is also rejected.

Having obtained an adaptive triangulation of the bifurcation surface, we have to consider how to display the set of triangles.
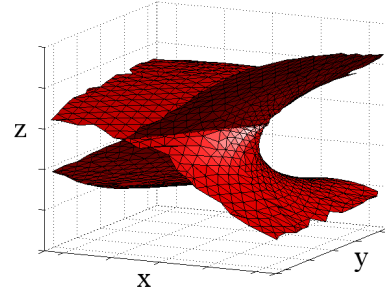
2.4.7   Level lines

One the one hand visualization of the edges of the triangles can lead to visual fallacies. Small triangles seem to be far away while large triangles may look very close. Focus points sometimes exacerbate this effect. On the other hand not displaying only the triangle surface without edges would deprive the viewer of clues on the three dimensional shape of the surface. We introduce level lines as a cosmetic tool. Like the level lines in a map we project certain values from the axes onto the surface.

Finally we demonstrate the ability of our algorithm by the computation of a Whitney umbrella type bifurcation surface which may appear as a higher codimension bifurcation for Hopf bifurcations (cf. Chapter 4, Sec. 4.4.2). In this case the bifurcation surface is twisted in itself (cf. Fig. 2.4). Even close to the end of the intersection line, where the crossing angle becomes small, no transitions occur. While in most regions the degree of curvature is quite small, a sharp edge appears close to the end of the line where the Hopf bifurcation intersects itself. Since the radius of curvature decreases rapidly at this edge from a quite high value to a very small one, the adaptive resolution control would fail to adapt the size of the triangles in this region. However, using focus points close to the end of the crossing line we can prevent bigger gaps in this region.

After the filling phase is completed (Fig. 2.4(b)) we cut off the outer triangles in order to obtain even margins at the boundary of the region in parameter space. Instead of the triangles we display now the level lines on the surface for both horizontal axes in Fig. 2.4(c). As mentioned above not only the bifurcation surfaces but also the intersection lines are of interest since they form bifurcations of higher codimension. In order to highlight these bifurcations we finally mark the intersection line and its endpoint as shown in Fig. 2.4(d).
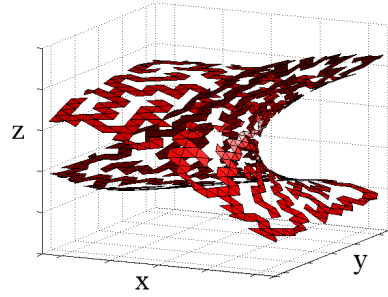
(a) The trace of triangles follows the evolution of the surface.

(b) Whitney umbrella surface after the filling phase.
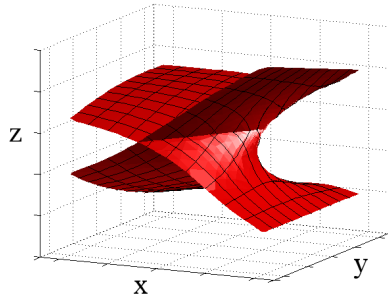
(c) Whitney umbrella surface after the filling phase with level lines (no highlighting of the triangle edges).
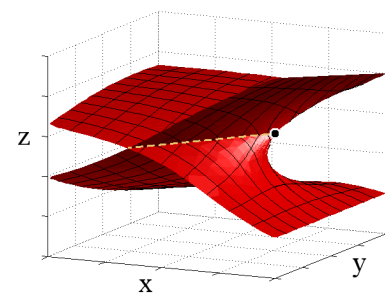
(d) Marking of intersection line and its endpoint

Figure 2.4: Construction of a Whitney umbrella shaped surface. While the upper subplots (a) and (b) show the two phases of the triangulation algorithm, the lower subplots (c) and (d) illustrate the preparation of the resulting diagram.

2.5   Discussion

In this chapter we have proposed and applied a combination of generalized modeling, bifurcation theory and adaptive triangulation techniques. This approach has enabled us to compute and visualize the local codimension-1 bifurcation hypersurfaces of steady states. In order to obtain a faithful representation of the surface at a low computational cost the algorithm automatically adapts the size of the computed triangle elements to the local complexity of the surface. Due to the application of generalized modeling, the resulting bifurcation diagrams do not describe a single model, but a class of models that share a similar structure.

The proposed approach enables the researcher to rapidly compute three parameter bifurcation diagrams for a given class of models. By considering several of these diagrams with different parameter axes an intuitive understanding of the local dynamics in a given class of systems can be gained. In particular, the approach bridges the gap between applied and fundamental research as discussed in the Introduction. In the visualization of local bifurcations as surfaces in a three dimensional parameter space, certain local bifurcations of higher codimension can be easily spotted. In our experience the proposed approach reveals bifurcations of codimension two and three in almost every model studied. It thereby provides plentiful examples for mathematical analysis. In return insights gained from the investigation of higher-codimension bifurcations can directly feed back in the investigation of the system. In particular the implications of local bifurcations of higher codimension, discussed above, is intriguing in this context. Provided that the dynamical implications of a bifurcation are known from normal form theory, the appearance of such a bifurcation in the three parameter diagram, pinpoints a parameter region of interesting dynamics. This region can then be investigated in conventional models or experiments. In this way the investigation of models is facilitated by reducing the need for more costly parameter search in conventional models.

In the present thesis we have only used the proposed approach in conjunctions with testfunctions for two basic local bifurcations: the Hopf bifurcation and the tangent bifurcation. However, in principle, the approach can be extended to include testfunctions for codimension-2 bifurcations. This would allow the algorithm to adaptively decrease the size of triangles close to these bifurcations and continue the bifurcation lines directly once they are reached. Furthermore, being hyperlines, the codimension-2 bifurcation points form surfaces in a four dimensional parameter space. Once again these surfaces can be triangulated with the described algorithms. The four dimensional space could be visualized in a movie, where time represents the forth parameter or by collapsing and color coding one of the parameter dimensions. Both approaches would allow for the visual identification of bifurcations of codimension three

and higher.

At present the proposed approach has two limitations. First, the extraction of information is solely based on the Jacobian. Higher orders, which determine the normal form coefficients, are at present not taken into account. However, parameters that capture this information could be defined in analogy to the exponent parameters, which we have used to capture the required information on the nonlinearity of the equations of motion.

The second limitation is that the approach outlined here is presently only applicable to systems of small or intermediate dimension ($N < 10$) as the analytical computation of the testfunctions becomes cumbersome for larger systems. This problem can be avoided by combining the triangulation techniques proposed here with the numerical investigation of generalized models demonstrated in (Steuer et al., 2006).

Chapter 3

Stoichiometric producer-grazer systems[*]

3.1 Abstract

We analyze how stoichiometric constraints affect the dynamics of producer-grazer systems. The approach of generalized modeling is used to identify generic stability properties and global dynamics. We find a Takens-Bogdanov bifurcation that leads to the disappearance of the paradox of enrichment in certain parameter regions. Further, the Takens-Bogdanov bifurcation indicates the presence of homoclinic bifurcations. These findings are compared to different specific modeling approaches.

3.2 Introduction

Traditionally most ecological models quantify energy and biomass flow solely in terms of carbon. Stoichiometric constraints arising in part from different nutrient ratios in the populations are only captured indirectly. However, in recent years it has been shown that already minor extensions can make carbon-based models stoichiometrically explicit and thus significantly enhance the qualitative understanding of laboratory experiments and field observations. Presently, the effects of stoichiometric constraints are thus receiving more and more attention (Sterner and Elser, 2002).

In particular the conversion efficiency from the first to the second trophic level as well as the rate of primary production have been found to be strongly affected by stoichiometric constraints (Andersen et al., 2004). Most primary

---

[*]This Chapter has been submitted in a condensed version to The American Naturalist. Especially, the discussion of the generalized parameters in Sec.3.3 and the final discussion Sec. 3.6 are much more detailed than in this Chapter.

producers are flexible in their use of nutrients and are thus characterized by highly variable nutrient content. By contrast grazers growing by consumption of the primary producers have a relatively fixed internal stoichiometry. Thus conversion efficiency of producer into grazer biomass can depend strongly on the nutrient content of the producer.

The producer's nutrient content depends on the many complex processes governing nutrient flows (DeAngelis, 1992), but is particularly dependent on grazing. Although grazing can enhance the recycling of nutrients in the system (Sterner, 1986), it also sustains accumulation of biomass on higher trophic levels which can lead to a storage of nutrients in the biomass of grazers and predators. In systems in which the recycling of nutrients is essential, storage of nutrients can lead to a depletion of nutrients available for primary producers and consequently decreases both the primary production and the grazers conversion efficiency.

Nutrient storage and variable conversion efficiency introduce a complex feedback mechanism as the rate of primary production and the growth of grazers become dependent on the biomasses of all populations in the system. Even in simple food chain models it has been shown that stoichiometric constraints arising from variable nutrient content lead to complex dynamics (Huxel, 1999; Loladze and Kuang, 2000; Sterner and Elser, 2002; Kooijman et al., 2004). A point of particular concern is that different, but seemingly similar, models can exhibit very different dynamics, depending on the functional forms that are used to describe the conversion efficiency. Since the metabolism of even a single cell is highly complex, every specific function formulated to describe stoichiometric constraints on the level of the population necessarily involves strong assumptions. It is therefore an important practical challenge to identify the decisive feature of the functional forms that have a strong impact on the dynamics and therefore have to be captured in the formulation of credible models.

In this Chapter we use the approach of generalized modeling (Gross et al., 2005; Gross and Feudel, 2006) to analyze the effects of stoichiometric constraints. In a generalized model the rates of processes do not need to be restricted to specific functional forms which enables us to investigate the dynamics of a large class of models comprising of several well studied examples. This allows us to compare the results of the generalized model to three specific models: the model of Kooijman et al. (2004) based on the Dynamic Energy Budget (DEB) theory (Kooijman, 2000), a model by Loladze and Kuang (2000) which uses Liebigs minimum law, and a related model with smooth functions based on the concept of synthesizing units (SU) (O'Neill et al., 1989; Kooijman, 2000). The generalized model provides an unifying framework that explains differences and commonalities between the different specific models, while the specific models allow for numerical investigation which reveal ad-

ditional insights beyond what can be extracted from the generalized model. Our analysis reveals that a variable conversion efficiency has a strong impact on population dynamics, leading to global bifurcations (Kuznetsov, 2004) and parameter regions where the paradox of enrichment (Rosenzweig, 1971) is avoided. However, the generalized analysis reveals a paradox of competition that is related to the paradox of enrichment but appears to be a generic property of the model class. By comparison, the functional dependence of the primary production on populations other than the primary producer appears to be of minor importance.

3.3 A generalized food chain model with variable efficiency

Our aim is to understand the effects of stoichiometric constraints on the primary production S and biomass conversion efficiency E. Therefore we consider one of the most fundamental classes of population models containing a primary producer X and a grazer Y as variables. For the sake of simplicity we assume that X and Y express the biomass densities in terms of carbon concentrations as it is the case for the specific models we analyze in Section 3.5.

As motivated in the introduction we assume that the the primary production $S(X,Y)$ and biomass conversion efficiency $E(X,Y)$ may depend on both variables, i.e. the primary producer and the grazer. The grazing is represented by the generalized per capita functional response $F(X)$. Finally we assume a linear mortality of the grazer with a constant rate D. Thus the model reads

$$
\begin{aligned}
\dot{X} &= S(X,Y) - F(X)Y , \\
\dot{Y} &= E(X,Y)F(X)Y - DY .
\end{aligned}
\tag{3.1}
$$

Usually the first step in the analysis is a local stability analysis of steady states. However, in contrast to specific models where the functional forms of the processes, namely $S(X,Y)$, $F(X)$ and $E(X,Y)$, are given explicitly, we can not compute the steady states of generalized models. Nevertheless, a normalization procedure described in (Gross and Feudel, 2006; Gross et al., 2004) enables a local stability analysis of generalized models in terms of bifurcation theory. This normalization is based on the assumption that at least one positive but not necessarily stable steady state (X^*, Y^*) exists. Additionally, this normalization technique leads to generalized parameters that can be interpreted by biological reasoning. In the following we demonstrate this method with a minimum of technical details (cf. Gross and Feudel (2006) for further details) in order to focus on the biological results.

Firstly, we define the normalized variables $x = X/X^*$ and $y = Y/Y^*$ as well as the normalized processes $s(x,y) = S(X^*x, Y^*y)/S(X^*, Y^*)$, $e(x,y) =$

$E(X^*x, Y^*y)/E(X^*, Y^*)$ and $f(x) = F(X^*x)/F(X^*)$. The normalized model reads then

$$\begin{aligned} \dot{x} &= s(x, y) - f(x)y \,, \\ \dot{y} &= r(e(x, y)f(x)y - y) \,, \end{aligned} \tag{3.2}$$

with $r := \frac{D}{S(X^*, Y^*)/X^*}$. The advantage of this normalization is that we know not only the steady state $x^* = y^* = 1$ but also the generalized processes in the steady state $s(x^*, y^*) = f(x^*) = e(x^*, y^*) = 1$.

The interpretation of the new parameter r is straightforward. From the model Eq.(3.2) we see that the parameter r is directly connected to the timescale of the grazer population y. Due to the normalization the parameter r describes the relative scale of the lifetime between the producer and the grazer in the steady state (X^*, Y^*). If $r = 1$ both variables have the same timescale in the steady state. We assume that the timescale of the grazer is slower than the timescale of the producer (Hendriks, 1999), i.e. $0 \le r \le 1$.

So far, we normalized the generalized model in order to avoid the unknown steady state (X^*, Y^*) and obtained the timescale parameter r. The next step is the stability analysis of the steady state under consideration in terms of bifurcation theory. The stability of the steady state is given by the eigenvalues of the Jacobian $\mathbf{J}$ in the steady state. A steady state is stable if the real parts of all eigenvalues are negative. Thus, only two bifurcation situations where the steady states becomes unstable are of interest: tangent bifurcations (where one real eigenvalue crosses the imaginary axis) or Hopf bifurcations (where a pair of complex conjugate eigenvalues crosses the imaginary axis). Note, since we focus on the eigenvalues only we do not distinguish between generic or degenerate types of these bifurcations in the generalized analysis.

The Jacobian of the normalized model in the steady state reads

$$\mathbf{J}|_{x=x^*, y=y^*} = \begin{vmatrix} \sigma_x - \gamma & \sigma_y - 1 \\ r(\eta_x + \gamma) & r\eta_y \end{vmatrix} \tag{3.3}$$

where we define

$$\begin{aligned} \gamma &:= \left. \frac{\mathrm{d}f(x)}{\mathrm{d}x} \right|_{x=x^*, y=y^*} , \\ \sigma_x &:= \left. \frac{\mathrm{d}s(x,y)}{\mathrm{d}x} \right|_{x=x^*, y=y^*} , \\ \sigma_y &:= \left. \frac{\mathrm{d}s(x,y)}{\mathrm{d}y} \right|_{x=x^*, y=y^*} , \\ \eta_x &:= \left. \frac{\mathrm{d}e(x,y)}{\mathrm{d}x} \right|_{x=x^*, y=y^*} , \\ \eta_y &:= \left. \frac{\mathrm{d}e(x,y)}{\mathrm{d}y} \right|_{x=x^*, y=y^*} , \end{aligned} \tag{3.4}$$

as the generalized parameters with $x^* = y^* = 1$. These parameters encode the required information about the mathematical form of the processes. Theoretically, we are now able to compute the bifurcation conditions mentioned

above based on the Jacobian (Eq. (3.3)). These bifurcation manifolds are hypersurfaces in parameter space that separate stable from unstable parameter regions. In principle, we could start to compute the bifurcation diagrams using the the technique introduced in Chapter 2. However, in order to benefit from these bifurcation diagrams, we first need bifurcation parameter that we understand from a biological perspective.

3.3.1 Ecological and stoichiometric restrictions

At this point we defined the model structure and obtained the timescale parameter and generalized parameters as potential bifurcation parameters. The interpretation of the generalized parameters in the light of stoichiometry requires a fundamental knowledge of the processes. For the bifurcation analysis it is further convenient to substitute some of the parameters. In the following we discuss the main ecological and stoichiometric restrictions on the processes and their mathematical consequences before we choose a set of bifurcation parameters having a biological interpretation.

First, it is reasonable to assume that the primary production $S(X, Y)$ grows proportional to the number of primary producers X if competition is low. However, as stated in the introduction each realistic system has limited resources. A storage of nutrients in biomass of X and Y could lead to a lack of available nutrients. Such a lack of a limiting nutrient would lead to low or even zero primary production.

Since a single grazer can only consume a limited amount of producers the consumption rate, i.e. the functional response $F(X)$ saturates for high producer densities. We assume that the functional response $F(X)$ growths monotonously with the density of primary producers X. This means that there are no inhibition effects due to high primary producer densities.

In our model class food quality effects does not affect directly the consumption rate but the conversion efficiency $E(X, Y)$ of the consumed biomass. Low food quality in terms of a lack of at least one essential nutrient tends to decrease the biomass production of the grazer and therefore $E(X, Y)$. But the food quality, the nutrient content of the primary producer is coupled to the availability of nutrients. For the same reasons as mentioned above, the biomass of X and Y tends to decrease the amount of available nutrients and therefore the nutrient content of X. Consequently, we assume that $E(X, Y)$ decreases monotonously with X and Y.

3.3.2 Mathematical consequences

For low values of X and Y resources are abundant and the competition pressure on X is low. Thus $S(X, Y)$ is approximately a linear function in X and

independent of Y as described above. The relations

$$
\begin{aligned}
\sigma_x &= \left.\frac{\mathrm{d}s(x,y)}{\mathrm{d}x}\right|_{x=x^*,y=y^*} = \left.\frac{X^*}{S(X^*,Y^*)}\frac{\mathrm{d}S(X,Y)}{\mathrm{d}X}\right|_{X=X^*,Y=Y^*}, \\
\sigma_y &= \left.\frac{\mathrm{d}s(x,y)}{\mathrm{d}y}\right|_{x=x^*,y=y^*} = \left.\frac{Y^*}{S(X^*,Y^*)}\frac{\mathrm{d}S(X,Y)}{\mathrm{d}Y}\right|_{X=X^*,Y=Y^*},
\end{aligned}
\tag{3.5}
$$

show that a linear approach, say $S(X,Y) = S(X) = \beta X$ where β is a constant factor, leads to $\sigma_x = (X^*/\beta X^*)\beta = 1$ and $\sigma_y = 0$. Since this situation is a limit case, we relate low competition to σ_x close to 1 and σ_y close to zero. By contrast, if available resources are scarce $S(X,Y)$ grows slower than linear in or even decreases with X and decreases monotonously with Y. Consequently, the parameters σ_x and σ_y are lower than 1 and 0, respectively. They go to $-\infty$ when a limiting nutrient becomes unavailable for primary production ($S(X^*,Y^*) \to 0$). Note that this is a limit case since $S(X^*,Y^*)$ is always larger than 0 for any positive steady state (X^*,Y^*). Due to our assumptions above we identify $1 \geq \sigma_x > -\infty$ and $0 \geq \sigma_y > -\infty$ as biologically reasonable ranges. In order to have a parameter within a limited range $[0,1)$ we define the parameters $c_x := (1-\sigma_x)/(2-\sigma_x)$ and $c_y := -\sigma_y/(1-\sigma_y)$ and substitute $\sigma_x = 2 - 1/(1-c_x)$ and $\sigma_y = 1 - 1/(1-c_y)$.

Since realistic functional responses $F(X)$ saturate for high producer densities, high values of $X^* \to \infty$ lead to $\gamma \to 0$. If producer is scarce the value of γ is higher. Typical values are $\gamma = 1$ and $\gamma = 2$ that are related to linear or quadratic consumption rates, respectively. As stated above we assumed that the conversion efficiency $E(X,Y)$ decreases monotonously, i.e. $\eta_x \leq 0, \eta_y \leq 0$. Further we assumed that $E(X,Y)$ tend to become small for high values of X and Y. If $E(X^*,Y^*) \to 0$ (while X^* and Y^* approach values larger than zero) then $\eta_x \to -\infty$ and $\eta_y \to -\infty$ as we see from Eq.(3.6).

$$
\begin{aligned}
\eta_x &= \left.\frac{\mathrm{d}e(x,y)}{\mathrm{d}x}\right|_{x=x^*,y=y^*} = \left.\frac{X^*}{E(X^*,Y^*)}\frac{\mathrm{d}E(X,Y)}{\mathrm{d}X}\right|_{X=X^*,Y=Y^*} \\
\eta_y &= \left.\frac{\mathrm{d}e(x,y)}{\mathrm{d}y}\right|_{x=x^*,y=y^*} = \left.\frac{Y^*}{E(X^*,Y^*)}\frac{\mathrm{d}E(X,Y)}{\mathrm{d}Y}\right|_{X=X^*,Y=Y^*}
\end{aligned}
\tag{3.6}
$$

Briefly we assume $-\infty < \eta_x \leq 0$ and $-\infty < \eta_x \leq 0$. Again we define new parameters $n_x := 1/(1-\eta_x)$ and $n_y := 1/(1-\eta_y)$ that are defined within the range $(0,1]$ respectively to substitute the unbounded parameters $\eta_x = 1-1/n_x$ and $\eta_y = 1 - 1/n_y$.

3.3.3   Bifurcation Parameters

In summary our bifurcation parameters are r, c_x, c_y, γ, n_x and n_y. Apart from γ all parameters are per definition limited in between 0 and 1. We identified the parameter r as the relative timescale between the producer X and the grazer Y. Following (Gross et al., 2005) we denote the parameter γ as

	Name	Range	Remarks
r	relative timescale	(0,1)	$\rightarrow 1$ no timescale separation, $\rightarrow 0$ infinite timescale separation
c_x, c_y	intra and inter specific competition	[0,1)	0 no competition ($S(X,Y)$ linear in X and independent of Y), $\rightarrow 1$ only competition($S(X^*,Y^*) \rightarrow 0$)
γ	sensitivity to prey	> 0	close to zero for saturated $F(X)$, 1 for $F(X)$ linear in X 2 for $F(X)$ quadratic in X
n_x, n_y	food quality	(0,1]	1 for good food quality $\rightarrow 0$ (constant $E(X,Y)$), for low food quality ($E(X^*,Y^*) \rightarrow 0$)

Table 3.1: Bifurcation parameters of the generalized model.

the (grazer) sensitivity to prey (producer). When the producer is abundant the grazer is not very sensitive to the amount of producers since predation is already quite saturated. In this case γ is close to zero as mentioned above.

We denote the parameters c_x and c_y as the intra-specific and inter-specific competition parameters, respectively. They are close to 0 if competition is low and close to 1 if limiting resources are scarce and competition leads to low primary production $S(X^*,Y^*)$.

In a similar way we interpret n_x and n_y as food quality parameters. As long as food quality is good in the sense that only food quantity limits growth these parameters are close to 1. In the case of low food quality these parameters are lower and approach 0 if the concentration of a limiting nutrient of the grazer approaches zero in the primary producer population. Table 3.1 gives an overview of all bifurcation parameters of the generalized model.

3.4 Generalized analysis

Now, after obtaining a reasonable parameter range for all parameters that appear in the Jacobian we can analyze which theoretically realistic parameter sets solve the bifurcation conditions mentioned above ($Re(\lambda_{1,2}) = 0$). Our particular emphasis lies on the impact of the functional form of the efficiency $E(X,Y)$. Hence, we first analyze the qualitative behavior with constant efficiency before we assume that E depends on the density of primary producers and grazers.
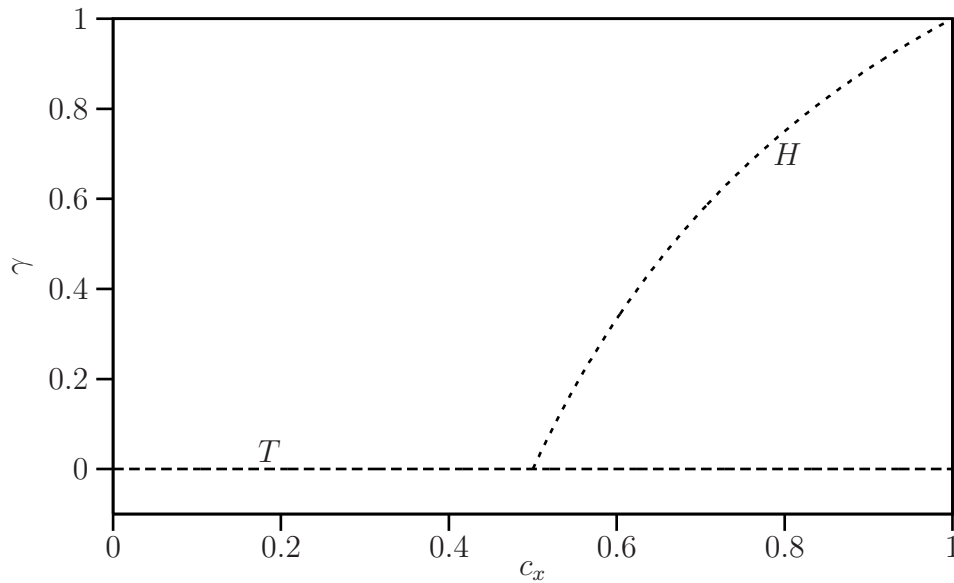
Figure 3.1: Bifurcation diagram of the generalized model with constant efficiency, i.e. $n_x = n_y = 1$. The steady state is stable in the top left region. A Hopf bifurcation line (H) and a tangent bifurcation line (T) are shown. The bifurcations are independent of the relative timescale r and the inter-specific competition parameter c_y. Note that the tangent bifurcation is at $\gamma = 0$ and is not present in models with monotone increasing functional response $F(X)$.

3.4.1   Constant efficiency

First, we consider the rather conventional case of a constant efficiency, i.e. $n_x = n_y = 1$. Figure 3.1 shows the resulting bifurcation diagram.

We find a tangent bifurcation line (T) and a Hopf bifurcation curve (H). The steady state of the normalization is stable in the top left region of the diagram. If one of the bifurcation lines is crossed due to a parameter variation the steady state becomes unstable.

First of all, it is remarkable that both bifurcations are independent of r and c_y. This means that timescale separation and the functional dependency of $S(X, Y)$ on Y (i.e. how X competes with Y) has no influence on the stability of the positive steady state.

The Hopf bifurcation curve exceeds the valid parameter range of $0 < c_x < 1$ for $\gamma \geq 1$. For this reason, a Hopf bifurcation cannot be found in this model class if $f(x)$ and therefore $F(X)$ are linear functions ($\gamma = 1$). One famous example is the Lotka-Volterra model with a logistic growth (Hofbauer and Sigmund, 1998). However, a Hopf bifurcation can appear in general if the

function $F(X)$ saturates and γ becomes lower than 1, e.g. models with Holling type II or type III functional response (Rosenzweig and MacArthur, 1963). In these models an increase of the intra-specific competition parameter c_x leads to a Hopf bifurcation and destabilizes the steady state. In ecology this Hopf bifurcation is usually related to a destabilization of the whole system, because in many models the oscillations beyond the Hopf bifurcation lead to low population densities and hence, increase the chance of a stochastic extinction of both populations. This counterintuitive effect of the intra-specific competition on the stability of the system is closely related to the paradox of enrichment (Rosenzweig, 1971).

The Hopf bifurcation ends at a tangent bifurcation line at $\gamma = 0$ in a codimension-2 Takens-Bogdanov bifurcation. Since we consider $F(X)$ as a monotonous function, i.e. $\gamma > 0$, the tangent and the Takens-Bogdanov bifurcation at $\gamma = 0$ can not be observed (as long as the conversion efficiency is a constant).

3.4.2 Variable efficiency

Let us now analyze the influence of a variable efficiency $E(X,Y)$ when the primary production $S(X,Y)$ is independent of Y leading to $c_y = 0$. Clearly, the food quality parameters n_x and n_y are not independent of each other. Since very low values of $E(X^*,Y^*)$ may lead to low values of n_x and n_y it is rather unrealistic to choose for instance n_x close to 0 and n_y close to one at the same time. However, the exact relation between n_x and n_y depends on the specific model. To see how the stoichiometry changes qualitatively the bifurcation diagram compared to results from constant efficiency models (shown in Fig. 3.1) we assume first that $n_x = n_y$. We will see in Sec. 3.5 that such a linear approach compares to one of our specific models as well.

Figure 3.2 shows the bifurcation diagram for a moderate timescale separation $r = 0.3$. Note, that the two-dimensional bifurcation diagram shown in Fig. 3.1 which we obtained for a constant efficiency (ideal food quality) can be seen as a cross section of this three-dimensional bifurcation diagram shown in Fig. 3.2 at $n_x = n_y = 1$.

We observe that the Hopf bifurcation surface can only be found in the region of relatively high food quality values. In the Appendix we show that generally no Hopf bifurcations can occur for $n_x \leq 0.5$. In that sense low food quality leads in general to the disappearance of the paradox of enrichment. However, this does not mean that low food quality necessarily stabilizes the system. From Fig. 3.2 we see that rather the opposite seems to be the case. A decreasing food quality can lead to a crossing of the tangent bifurcation surface and hence, into the unstable parameter volume. Beyond the tangent bifurcation the system leaves the steady state X^*, Y^* and approaches another

Figure 3.2: Bifurcation diagram of a generalized producer-grazer model. A surface of Hopf bifurcations (bright) and a surface of tangent bifurcations (dark) are shown. The bifurcation parameters are the sensitivity to prey γ, the food quality parameters $n_x = n_y$ and the intra-specific competition parameter c_x. The fixed parameters are $r = 0.3$ (moderate timescale separation) and $c_y = 0$ ($S(X, Y) = S(X)$). The steady state (X^*, Y^*) is only stable in the top front volume. Note that the cross section at $n_x = n_y = 1$ represents the bifurcation diagram in Fig. 3.1.

attractor.

Furthermore, we note that the Takens-Bogdanov bifurcation can occur as soon as the food quality parameters $n_x = n_y$ are lower than one. At this bifurcation the Jacobian has a double zero eigenvalue. In addition to the tangent bifurcation and the Hopf bifurcation a homoclinic bifurcation emerges from the Takens-Bogdanov bifurcation line (Kuznetsov, 2004). The homoclinic bifurcation is in general difficult to detect and can be related to sudden population bursts and to the vanishing of population cycles. Consequently, we can state that a variable food quality and therefore a variable conversion efficiency leads to new bifurcations and therefore enriches the system dynamics.

In the last section we have shown that the inter-specific competition parameter c_y has no influence on the stability of the steady state if the efficiency is constant. For variable efficiency models the inter-specific competition parameter c_y leads to a shift of the tangent bifurcation surface and therefore to a shift of the end of the Hopf bifurcation surface. However, for low to intermediate values of $c_y \leq 0.5$ the bifurcation diagram looks almost identical to Fig. 3.2 where we assumed $c_y = 0$ $(S(X, Y) = S(X))$. Figure 3.3 shows two bifurcation diagrams at $c_y = 0.6$ (left) and at $c_y = 0.95$ (right). We see that the effects become more pronounced for relative high values of $c_y \rightarrow 1$. However, we observe that the inter-specific competition parameter c_y does not change the results discussed above qualitatively. Nevertheless, it leads to a shift of the bifurcation surfaces and hence can influence the stability of the system.
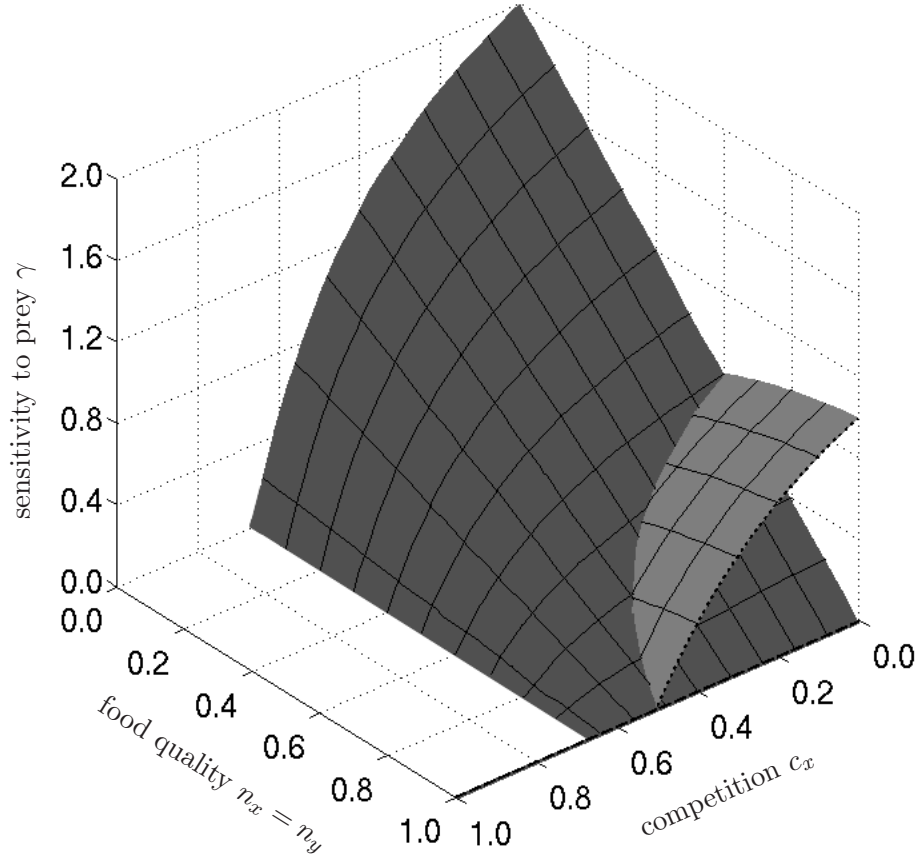
Figure 3.3: Bifurcation diagram of a generalized producer-grazer model. A surface of Hopf bifurcations (bright) and a surface of tangent bifurcations (dark) are shown. The fixed parameters are $r = 0.3$ and $c_y = 0.6$ (left diagram) and $c_y = 0.95$ (right diagram). The steady state (X^*, Y^*) is only stable in the top front volume.

To see whether these findings persist if we decrease n_x and n_y independently, we compute a bifurcation diagram for low competition ($c_x = 0.01$ and $c_y = 0$) and take n_x and n_y as bifurcation parameters. As shown in Fig. 3.4, for both parameters n_x and n_y a decrease leads to an upwards shift of the tangent bifurcation surface (dark). The parameter n_x causes additionally an upwards shift of the Hopf bifurcation surface (bright). However, the conclusions we derived from Fig. 3.2 do not depend on the specific coupling of n_x and n_y as long as one or both of these parameters decrease.
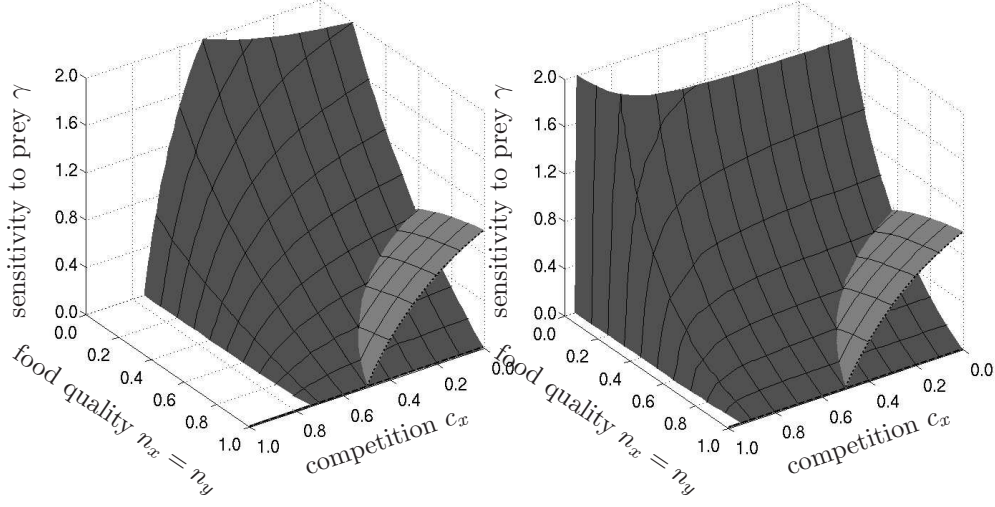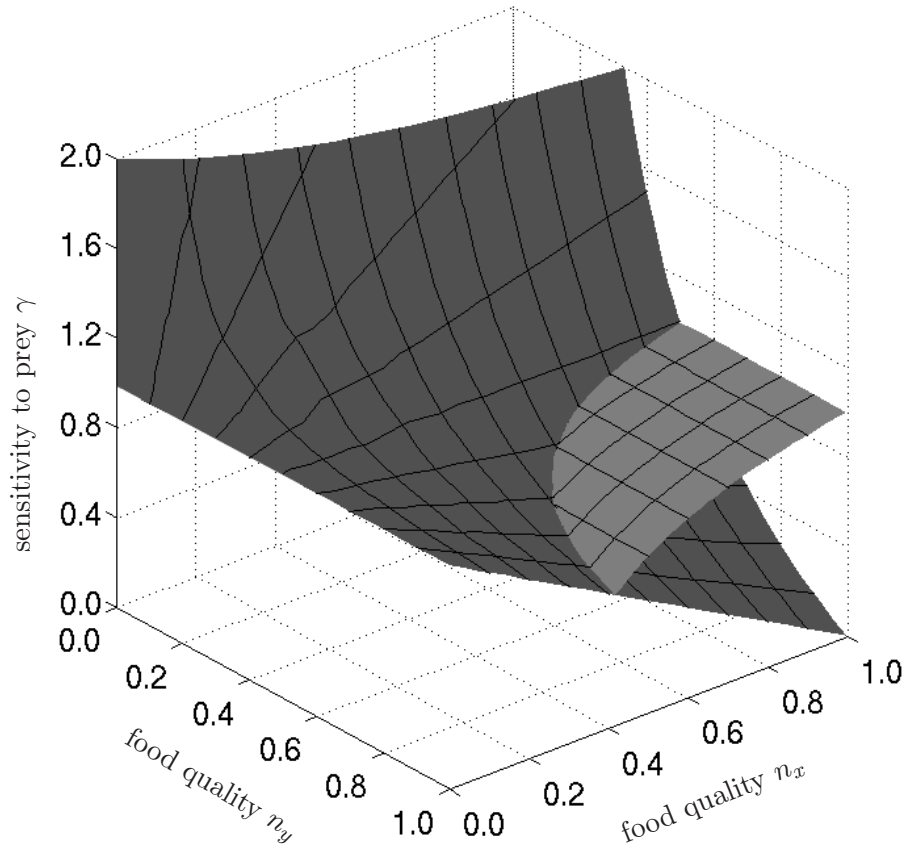
Figure 3.4: Bifurcation diagram of a generalized producer-grazer model. A surface of Hopf bifurcations (bright) and a surface of tangent bifurcations (dark) are shown. The fixed parameters are $r = 0.3$, $c_x = 0.01$ and $c_y = 0$. The steady state (X^*, Y^*) is only stable in the top front volume.

In summary, the analysis of the generalized model showed that for a constant efficiency a decreasing intra-specific competition (i.e. competition parameter c_x) tends to destabilize the system due to a Hopf bifurcation. The timescale r as well as the inter-specific competition parameter c_y and therefore the functional dependency of $S(X, Y)$ on Y have no effect.

Although in variable efficiency models the inter-specific competition parameter c_y has an influence on the bifurcation surfaces for $n_x < 1, n_y < 1$ the effects are qualitatively low. We can clearly ascribe the presence of tangent and Takens-Bogdanov bifurcations to a variability of the conversion efficiency for the model class under consideration. Further homoclinic bifurcations are in general present for variable conversion efficiency emerging from the Takens-Bogdanov bifurcations. In other words, although both processes, the primary production $S(X, Y)$ and the conversion efficiency $E(X, Y)$ are obviously constrained due to stoichiometry, the latter appears to be much more important for the system dynamics. Even low effects of a variable food quality may cause population bursts and the disappearance of population cycles, as stated above.

The Hopf bifurcation ends for decreasing food quality (i.e. at a certain value of n_x and n_y) in a Takens-Bogdanov bifurcation. The paradox of enrichment is therefore absent for low food quality parameters. However, a decreasing intra-specific competition (i.e. the competition parameter c_x) still tends to destabilize the steady state under consideration due to a tangent bifurcation.

3.5   Specific stoichiometric modeling approaches

The generalized analysis is of most advantage if the functional forms of the processes are unknown. As we have seen above it allows to gain insights on stability properties and global dynamics from very fundamental assumptions about the considered processes. A major drawback of the generalized analysis is that we have no information about the response of the steady state values (X^*, Y^*) on parameter variations.

In specific models usually rather simple functional forms are used that incorporate the basic knowledge about the underlying processes. This specific model description allows for a numerical as well as an analytical analysis. A drawback of specific models is that it is difficult to distinguish generic system properties from artifacts or degenerations due to the simplifications made in order to formulate the specific model. In the following we present a fruitful combination of generalized and specific bifurcation analysis in order to relate generalized and specific model properties.

Please note that in the following model descriptions small and capital letters no longer relate to normalized or non-normalized variables and processes.

We will instead use the notations of the variables from the formulations of the original models. The bifurcation diagrams of the specific models are obtained by numerical continuation using the software AUTO Doedel et al. (1997); Doedel and Oldeman (2009).

3.5.1 DEB model and simplified DEB model

A first central result of the generalized analysis is that the functional dependency of the primary production on the grazer population expressed by c_y has no or a qualitatively rather low influence on the bifurcation manifolds. The appearance of new local and global bifurcations is clearly related to the variable efficiency in the model class under consideration.

The following specific example is a DEB model which has been introduced by (Kooijman et al., 2004, 2007). It considers the dynamics of a producer P and a consumer C. In this model the primary production depends not only on the density of primary producers but also on the grazer density. It was formulated as a variable efficiency model as well as a simplified constant efficiency model. In the following we compare the dynamics of the two models to our generalized analysis.

We follow the model formulation in (Kooijman et al., 2007) without maintenance costs. In the DEB model the producer consists of two compartments. Assimilated nutrients are added first to a reserve or storage compartment. In a second step reserves are used for growth. Since the producers take up nutrients from the environment fast and efficiently, we assume that all nutrients are either in the structure or reserves of the producers $P(t)$ or in the structure of the consumers $C(t)$.

Here the producer's reserve density m_N is obtained from the conservation of nutrient in the system

$$m_N(t) = N/P - n_{NC}\, C/P - n_{NP} \tag{3.7}$$

for a total constant amount of nutrient N. The chemical indices n_{NP} and n_{NC} stand for producers' and consumers' nutrient content per carbon and are constant as well. This means that $P(t) \in (0, N/n_{NP})$ and $C(t) \in [0, N/n_{NC})$.

Following (Muller et al., 2001), the time evolution of the amounts of producers P and consumers C is given by

$$\frac{d}{dt}P = r_P P - j_P C \quad \text{with } r_P = \frac{k_N m_N}{y_{NP} + m_N} \quad \text{and } j_P = \frac{j_{Pm} P}{K + P} \tag{3.8}$$

$$\frac{d}{dt}C = (r_C - h_C)C \quad \text{with } r_C = \left(r_{CP}^{-1} + r_{CN}^{-1} - (r_{CP} + r_{CN})^{-1}\right)^{-1} \tag{3.9}$$

$$r_{CP} = y_{CP}\, j_P \quad \text{and}$$
$$r_{CN} = y_{CN}\, m_N\, j_P$$

	Name	Value	Units
N	Total nutrient in the system	0-8.0	mol l^{-3}
n_{NC}	Chemical index of nutrient in C	0.25	mol mol^{-1}
n_{NP}	Chemical index of nutrient in P	0.15	mol mol^{-1}
k_N	Reserve turnover rate	0.25	h^{-1}
y_{NP}	Yield of N on P	0.15	mol mol^{-1}
j_{Pm}	Maximum specific assimilation rate	0.4	mol mol^{-1} h^{-1}
K	Half saturation constant	10	mM
$y_C P$	Yield of C on P	0.5	mol mol^{-1}
$y_C N$	Yield of C on N	0.8	mol mol^{-1}
j_{PAm}	Maximum specific assimilation rate	0.15	mol mol^{-1} h^{-1}

Table 3.2: Parameter table of the model by (Kooijman et al., 2007)

where the specific growth rate of the producers r_P follows from Droop-kinetics and the specific feeding rate j_P is the Holling type II functional response. The specific growth rate r_C of the consumers results from the standard SU rules for the parallel processing of complementary compounds, here producer's reserve and structure (O'Neill et al., 1989; Kooijman, 2000). The flux r_{CP} represents the contribution of the producer's structure to consumer's growth, and r_{CN} that of producer's reserve, while both compounds are required in the fixed stoichiometric ratio y_{CP}/y_{CN}.

For the simplified constant efficiency version of model Eqs. (3.8, 3.9) we assume that the consumer takes the structural part of the producer only. Then the growth rate of the consumer follows a simple Holling type II functional response, that is $r_C = r_{CP}$.

$$\frac{d}{dt}P = r_P P - j_{PA} C \quad \text{with } r_P = \frac{k_N m_N}{y_{NP} + m_N} \quad \text{and } j_{PA} = \frac{j_{PAm} P}{K + P} \tag{3.10}$$

$$\frac{d}{dt}C = (r_{CP} - h)C \quad \text{with } r_{CP} = y_{CP} j_{PA} \tag{3.11}$$

In order to compare the dynamics of both model formulations Eqs. (3.8,3.9) and Eqs. (3.10, 3.11) for different amounts of available nutrients N, we compute two bifurcation diagrams Fig. 3.5 and Fig. 3.6.

Figure 3.5 shows the bifurcation diagram of the simplified DEB model (3.10, 3.11) for a variation of the total nutrient N. We see that a positive steady state emerges from a transcritical bifurcation TC and becomes unstable in a Hopf bifurcation H where a stable limit cycle emerges. This bifurcation scenario is typical for many constant efficiency models (Van Voorn et al., 2008) although the primary production here is modeled in a different way.
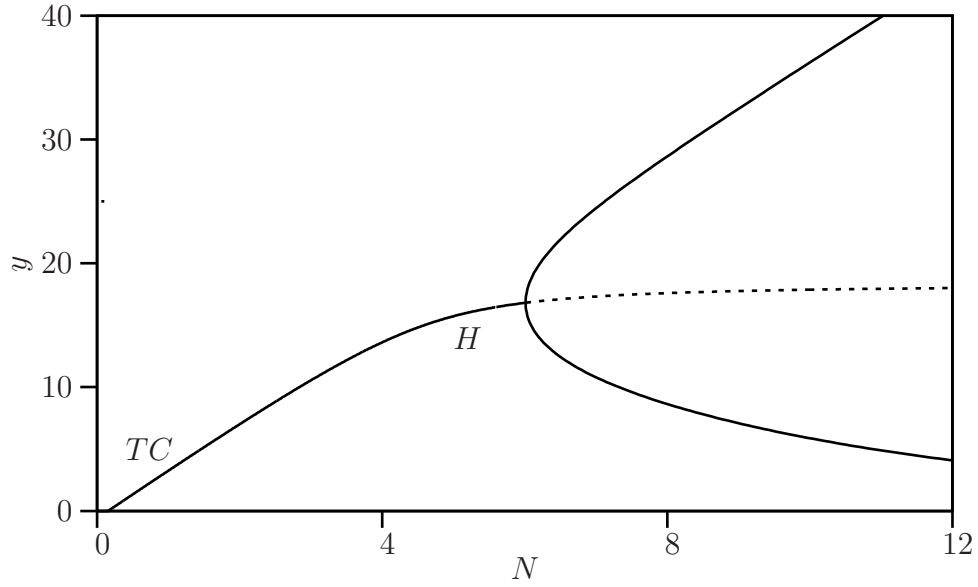
Figure 3.5: Bifurcation diagram of the simplified DEB model. The stable positive steady states emerges from a transcritical bifurcation TC and becomes unstable in a Hopf bifurcation H. From the Hopf bifurcation emerges a stable limit cycle.

Note that the parameter N is not equivalent to the carrying capacity K of the frequently used logistic growth. However, from the generalized point of view it is not surprising that we obtain a similar bifurcation diagram since all constant efficiency models in the model class under consideration share the same rather simple bifurcation diagram shown in Fig. 3.1.

Due to the results from the generalized analysis we expect a much more complicated bifurcation scenario for the variable efficiency DEB model Eqs. (3.8, 3.9). Figure 3.6 shows the bifurcation diagram for the DEB model with variable efficiency. The positive stable equilibrium emerges from a tangent bifurcation instead of a transcritical one. Biologically, this tangent bifurcation can be interpreted as an Allee-effect: The initial population size of the grazer has to be large enough (above the unstable solution emerging from the tangent bifurcation) in order to persist. By increasing the amount of Nutrient N the stable equilibrium becomes unstable in a Hopf bifurcation H and as in the simplified model a stable limit cycle emerges. In contrast to our previous observations for the simplified constant efficiency model Eqs. (3.10, 3.11) the stable limit cycle vanishes for even higher values of N in a homoclinic bifurcation. After this global bifurcation the zero equilibrium is the global attractor for the system.
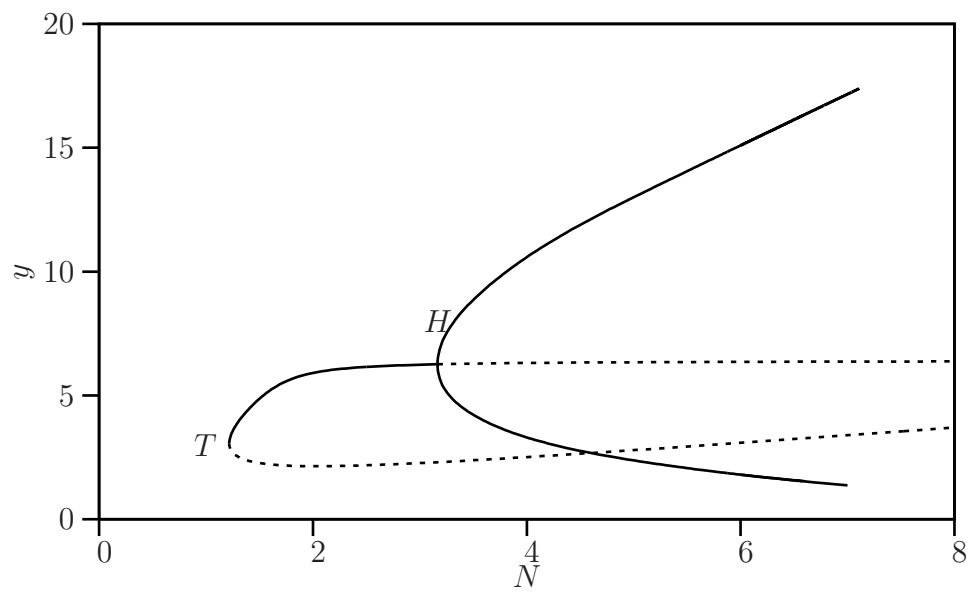
Figure 3.6: Bifurcation diagram of the DEB model with variable efficiency. A stable (solid line) and an unstable (dashed line) solution emerge from a tangent bifurcation T. The stable solution becomes unstable in a Hopf bifurcation H and a stable limit cycle emerges. The limit cycle disappears in a homoclinic bifurcation when increasing N.
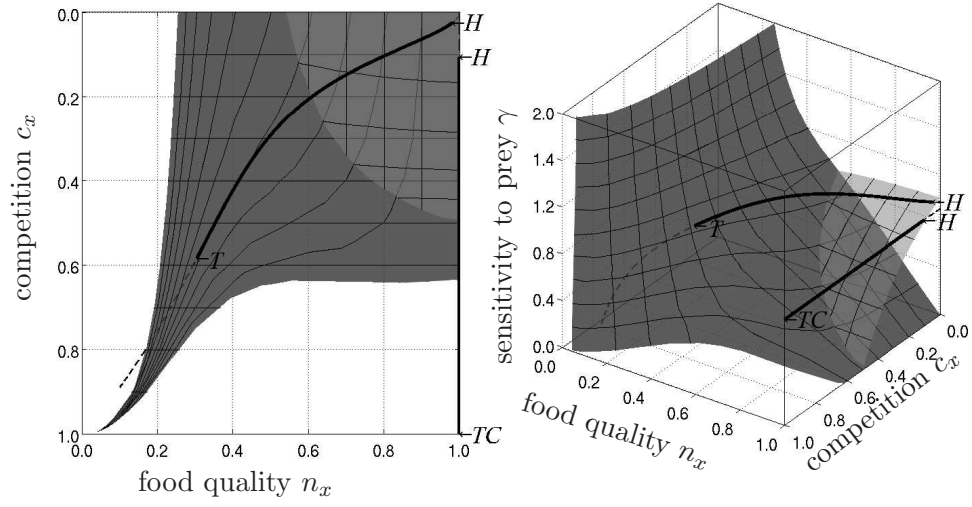
Figure 3.7: Bifurcation diagram of the generalized producer-grazer model from top (left) and side (right) view. A surface of Hopf bifurcations (transparent grey) and a surface of tangent bifurcations (dark grey) are shown. Additionally, the steady state solutions from Fig. 3.5 (at $n_x = 1.0$) and from Fig. 3.6 ($0 \leq n_x \leq 1$) are shown. In contrast to Fig. 3.2, the relation $n_y = n_y(n_x)$ is derived to fit the computation shown in Fig. 3.6. The fixed parameters are $r = 0.02$ and $\sigma_y = -2.37$ (i.e. $c_y \approx 0.77$)

Although the bifurcation types that can be found are in line with the generalized analysis it is not a priori clear where these bifurcations occur. In order to see how the specific bifurcation diagrams compare to the generalized analysis, we transfer the curves in Fig. 3.5 and Fig. 3.6 into the generalized parameter space. For each point in Fig. 3.5 and Fig. 3.6 we compute the related generalized parameter set.

While we used the *ad hoc* approach $n_x = n_y$ in our previous analysis we can now obtain the relation directly from the transferred bifurcation curves. Figure 3.7 shows the resulting bifurcation diagram. Note that the derived relation between n_x and n_y is specific for the DEB model and for the parameter used in Fig. 3.6. However, the qualitative results we derived in Sec. 3.4.2 from Fig. 3.2 assuming $n_x = n_y$ hold for Fig. 3.7 as well.

In addition to the bifurcation surfaces we see two curves partly solid and partly dashed. The right hand side curve at $n_x = 1$ relates to the positive steady state of the simplified DEB model shown in Fig. 3.5. The TC is located at $c_x = 1$ in the generalized diagram. At this point the positive steady state intersects with the zero equilibrium ($Y^* \to 0$) where the grazing as well as the primary production become zero. From Sec. 3.5 we already know that $S(X,Y) \to 0$ is related to $c_x \to 1$. The Hopf bifurcation point H where the stable positive steady state (solid line) becomes unstable (dashed line) fits to the Hopf surface of the generalized analysis.

The other curve is transferred from the bifurcation diagram of the DEB model with variable efficiency shown in Fig. 3.6. It intersects the tangent bifurcation surface at T. This is exactly the point T from Fig. 3.6 in generalized coordinates. The dashed part of the curve is the unstable steady state while the solid part is the stable steady state that coalesce in the tangent bifurcation T. The stable steady state becomes unstable when it intersects the Hopf bifurcation surface at H. Note that at the tangent bifurcation T both parts of the curve evolve into two different directions in the generalized parameter space. The reason is that both parts of the curve are related to two different steady states. Consequently, both curves are normalized to different steady states.

From the generalized analysis we expect the presence of a homoclinic bifurcation due to the Takens-Bogdanov bifurcation. At the homoclinic bifurcation the limit cycle that emerges from the Hopf bifurcation intersects the unstable steady state from the tangent bifurcation and disappears. Biologically speaking, close to the homoclinic bifurcation the population typically remains for a long time close to the unstable equilibrium before it rapidly breaks out and comes back to the equilibrium. After the bifurcation the population approaches another attractor. In this example both populations die out.

From Fig. 3.7 we see that this scenario is impossible for the simplified constant efficiency DEB model. The tangent bifurcation as well as the Takens-

Bogdanov bifurcation are out of the feasible range $\gamma > 0$.

In summary, the generalized framework allows for a comparison of the DEB model and the simplified DEB model. The combined diagram in Fig. 3.7 visualizes that the simplification to a constant efficiency model leads to a reduced bifurcation scenario. Or in other words, that an extension to a variable efficiency model leads to much richer dynamics.

3.5.2 Non-smooth model by Loladze and Kuang 2000

Another central result of the generalized analysis is the disappearance of Hopf bifurcations and as a consequence, the disappearance of the paradox of enrichment for low food quality parameters n_x or n_y.

A specific stoichiometric model where the disappearance of the paradox of enrichment has been observed was proposed and analyzed in (Loladze and Kuang, 2000). In contrast to our first example two different essential nutrients are considered here namely carbon and phosphorus. Further, no storage of nutrients is modeled explicitly. The density of phosphorus $\eta(t)$ in the producers population x is variable but not less than a minimal density q. The density of phosphorus θ in the grazer population y is assumed to be constant.

The primary production follows a logistic growth with carrying capacity K if carbon is limiting. However, if phosphorus is limiting the carrying capacity is given by the upper limit for the producer density which is the total available phosphorus $(P - \theta y)$ divided by the minimal phosphorus density in the primary producer q. Hence, the classical carrying capacity is replaced by the minimum function $\min(K, (P - \theta y)/q)$.

The producer is consumed by the grazer with rate $cf(x)$ carbon and at the same time phosphorus with a rate $\eta(t)cf(x)$. If the growth of the grazer is carbon limited the conversion efficiency is assumed to be constant $\hat{e}$. As soon as the phosphorus density of the producer $\eta(t)$ is below the phosphorus density of the grazer the growth of the grazer is phosphorus limited. The conversion efficiency is decreased by the ratio $\eta(t)/\theta$. Consequently, we define the conversion efficiency as $\min(\hat{e}, \hat{e}\eta/\theta)$.

The model equations read

$$\frac{dx}{dt} = bx\left(1 - \frac{1}{\min(K/x, \eta/q)}\right) - cf(x)y \qquad (3.12)$$

$$\frac{dy}{dt} = \hat{e}\min\left(1, \frac{\eta}{\theta}\right)cf(x)y - dy \qquad (3.13)$$

where

$$f(x) = \frac{x}{a + x} \qquad (3.14)$$

	Name	Value	Units
P	Total phosphorus	0.025	mg P l^{-1}
$\hat{e}$	Maximal production efficiency in carbon terms	0.8	
b	Maximal growth rate of the producer	1.2	day^{-1}
d	Grazer loss rate (includes respiration)	0.25-0.27	day^{-1}
θ	Grazer constant P/C	0.03	(mg P)(mg C)$^{-1}$
q	Producer minimal P/C	0.0038	(mg P)(mg C)$^{-1}$
c	Maximum ingestion rate of the grazer	0.81	day^{-1}
a	Half-saturation of grazer ingestion response	0.25	mg C l^{-1}
K	Producer carrying capacity limited by light	0.25-2.0	mg C l^{-1}

Table 3.3: Parameter table of the model by Loladze and Kuang (2000).

and the variable

$$\eta(t) = \frac{P - \theta y(t)}{x(t)} \tag{3.15}$$

where the constant P is the total amount of phosphorus in the closed system.

Observe that the grazer egests nutrient that is not used for growth. The egested products are mineralized and sequestered by the producer instantaneously. As a result, no external carbon and phosphorus pools are assumed.

Since η is variable also the conversion efficiency $\hat{e}\min(1, \eta/\theta)$ is variable if phosphorus is limiting. In this case, as in our last example we expect from the generalized analysis that tangent bifurcations as well as homoclinic bifurcations can be found. Figure 3.8 shows a one parameter bifurcation diagram of this model for a variable carrying capacity K. The positive stable steady state starts from a transcritical bifurcation $TC1$ and becomes unstable at a Hopf bifurcation. This bifurcation scenario is similar to constant efficiency models as we have seen for the simplified DEB model. However, for higher values of K we see additionally another stable and another unstable solution emerging from a tangent bifurcation T. The limit cycle emerging from the Hopf bifurcation vanishes in a saddle-node homoclinic bifurcation at T. At this point T another unstable and a stable solution emerge on the limit cycle and turn the limit cycle into a homoclinic loop.

As mentioned above, another central result of the generalized model is in line with the results from the model analysis in (Loladze and Kuang, 2000): The disappearance of the paradox of enrichment for low food quality (low total phosphorus concentrations, see Eq.(3.15))). From the generalized modeling point of view, the disappearance of the paradox of enrichment is related
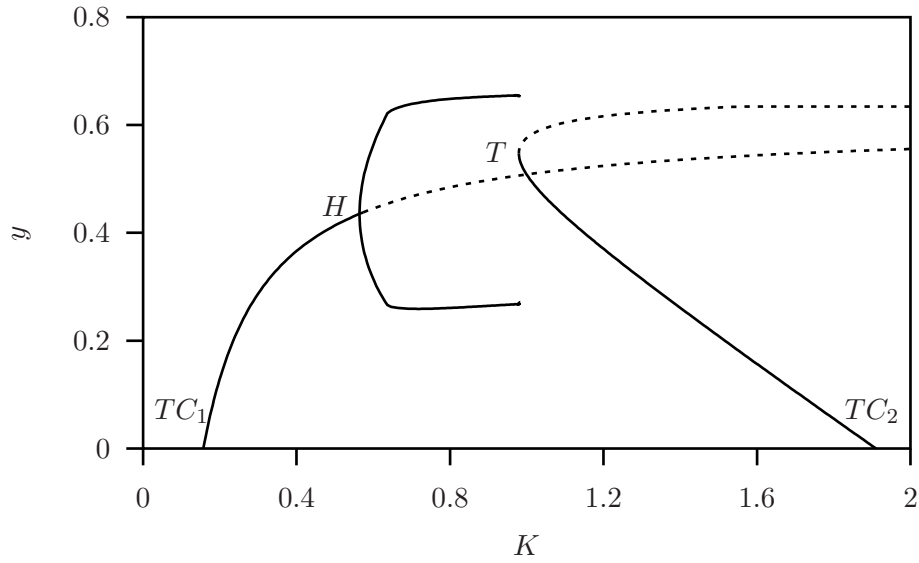
Figure 3.8: One-parameter bifurcation diagram with the carrying capacity K on the abscissa, and the grazer biomass on the ordinate. A stable positive solution that emerges from a transcritical bifurcation TC_1 (solid line) becomes unstable (dashed line) at the Hopf bifurcation H. A stable limit cycle that emerges at the Hopf bifurcation vanishes for increasing K in a saddle-node homoclinic bifurcation where another stable and an unstable solution emerge from the tangent bifurcation T. The stable solution of the tangent bifurcation exchanges stability with the zero equilibrium in another transcritical bifurcation TC_2.

to a switch of the generalized parameter n_x. By comparing Eq. (3.1) and Eq.(3.13) we see that the efficiency is given as $\hat{e}c\min\left(1, \frac{\eta}{\theta}\right)$. This means that the efficiency switches from a constant function to a function that is inverse proportional to x if phosphorus becomes limiting. In the generalized parameter space this is related to a switch of n_x from 1 to 0.5. As we have shown the value $n_x = 0.5$ is exactly the limit where the Hopf bifurcation disappears. In that sense we understand the disappearance of the paradox of enrichment in the model by Loladze and Kuang (2000) as a generic property of all models that allow for low values of the food quality parameter ($n_x \leq 0.5$).

In order to visualize the switch we show in Fig. 3.9 a two-parameter bifurcation diagram of the model by Loladze and Kuang (2000) similar to Fig. 5 in (Loladze and Kuang, 2000). Figure 3.9 shows the switch explicitly as a curve A and additionally a homoclinic bifurcation G. We note that the Hopf bifurcation as well as the homoclinic and the tangent bifurcation end at the switch. At first sight, it seems confusing that Hopf and tangent bifurcation appear at the same side of the switch. The reason for this is that the tangent bifurcation line and the Hopf bifurcation line are related to different steady states as we show in Fig. 3.8. This difference in the steady state leads to different generalized parameters due to the normalization. For the steady state of the Hopf bifurcation the switch A is from $n_x = 1$ to $n_x = 0.5$. By contrast, for the steady states at the tangent bifurcation the switch A is from $n_x = 0.5$ to $n_x = 1$.

In the generalized model we observe that a decrease of competition always tends to destabilize the steady state. At low food quality where no Hopf bifurcations can be found this destabilization is caused by a tangent bifurcation. We see from Fig. 3.9 that, in the model by Loladze and Kuang (2000) the same bifurcation scenario can be found when phosphorus is limiting: an increasing total phosphorus concentration can lead to a destabilization due to the tangent bifurcation T. Loladze and Kuang (2000) denoted this paradoxical effect as the paradox of nutrient enrichment. From the generalized point of view both the paradox of enrichment and the paradox of nutrient enrichment are combined by the paradox of competition.

In contrast to Fig. 5 in (Loladze and Kuang, 2000), Fig. 3.9 shows not only the switch but also the location of the homoclinic bifurcation. From the generalized analysis we know that a homoclinic bifurcation is present because of the Takens-Bogdanov bifurcation line we found. However, the Takens-Bogdanov bifurcation can not be found in this specific model because the switch of n_x from 1 to 0.5 avoids the parameter region where the Takens-Bogdanov bifurcation is present. Therefore, it is an open question whether the additional homoclinic connection of the saddle emerges from the Takens-Bogdanov bifurcation found in the generalized analysis. A path following of the homoclinic connection stops at the switch A in the model as shown in
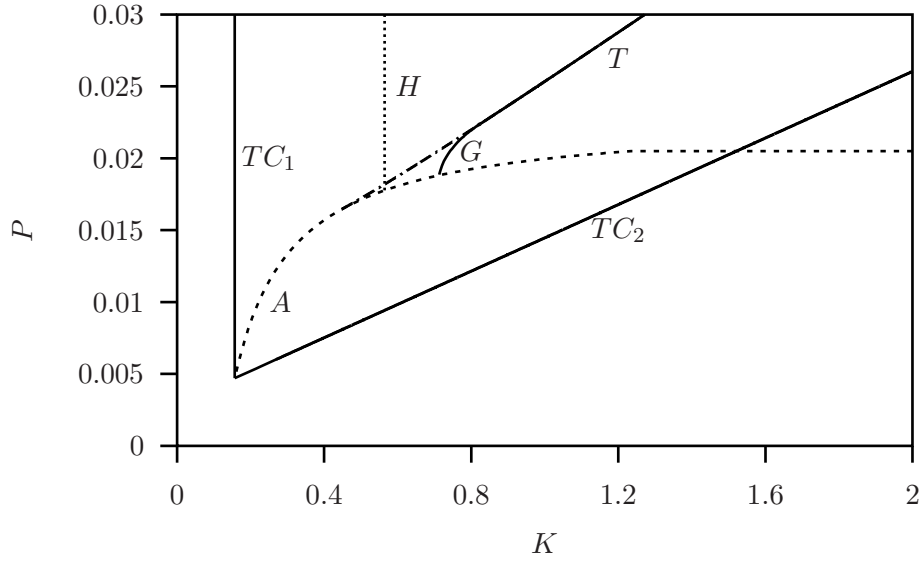
Figure 3.9: Bifurcation diagram in a two-parameter plane spanned by total phosphorus content P and carrying capacity K for the non-smooth model by Loladze and Kuang (2000), with $d = 0.32$. The (saddle) homoclinic bifurcation curve G merges with the tangent bifurcation curve T in a saddle-node homoclinic bifurcation. A is the curve where the grazer minimum function $((P - \theta y)/x)/\theta = 1$, i.e. a stoichiometric switch occurs. The Hopf bifurcation curve H and the tangent bifurcation curve T both terminate at the curve A. The curves TC_1 and TC_2 define the transcritical boundary. Before TC_1 and beyond or rather below TC_2 the grazer becomes extinct.

Fig. 3.9. In order to find the Takens-Bogdanov bifurcation as the organizing center of the Hopf and the homoclinic bifurcation we formulate a smooth analogon to this model to avoid the switch which introduces a discontinuity.

3.5.3   Smooth analogon model

To overcome discontinuities in derivatives which cause problems for a bifurcation analysis we now set up a new model which is a smooth approximation of the model Eqs. (3.12, 3.13) analyzed in (Loladze and Kuang, 2000). The closed system consists of the producer, the grazer and the environment. Just as in (Loladze and Kuang, 2000) we assume that there is no phosphorus in the environment, but there is an external carbon pool for the two biota. The pool represents the resources for the producers modeled in (Loladze and Kuang, 2000) by introducing the carrying capacity K.

Let x denote the biomass density of the producer and y the biomass density of the grazer, both represented in mg C per volume of the environment. Then the model reads

$$\frac{dx}{dt} = bx \frac{j_m}{1 + \frac{K_{PC}}{(C-x)B_C} + \frac{K_{PC}}{(P-\theta y-qx)B_P} - \frac{K_{PC}}{(C-x)B_C+(P-\theta y-qx)B_P}} - cf(x)y \tag{3.16}$$

$$\frac{dy}{dt} = \hat{e}\frac{1.2}{1 + \frac{\theta}{\eta} - 1/(1 + \frac{\eta}{\theta})}cf(x)y - dy \tag{3.17}$$

where the constant C is the total amount of carbon in t, P is the total amount of phosphorus and

$$j_m := 1 + \frac{K_{PC}}{CB_C} + \frac{K_{PC}}{PB_P} - \frac{K_{PC}}{CB_C + PB_P} \tag{3.18}$$

so that b is the maximum initial producer growth rate (i.e. for $x \to 0$,$y \to 0$). The parameter θ is again the phosphorus density in the grazer and $\eta(t)$ the phosphorus density in the producer. The parameters B_C and B_P are the assimilation preferences of the producer for C and P respectively. The parameter K_{PC} is a saturation constant.

The producer consists of two components, its structure and a phosphorus pool. The structure has a fixed stoichiometry, that means the phosphorus density P/C ratio denoted by q is fixed. The total phosphorus density in the producer is denoted by η: hence, the phosphorus of the pool is $\eta - q$.

To model the assimilation of the producer (Eq.(3.16), the SU-formulation (O'Neill et al., 1989; Kooijman, 2000) is used where both nutrients are assumed to be essential. Note that this rate determines the growth rate of the

	Name	Value	Units
$K_P C$	Saturation constant	1	
B_C	Producer assimilation preferences for C	0.002	l $(mg\ C)^{-1}$
B_P	Producer assimilation preferences for P	2	l $(mg\ P)^{-1}$

Table 3.4: Parameter table of the smooth analogon to the model by Loladze and Kuang (2000) (b, C, P, θ, η, c and $\hat{e}$ same as in Tab.3.3).

producer measured as carbon content while the phosphorus is already fixed by the conservation law applied to the closed system and the assumption that all phosphorus is in the biota. As a result the phosphorus density in the pool $\eta - q$ and consequently the total phosphorus density η are time-dependent.

Furthermore, in this formulation the growth depends on carbon influx from the environment proportional to $C - x$ and internal phosphorus from the pool $P - \theta y - qx$. In the mass-balance model formulation the densities of the two nutrients available for growth are $C - x - y$ and $P - \theta y - qx$. Note that now not $C - x - y$ but $C - x$ is used for the carbon in order to obtain the same approximation as in the model of Loladze and Kuang (2000). This reflects the fact that the model formulation with the logistic growth for the producer in absence of the grazer does not obey mass-conservation (Kooi et al., 1998). However, in Sec. 3.5.4 we also analyze a model formulation with mass-conservation to investigate its impact on the dynamics.

The consumed amount of carbon and phosphorus by the grazer are both proportional to $cf(x)$ while η, is time-dependent. In this process there is no distinction between the origin of the phosphorus: either from the structure of the producer or from its phosphorus pool. In (3.17) the SU-formulation for the two momentary fluxes is used. However, in this formalism both fluxes need to be independent. Application of this formalism is justified by assuming that after ingestion both nutrients from the assimilation (catabolic) process become available for growth as unrelated chemical substances whereby the two nutrients are both essential. The factor 1.2 is used to get a better match between the smooth model (Eqs. (3.16, 3.17)) and its non-smooth counterpart (Eqs. (3.12, 3.13)). Indeed, we obtain a very similar bifurcation diagram when increasing the total carbon concentration C that compares to the carrying capacity K in the model by Loladze and Kuang (2000).

Figure 3.10 shows a bifurcation diagram of the smooth SU model formulation. The variation of the total carbon C leads to a qualitatively as well as quantitatively similar bifurcation diagram compared to Fig. 3.8 where we increased the capacity K from the logistic growth formulation. Again the appearance of the tangent and the homoclinic bifurcation are in line with the
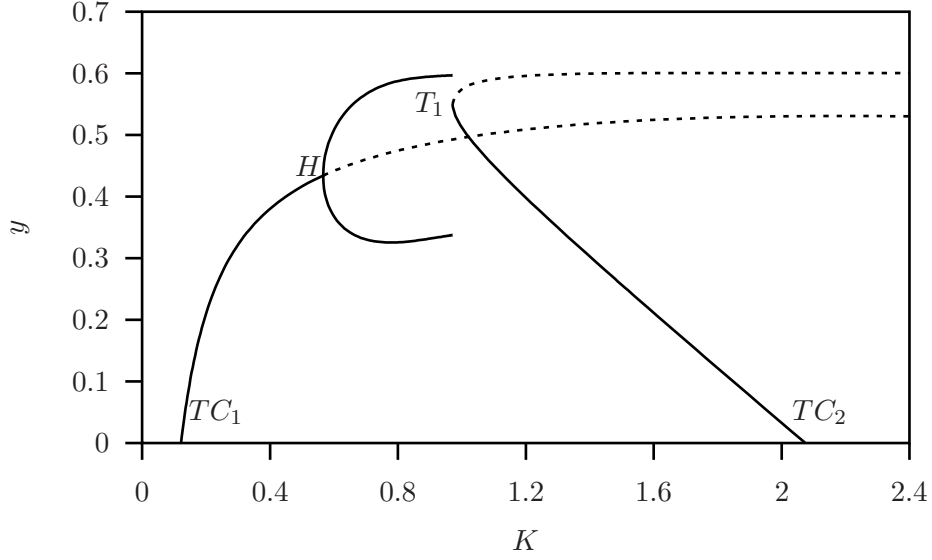
Figure 3.10: One-parameter bifurcation diagram with total carbon concentration C on the abscissa, and the grazer biomass on the ordinate. A stable positive solution that emerges from a transcritical bifurcation TC_1 (solid line) becomes unstable (dashed line) at the Hopf bifurcation H. A stable limit cycle that emerges at the Hopf bifurcation vanishes for increasing K in a saddle-node homoclinic bifurcation where another stable and an unstable solution emerge from a tangent bifurcation T. The stable solution of the tangent bifurcation exchanges stability with the zero equilibrium in another transcritical bifurcation TC_2.

results from the generalized analysis. As mentioned above, we expect from the generalized analysis a Takens-Bogdanov bifurcation to be the organizing center of the Hopf and the homoclinic bifurcation. However, the tangent and the Hopf bifurcation can not meet in a Takens-Bogdanov bifurcation since both belong to different steady states. We need to find a tangent bifurcation of the steady state of the Hopf bifurcation. Indeed, by decreasing d slightly from 0.25 to 0.27 we observe that the steady state which becomes unstable in the Hopf bifurcation undergoes a tangent bifurcation T_2 and turns into a stable steady state in the tangent bifurcation T_1. The resulting bifurcation diagram is shown in Fig. 3.11.

In contrast to the non-smooth model by Loladze and Kuang (2000), the smooth model formulation enables us to map the specific bifurcation diagram into the generalized parameter space as we did for the DEB model in Fig. 3.7.
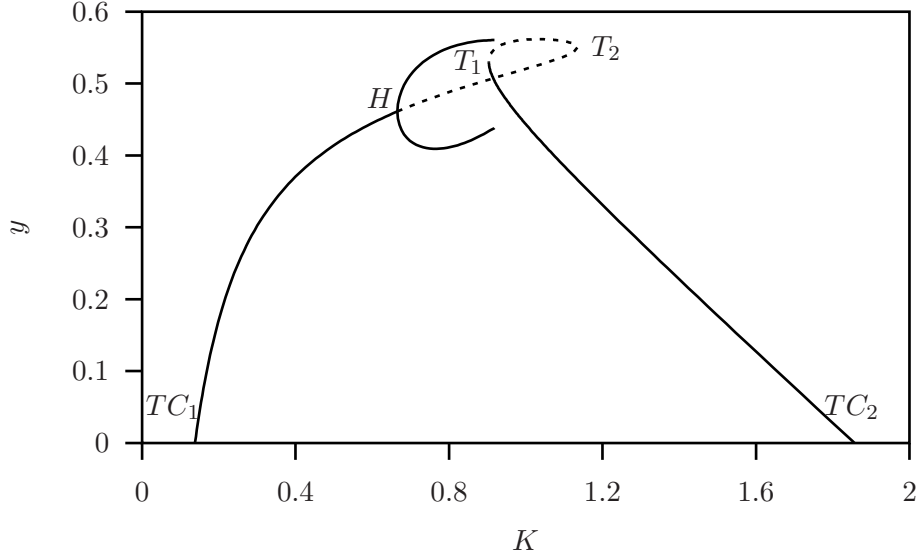
Figure 3.11: One-parameter bifurcation diagram with total carbon concentration C on the abscissa, and the grazer biomass on the ordinate. A stable positive solution that emerges from a transcritical bifurcation TC_1 (solid line) becomes unstable (dashed line) at the Hopf bifurcation H. A stable limit cycle that emerges at the Hopf bifurcation vanishes for increasing K in a saddle homoclinic bifurcation. The saddle emerges together with another stable solution from a tangent bifurcation T_1. The stable solution of the tangent bifurcation exchanges stability with the zero equilibrium in another transcritical bifurcation TC_2. In contrast to Fig. 3.10 where we used the same parameter set except $d = 0.25$ instead of $d = 0.27$, the two unstable solutions merge and disappear in another tangent bifurcation T_2.

However, in contrast to the DEB model a linear approach for the relation between n_x and n_y is sufficient to get a match between the bifurcation points of the specific model and the bifurcation surfaces of the generalized bifurcation diagram. Figure 3.12 shows the combined bifurcation diagram.

Again the transcritical bifurcations are located at the cross section at $c_x = 1$. At this plane the first positive steady state starts at TC_1. A further increase of C leads to a decreasing intra-specific competition parameter c_x. At first the Hopf bifurcation surface is crossed at H before the unstable steady state connects to the other steady state at the tangent bifurcation point T_2.

The tangent bifurcation point T_1 is located at the same bifurcation surface. For the stable solution of the tangent bifurcation T_1 the relation of c_x and C
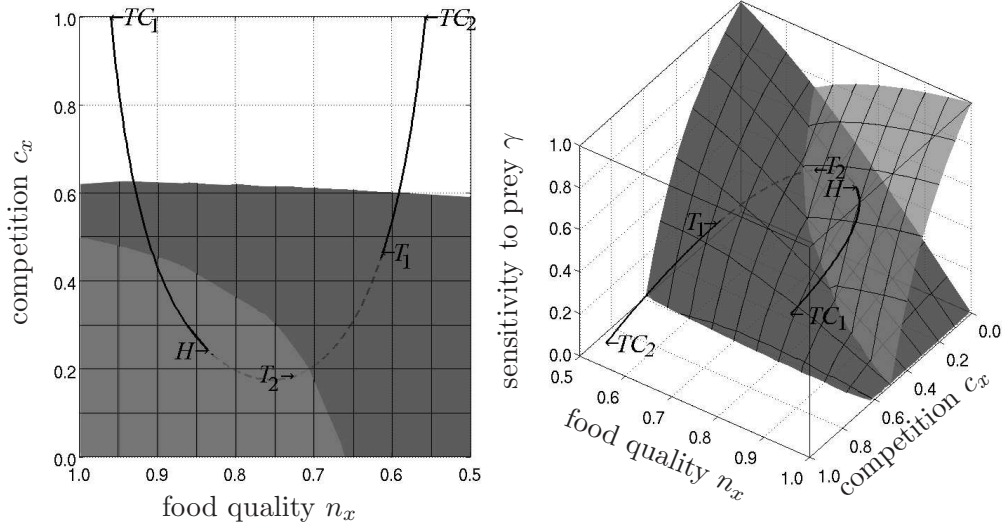
Figure 3.12: Bifurcation diagram of a generalized producer-grazer model. A surface of Hopf bifurcations (bright) and a surfaces of tangent bifurcations (dark) are shown. The fixed parameters are $r = 0.28$ and $c_y = 0$. The steady state (X^*, Y^*) is only stable in the top front volume.

is counterintuitive: An increase of C is related to a decrease of c_x. The stable solution exchanges stability in the other transcritical TC_2 at the plane $c_x = 1$. Again, it is important to note that each point on the curve in Fig. 3.12 is related to different steady state values and consequently to a different normalization.

As discussed above, based on the results of the generalized analysis we expect that the Hopf bifurcation H and the tangent bifurcation point T_2 intersect in a Takens-Bogdanov bifurcation. This Takens-Bogdanov line is expected to be the origin of the homoclinic bifurcation. A two parameter continuation of the bifurcations presented in Figure 3.13 shows exactly this bifurcation scenario for the smooth SU model. The Hopf bifurcation line ends for a decreasing total phosphorus content P in a Takens-Bogdanov bifurcation which is also the starting point of the homoclinic bifurcation which causes the breakdown of the limit cycle shown in Fig. 3.10 and Fig. 3.11. It shows further that the additional tangent bifurcation T_2 in Fig. 3.11 emerges together with T_1 from a cusp bifurcation N. At $d = 0.25$ we are above the T_2 curve and therefore, the second tangent bifurcation is absent in Fig. 3.10.

In summary, compared to the non-smooth model by Loladze and Kuang (2000) the SU formulation leads qualitatively to similar results. A main difference is that the disappearance of the paradox of enrichment is not related to a sudden switch of underlying processes but to a Takens-Bogdanov bifurcation that determines the end of Hopf bifurcations.

Figure 3.13: Bifurcation diagram in parameter space spanned by carbon content C and phosphorus P, of the smooth analogon to the model by Loladze and Kuang (2000), with $d = 0.25$. There exists a homoclinic bifurcation curve (solid curve) G that originates from the Takens-Bogdanov point TB, which is also the origin for the Hopf bifurcation curve H. As in Fig. 3.9 the (saddle) homoclinic bifurcation merges with the tangent bifurcation T_1 to a saddle-node homoclinic bifurcation. The tangent bifurcation lines T_1 and T_2 emerge from a cusp bifurcation N. In this 2 parameter bifurcation diagram the two transcritical bifurcations TC_1 and TC_2 (cf. Fig. 3.10,3.11) are shown as one curve with a decline part TC_1 and an increasing part TC_2.

3.5.4 Smooth mass balance

In order to adapt the SU model to the model by Loladze and Kuang (2000), we have assumed that the total free carbon is given by $C - x$. As mentioned above this is necessary to match their assumption of a logistic growth when carbon or light is limiting. This approach is rather problematic as soon as more than one species is involved (Kooi et al., 1998). But how does the results change if we assume mass-conservation and therefore $C - x - y$ as the free carbon concentration? From the generalized analysis, we expect that the dependency of the primary production on the grazer population does not change the results qualitatively. Figure 3.14 shows the two parameter bifurcation diagram for the SU model taking into account the mass conservation.

We see that the transcritical bifurcation line TC is not affected since the grazer population is absent at the transcritical. Except for the transcritical bifurcation line the mass conservation leads to a shift of the whole bifurcation scenario to higher values of C and lower values of P. Quantitatively the changes are remarkable: The stable region between the transcritical TC_2 and the tangent bifurcation T is much more narrow while the stable region between the transcritical TC_1 and the Hopf bifurcation H is now larger than in Fig. 3.13. However, the shift does not change the qualitative results are as expected the same as above.

3.6 Discussion

Stoichiometric ecology has brought the concept of food quality into theoretical ecology. The variability of food quality for grazers in terms of a variable nutrient content of primary producers leads consequently to a variable conversion efficiency between these trophic levels. It has been shown before that a variable conversion efficiency leads to new bifurcations and richer dynamics even in the most fundamental food chain models. While early variable food quality models were rather based on *ad hoc* approaches for the variable efficiency function (Koppel et al., 1996; Huxel, 1999) recent models are more explicit in stoichiometry and the resulting constraints on growth processes (e.g. Loladze and Kuang (2000); Muller et al. (2001); Hall (2004); Kooijman et al. (2007); Sui et al. (2007); Wang et al. (2008)). These constraints affect not only the conversion efficiency but also the primary production. Since higher trophic levels utilize nutrients for their growth processes they reduce the amount of nutrients available for the producer. This indirect intra-specific competition leads to a dependency of the primary production on higher trophic levels. However, any specific approach to include these constraints on the primary production and conversion efficiency in ecological models is as ecological modeling itself a simplification of nature. Consequently, it remains always the
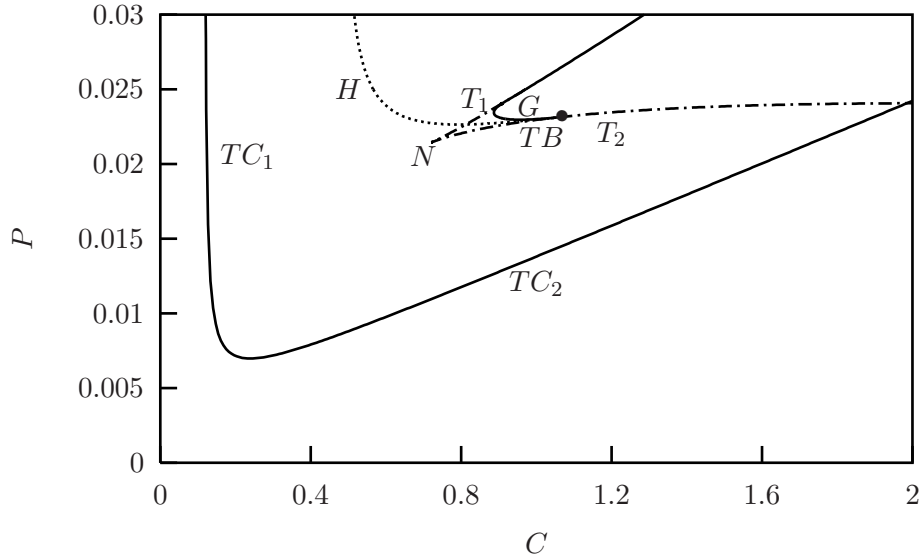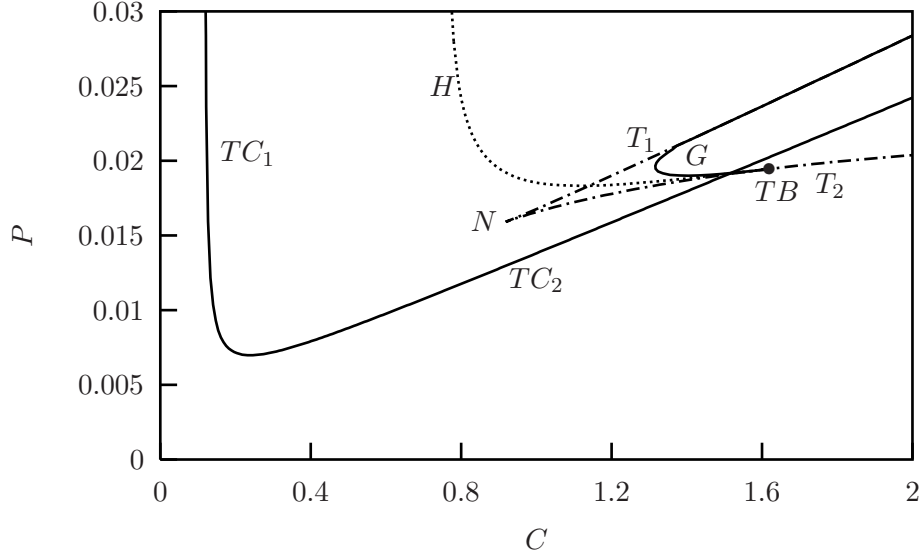
Figure 3.14: Bifurcation diagram in parameter space spanned by carbon content C and phosphorus P, of the smooth analogon to the model by Loladze and Kuang (2000), with $d = 0.25$. There exists a homoclinic bifurcation curve (solid curve) G that originates from the Takens-Bogdanov point TB, which is also the origin for the Hopf bifurcation curve H. The (saddle) homoclinic bifurcation merge with the tangent bifurcation T_1 to a saddle-node homoclinic bifurcation. In this 2 parameter bifurcation diagram the two transcritical bifurcations TC_1 and TC_2 (cf. Fig. 3.10,3.11) are shown as one curve with a decline part TC_1 and an increasing part TC_2. Compared to the model without mass conservation the whole bifurcation scenario is shifted to higher values of C and slightly to lower values of P except the transcritical curve TC_1, TC_2.

question if properties of specific models are system inherent or artifacts of the simplifications.

By using the generalized approach, a normalization technique allows for an analysis without a further specification of the processes in terms of its mathematical form. Consequently, the generalized modeling helps to identify generic properties of model classes that share the same structure. However, a drawback of the generalized analysis is that due to the normalization all informations about the steady state values and total rates are lost. Because all positive steady states share the same generalized bifurcation diagram, multi-stability i.e. the coexistence of different stable states for a given set of parameters, can not be detected by the generalized analysis. Also simulations and as a consequence certain numerical methods can not be applied. Therefore it can be of advantage to combine the generalized analysis with specific modeling approaches.

In (Van Voorn et al., 2008) we analyzed stabilizing mechanisms observed in specific models by using the formalism of the generalized models. The comparison of both approaches has led to a better understanding of these mechanisms. In the presented thesis we go the opposite way. We find insights of the generalized model and use them to understand, predict and compare the properties of different specific models.

The generalized analysis reveals that for constant conversion efficiency models neither the relative timescale r nor the inter-specific competition c_y influence the stability of steady states. Further, we find a counterintuitive effect of intra-specific competition for the whole producer-grazer model class: Increasing intra-specific competition (in terms of the parameter c_x) leads to a destabilization of the system due to a Hopf bifurcation. This effect is closely related to the paradox of enrichment (see Sec. 3.5.1). However, it shows that the introduction of a variable conversion efficiency greatly affects not only these local stability properties but also the global system dynamics.

For variable efficiency we find tangent bifurcations and a line of codimension-2 Takens-Bogdanov bifurcations in addition to the Hopf bifurcation. The bifurcations are not independent of the relative timescale r and the inter-specific competition c_y anymore. On the the one hand, the Takens-Bogdanov bifurcation line provides evidence of global bifurcations in variable efficiency models. On the other hand, the Takens-Bogdanov bifurcation line determines the end of the Hopf bifurcation surface. We show that for low food quality ($n_x \leq 0.5$) no Hopf bifurcations can be found. In that sense, variable food quality leads to the disappearance of the paradox of enrichment. Since these observations are not related to the magnitude of the variation of the conversion efficiency, the subclass of constant conversion efficiency models appears, from the generalized analysis point of view, as a degenerated model class.

Our examples of a specific stoichiometric models show, as expected, that

in addition to Hopf bifurcations tangent and homoclinic bifurcations can be found. Based on the generalized analysis we can ascribe these additional bifurcations to the variability of the conversion efficiency in the model. Although it is possible to transfer qualitative results from the generalized analysis to specific models it is rather problematic to map bifurcation diagrams obtained from the different modeling approaches onto each other. One problem is that each change of system parameters can change the steady state itself. Since the parameters of generalized models are usually linked to steady state values, the change of a single parameter of a specific model may change all parameters of the generalized model at the same time and vice versa. The second problem is that the analytical dependency of the steady state on the system parameters is in general not known explicitly.

Here we present the possibility to overcome these problems. The path following methods used for the bifurcation analysis of the specific models compute the steady state values simultaneously. From the generalized analysis we identify four generalized parameters as the most important ones. Since we can only visualize 3 dimensions we fit one parameter as a function of another related parameter ($n_y = n_y(n_x)$). We use this fit to compute the three-dimensional bifurcation diagram of the generalized model. Since we know how the steady state values change depending on the parameters from the numerical bifurcation analysis of the specific model we can compute the associated bifurcation parameters of the generalized model as well. This technique enables us to plot the bifurcation curves of the specific model into the generalized bifurcation diagram.

The combined bifurcation diagrams allow for a direct comparison of different models. For instance, we present in our analysis a bifurcation diagram (Fig. 3.7) were the bifurcation scenario of a variable efficiency DEB-model proposed by Kooijman et al. (2007) and a simplified DEB-model are shown in one generalized diagram. Thereby, we see that the bifurcation points of the specific models coincide with the bifurcation surfaces of the generalized analysis. Moreover it shows that the curve of the simplified model is located in the front plane of the diagram. This subspace where the bifurcation scenario is much simpler as the rest of the generalized diagram is dedicated to the class of constant efficiency models. With this in mind, it is not surprising that all the additional bifurcations and global dynamics related to the variable efficiency disappear from the DEB model in Sec. 3.5.1 if the model is simplified to a constant efficiency model. In that sense the simplification of the DEB-model represents the generic effect of a transition into the class of constant efficiency models visualized in the combined diagram.

The generalized analysis as well as numerical bifurcation analysis require continuously differentiable models. Therefore, another difficulty arise from models with non-smooth processes. A frequently assumed non-smooth ap-

proach in stoichiometric models is Liebig's minimum law as used in the model by Loladze and Kuang (2000). Although such a sudden switch is problematic from the analytical point of view, the model by Loladze and Kuang (2000) shares some important properties to the generalized model: the appearance of tangent and homoclinic bifurcations as well as the disappearance of the Hopf bifurcation and the paradox of enrichment for low food quality. However, from the generalized analysis we expect a Takens-Bogdanov bifurcation acting as an organizing center, the origin of the homoclinic bifurcation and the end of the Hopf bifurcation.

Using the synthesizing units approach we propose a smooth analogon to the model by Loladze and Kuang (2000) that complies with the predictions from the generalized analysis. In order to adapt the SU model to the model by Loladze and Kuang (2000) we had to neglect the inter-specific competition for carbon between producer and grazer in the primary production. However, as we expect from the generalized analysis the inter-specific competition for carbon leads only to a shift of the bifurcation scenario and does not change the qualitative results of our analysis. Nevertheless, such shifts can be quantitatively of importance in applied modeling. Technically, a smooth description is of advantage since it does not create problems for analytical and numerical bifurcation analysis. Biologically, the disappearance of the paradox of enrichment due to a Takens-Bogdanov bifurcation appears less artificial as a sudden non-smooth switch of underlying processes.

Although the projections of the numerical bifurcation curves of the smooth analogon model fit the bifurcations obtained from the generalized model very well, it becomes clear that the translation is not trivial. The relation between specific parameters and the generalized parameters depends on the steady state under consideration and can be even counterintuitive as we have shown in Sec. 3.5.1 and Sec. 3.5.3. Especially, the relation between resources and the intra-specific competition c_x is crucial for the question whether the paradox of enrichment can be observed in a model or not. Gross et al. (2004) analyzed the impact of different forms of predator-prey interaction on the paradox of enrichment. In our analysis we found a destabilization due to decreasing intra-specific competition. The paradox of enrichment is instead generally related to increasing resources. The relation between resources and competition depends on the response of the steady state values. If for instance X^* and Y^* grow proportional to the resources the enrichment has probably no effect on competition and the paradox of enrichment can not be observed (Arditi and Ginsburg, 1989). As we have shown in Fig. 3.7 and Fig. 3.12 an increase of resources (i.e. the total nutrient N or the total carbon C respectively) can increase or even decrease the intra-specific competition parameter c_x, depending on the steady state under consideration. Whether the paradox of enrichment can be observed in a model or not depends therefore on the model specific

response of the steady state under consideration.

Using the approach of generalized models we have shown that the paradox of enrichment can in general not be found for low food quality values ($n_x \leq 0.5$). Therefore, the variability of food quality is another mechanism to invalidate the paradox of enrichment. However, the paradox of intra-specific competition is still present since a decreasing of the competition parameter still tends to destabilize due to a tangent bifurcation. In that sense, each parameter variation that decreases the competition parameter c_x potentially destabilizes the system. Consequently, the paradox of competition observed in the generalized model analysis is a generic paradox of the whole model class.

Appendix

The paradox of enrichment is related to a destabilization of the system due to a Hopf bifurcation. Here we show that no Hopf bifurcations can be found if the food quality parameter is low, $n_x \leq 0.5$. This condition is related to $\eta_x \leq -1$. From Sec. 3.3 we know that the Hopf bifurcation condition as well as the tangent bifurcation condition depend on the eigenvalues of the Jacobian. To be specific the Hopf bifurcation requires center symmetric eigenvalues which are given if $trace(J) = 0$ and therefore

$$\gamma_{\mathrm{H}} = -r\eta_y + \sigma_x. \tag{3.19}$$

The tangent bifurcation requires a zero eigenvalue which is given if $det(J) = 0$ and therefore

$$\gamma_{\mathrm{T}} = -\frac{\eta_x\sigma_y - \eta_x - \eta_y\sigma_x}{\sigma_y - 1 + \eta_y}. \tag{3.20}$$

From our analysis in Sec. 3.4 we know that the Hopf bifurcation ends at the tangent bifurcation in a Takens-Bogdanov bifurcation. Consequently we can find no Hopf bifurcation below the tangent bifurcation and $\gamma_{\mathrm{H}} \geq \gamma_{\mathrm{T}}$ is an additional condition for the Hopf bifurcation. Let us assume that $\eta_x \leq -1$. Since $\sigma_x \leq 1$ we see that

$$(\sigma_x + \eta_x) < 0. \tag{3.21}$$

We multiply by the negative expression $(\sigma_y - 1)$ and obtain

$$(\sigma_y - 1)(\sigma_x + \eta_x) > 0. \tag{3.22}$$

On the left hand side we add the three negative terms $r\eta_y\sigma_y - r\eta_y + r\eta_y^2$ and obtain

$$r\eta_y\sigma_y - r\eta_y + r\eta_y^2 + \sigma_y(\sigma_x + \eta_x) - (\sigma_x + \eta_x) > 0. \tag{3.23}$$

Finally we divide by the negative term $\sigma_y - 1 + \eta_y$ and get

$$\frac{r\eta_y\sigma_y - r\eta_y + r\eta_y^2 + \sigma_y\sigma_x + \sigma_y\eta_x - \sigma_x - \eta_x}{\sigma_y - 1 + \eta_y} < 0. \tag{3.24}$$

Using Eq.(3.19) and Eq.(3.20) this is equivalent to

$$\gamma_{\mathrm{H}} - \gamma_{\mathrm{T}} < 0 \tag{3.25}$$

which contradicts the condition of Hopf bifurcations Eq.(3.19). Consequently, no Hopf bifurcations can be found if $n_x \leq 0.5$.

Chapter 4

Evidence of chaos in eco-epidemic models*

4.1 Abstract

We study an eco-epidemic model with two trophic levels in which the dynamics is determined by predator-prey interactions as well as the vulnerability of the predator to a disease. Using the concept of generalized models we show that for certain classes of eco-epidemic models quasiperiodic and chaotic dynamics is generic and likely to occur. This result is based on the existence of bifurcations of higher codimension such as double Hopf bifurcations. We illustrate the emergence of chaotic behavior with one example system.

4.2 Introduction

Mathematical models are essential tools in order to understand the mechanisms responsible for persistence or extinction of species in natural systems. In ecological models persistence is in general desired. By contrast, investigations in epidemic models usually aim at finding mechanisms that lead to the extinction of the parasites or infections (e.g. Liu et al. (2008)). However, it is known that diseases can not only greatly affect their host populations, but also other species their host populations interact with (e.g. Anderson et al. (1986)).

---

*This Chapter is a slightly modified version of the manuscript (Stiefs et al., 2009). The manuscript has been accepted for publication in the journal Mathematical Bioscience and Engineering. Some notations have changed in order to be consistent with the Chapter 2 and 3. Further, Fig. 4.1 and Fig. 4.2 are not colored in the accepted manuscript. The Appendix contains an additional Section that shows the relation of two parameters from Chapter 3 and 4.

In recent decades theoretical ecologists as well as epidemiologists became increasingly interested in so-called eco-epidemiology. Eco-epidemic models describe ecosystems of interacting populations among which a disease spreads Arino et al. (2004); Beltrami and Carroll (1994); Chattopadhyay and Arino (1999); Hadeler and Freedman (1989); Hethcote et al. (2004); Saenz and Hethcote (2006); Venturino (1994, 2001, 2002b). It has been shown that invading diseases tend to destabilize the predator-prey communities Anderson et al. (1986); Dobson (1988); Hadeler and Freedman (1989); Xiao and Bosch (2003). However, Hilker and Schmitz Hilker and Schmitz (2008) show that predator infection can also have a stabilizing effect.

Most of the existing models in eco-epidemiology consider a disease in the prey population Arino et al. (2004); Chattopadhyay and Arino (1999); Venturino (1995). There are only a few models where the predator population is infected Venturino (2002a). Some of the latter can exhibit sustained oscillations which are absent from the uninfected ecological model under consideration Anderson et al. (1986); Xiao and Bosch (2003).

In ecology as well as in epidemiology oscillations are associated with destabilization. The reason is that extinction of the population due to natural fluctuations becomes very likely when the oscillation drives the population to low abundances d'Onofrio and Manfredi (2007); Rosenzweig (1971); Van Voorn et al. (2008). Such extinction events are less critical if a species is spatially separated in several subpopulations. The subpopulations allow for a repopulation by migration after the extinction of one subpopulation. However, in such a case synchronous dynamics between the subpopulations due to the coupling by migration can have a devastating effect: it increases the possibility of global extinction of the whole species Heino et al. (1997); Holt and McPeek (1996) when all subpopulations have a minimum at the same time. In epidemiology such a synchronization of the dynamics can again be desired and induced by pulse vaccinations Grenfell et al. (1995) in order to cause the extinction of the disease.

In some models where the prey is infected also chaotic long-term dynamics have been observed Chatterjee et al. (2007). In contrast to oscillations, the effect of chaos on the stability in ecological models is a question of debate for a long time Gross et al. (2005); Hastings et al. (1993); Ruxton and Rohani (1998). A popular view has been that chaos has a destabilizing effect because of the associated *boom and burst* dynamics Berryman and Millstein (1989). However, for a population that consists of subpopulations as described above it has been shown that chaotic dynamics can be of advantage in order to stabilize the whole population. Although chaotic dynamics increase the number of local extinctions of subpopulations it reduces the degree of synchrony between different patches. Consequently it reduces the probability of a global extinction Allen et al. (1993); Ruxton (1994). Thereby it seems essential that the

subpopulations are chaotic in isolation Earn et al. (1998). With the coupling the subpopulations can show simpler dynamics but the subpopulations tend to be out of phase. In this sense it can be of advantage for the total population if the subpopulations exhibit chaotic dynamics or are close to chaotic parameter regions. This observation may explain why some ecological systems appear to be at the edge of chaos Turchin and Ellner (2000). Further, diffusion-induced complex dynamics as been found in continuous spatial predator-prey systems Baurmann et al. (2007); Pascual (1993); Upadhyay et al. (2008). But also isolated populations can exhibit persistent chaotic dynamics. Benincà et al. Benincà et al. (2008) observed chaotic dynamics of a food web in laboratory mesocosm that last for more than 6 years. From an evolutionary point of view ecological models should evolve into chaotic parameter regions if chaotic dynamics are of advantage for the population persistence.

To study stabilizing or destabilizing effects bifurcation theory is often applied to find the parameter regions where the steady state for the ecological or epidemiological model is stable with respect to perturbations. These analyses are based on specific models describing the relevant processes in form of ordinary differential equations (ODEs). Recently another approach has been developed which is based on generalized models where the exact mathematical form of the processes entering the right hand side of the ODEs is not specified Gross and Feudel (2006). In spite of the fact that the mathematical functions are not known in detail, it is possible to analyze the stability properties of the steady state and draw conclusions about possible destabilization mechanisms of the steady state when a system parameter is varied Gross and Feudel (2004), as well as the emergence of chaotic dynamics Gross et al. (2005).

In this Chapter we use the concept of generalized model to study the impact of a disease of the predator on the dynamics of a predator-prey system. To this end we couple a generalized ecological model with an epidemic one and study the stability properties of the steady state. The advantage of the method is that our results are not restricted to a particular model but apply to certain classes of models since we use parameters encoding the shape of predator-prey functional responses and incidence functions as bifurcation parameters. We find that the coupling of both models introducing a disease in the predator population leads to complex dynamics such as quasiperiodic and chaotic motion. This complex dynamics are solely based on the interplay of demographic and epidemic modeling since the demographic and the epidemic model alone are not capable to exhibit chaotic motion. As a result we show that chaos is generic and prevalent for certain classes of eco-epidemic models.

The Chapter is organized as follows: In Sec. 4.3 we discuss the demographic as well as the epidemic model and introduce the eco-epidemic model. Furthermore, we normalize the model and discuss the possible emergence of bifurcations for the steady state. In Sec. 4.4 we analyze the stability properties

of the steady state for the predator-prey model with and without the disease
in the predator population and compare the results. As a conclusion we ob-
tain classes of systems in which we expect to find quasiperiodic and chaotic
behavior. Since these findings are based on mathematical theorems we can
only state the existence of parameter regions where the dynamics is chaotic.
To find out the size of these parameter regions and the hence, their relevance
for the dynamics of the eco-epidemic model we investigate a specific model
in Sec. 4.5 to show explicitly the emergence of chaotic dynamics. Finally we
summarize the results in Sec. 4.6.

4.3   The generalized eco-epidemic model

Before we begin our analysis we will briefly outline the construction of one of
the simplest predator-prey models and of one of the most elementary epidemic
models, which together form the building blocks for the more general eco-
epidemic model we would like to consider.

The basic demographic model in general accounts for two interacting species.
The nature of interactions can be of competing, predator-prey or symbiotic
nature. A typical formulation for a predator-prey model is given by

$$
\begin{aligned}
\dot{X} &= SX - M_X X^2 - G(X)Y, \\
\dot{Y} &= EG(X)Y - M_Y Y \ ,
\end{aligned}
\tag{4.1}
$$

where S is the specific growth rate of the prey X. Apart from predation the
growth of the prey is limited by intra-specific competition assumed to increase
quadratically in X with the coefficient M_X thereby giving a logistic evolution
for the prey dynamics. The predation is expressed by the so-called per capita
functional response $G(X)$. The efficiency of biomass conversion is given by
the yield constant E. M_Y is the mortality rate of the predator population.

This simple model structure has been analyzed for a variety of different
functional responses $G(X)$ describing the prey-dependent predation rate (e.g.
Holling (1959)). However, in our case the function $G(X)$ is not specified
in order to keep the model more general. In Sec. 4.4 we will discuss some
properties of this underlying ecological model.

Classical epidemic models partition the population into several epidemi-
ological classes, for a thorough review see Hethcote (2000). The population,
in our case the predator population Y, is usually split into susceptibles Y_S,
infected Y_I, and recovered Y_R. The latter may be thought of as being immun-
ized, at least for a period of time, after which they return into the class of
susceptibles. Following this population division, in absence of vital dynamics,
i.e. demographic terms to account for births and natural deaths, a simple

SIRS model would be written as

$$
\begin{aligned}
\dot{Y}_S &= -\lambda(Y_S, Y_I) + \delta Y_R \\
\dot{Y}_I &= \lambda(Y_S, Y_I) - \gamma Y_I \\
\dot{Y}_R &= \gamma Y_I - \delta Y_R
\end{aligned}
\tag{4.2}
$$

assuming linear transition rate γ from the infected to the recovered class. The recovered become susceptible again with a fixed rate δ.

In general, pathogen transmission is expressed by interactions among individuals. The latter are modeled by the incidence function $\lambda(Y_S, Y_I)$, for which the most common approaches are the mass action $\lambda(Y_S, Y_I) = bY_S Y_I$ and the so-called standard incidence function or frequency-dependent transmission $\lambda(Y_S, Y_I) = bY_S Y_I/(Y_S + Y_I)$. In both cases susceptibles Y_S and infected Y_I are assumed to be well-mixed and hence, to interact randomly. However, it is not clear if the assumption of random interactions and an equal distribution of infected and uninfected is appropriate to describe pathogen transmission in wild populations. Both, small-scale experiments as well as observed disease dynamics, give evidence that simple mass action is not an adequate model in many situations McCallum et al. (2001). The simplest argument for an asymmetry of the incidence function is that due to a patchiness in the disease on average each infected individual is more likely to have an infected neighbor. The more biological details are taken into account, the more complex the incidence function may be. For instance, Capasso and Serio Capasso and Serio (1978) introduced a saturated incidence function. Such a saturation can be caused by crowding effects at high infection levels or by protection measures the susceptible individuals take. Liu et. al. Liu et al. (1986) proposed a more general incidence function of the form $\lambda(Y_S, Y_I) = kY_S Y_I^p/(1 + mY_I^p)$. Additionally a variety of other incidence functions have been investigated by various authors (e.g. Table 4.1). A universal approach has not been found yet. However, using the generalized approach we avoid to specify the incidence function but study more generic properties of the model class under consideration.

To analyze the effect of a disease in the predator population Y on the dynamics of interaction with the prey X we combine the demographic model Eqs. (4.1) with the SIRS epidemic model Eqs. (4.2) as follows

$$
\begin{aligned}
\dot{X} &= SX - G(X)(Y_S + Y_R + \alpha Y_I) - M_X X^2, \\
\dot{Y}_S &= EG(X)(Y_S + Y_R + \alpha\beta Y_I) - M_Y Y_S + \delta Y_R - \lambda(Y_S, Y_I), \\
\dot{Y}_I &= \lambda(Y_S, Y_I) - (M_Y + \mu)Y_I - \gamma Y_I, \\
\dot{Y}_R &= \gamma Y_I - \delta Y_R - M_Y Y_R.
\end{aligned}
\tag{4.3}
$$

Here we assume neither vertical transmission, nor vertical immunity, i.e. that the infected predators as well as the recovered predators reproduce only susceptibles. Furthermore, we suppose that the disease can, in principle, influence

Functional form	Comments	Citations
$\sim SI$	mass action	Anderson and May (1979)
		May and Anderson (1979)
$\sim \frac{SI}{S+I}$	standard incidence	May and Anderson (1987)
$\sim SI(1-CI)$		Yorke and London (1973)
$\sim \frac{IS}{1+AI}$		Capasso and Serio (1978)
$\sim S^p I^q$	power relationship	Liu et al. (1986)
$\sim S ln(1+BI/k)$		Barlow (2000)
$\sim S^p \frac{I^q}{B+I^q}$	$p>0,\ q>0$	Liu et al. (1986)
$\sim S \frac{I}{A+I^2}$	non-monotone incidence	Xiao and Ruan (2007)
$\sim S \frac{I}{A+S+I}$	asymptotic incidence	Diekmann and Kretzschmar (1991)
		Roberts (1996)

Table 4.1: Different proposed functional forms for the incidence function

the demographic parameters. The disease may induce a disease related mortality rate μ and reduce the predation and reproduction rates of the infected Y_I expressed by the factors α and β respectively.

All parameters and terms denoted by Greek letters are related to the disease. Note, that in the absence of weakening effects of the disease (i.e. $\alpha = \beta = 1$ and $\mu = 0$) the combined model Eq.(4.3) reproduces the population dynamics of the uninfected model Eqs.(4.1) , with $Y = Y_S + Y_I + Y_R$. This means that the disease could have in principle no influence on the ecological dynamics.

To analyze the dynamics of model (4.3) one would start by computing the steady state and its stability with respect to perturbations. But a local stability analysis cannot be performed since an analytical computation of the steady states is impossible because $G(X)$ and $\lambda(Y_S, Y_I)$ are not specified but assumed to be general functions. However, this difficulty can be overcome using the normalization procedure for the generalized models described in Gross and Feudel (2006). To use this approach we assume that a positive steady state $(X^*, Y_S^*, Y_I^*, Y_R^*)$ exists.

We now define normalized variables $x := X/X^*, y_s := Y_S/Y_S^*, y_i := Y_I/Y_I^*$ and $y_r := Y_R/Y_R^*$. Further, we define a normalized functional response $g(x) := G(X^*x)/G(X^*)$ and $l(y_s, y_i) := \lambda(Y_S^*y_s, Y_I^*y_i)/\lambda(Y_S^*, Y_I^*)$ as a normalized incidence function. Note, that in the space of normalized state variables the steady state is by definition $(x^*, y_s^*, y_i^*, y_r^*) = (X^*/X^*, ...) = (1,1,1,1)$. In the same manner, we obtain $l(y_s^*, y_i^*)=g(x^*)=1$. Following the

normalization procedure we can rewrite Eqs. (4.3) as

$$
\begin{aligned}
\dot{x} &= a_x \quad (x - \tilde{m}_x g(x)(\tilde{f}_\alpha(by_s + \tilde{b}y_r) + f_\alpha y_i) - m_x x^2), \\
\dot{y}_s &= a_s \quad (e_s g(x)(\tilde{f}_\beta(by_s + \tilde{b}y_r) + f_\beta y_i) - m_y y_s + \tilde{e}_s y_r - \tilde{m}_y l(y_s, y_i)), \\
\dot{y}_i &= a_i \quad (l(y_s, y_i) - y_i). \\
\dot{y}_r &= a_r \quad (y_i - y_r).
\end{aligned}
$$

$$(4.4)$$

The details of the normalization and the definitions of the newly introduced scale parameters $a_i, b, \tilde{b}, f_\alpha, \tilde{f}_\alpha, f_\beta, \tilde{f}_\beta, e_s, \tilde{e}_s, m_x, \tilde{m}_x, m_y$ and $\tilde{m}_y$ are given in the Appendix. As an advantage of this approach these parameters are easy to interpret in the biological context. The scale parameters a_x, a_s, a_i and a_r for instance encode the inverse timescales of the normalized state variables. They measure the relation between the lifetimes of the different species. All other scale parameters are between 0 and 1 and describe weight factors of certain processes of the model at the steady state.

The losses due to intra-specific competition relative to the total losses within the prey are represented by the parameter m_x. To be specific, if m_x is close to 1 the losses of prey due to intra-specific competition preponderate. In the Appendix, we show that the inter-specific competion parameter c_x defined in Chapter 3 is equal to the weight faktor m_x for the considered models. The parameter $\tilde{m}_x = 1 - m_x$ expresses losses caused by predation. f_α and $\tilde{f}_\alpha$ are the fractions of prey consumed by infected predators and healthy predators respectively. In the same way b is the fraction of healthy predators that are susceptible and $\tilde{b} = 1 - b$ the fraction of healthy predators that are recovered. Further, the parameter e_s represents the weight factor of the natural growth terms of susceptibles due to consumption of X. At the steady state the fraction of gains due to recovered predators that become susceptible again is given by $\tilde{e}_s = 1 - e_s$. The natural mortality for the predator relative to the total losses is expressed by m_y.

In the normalized model the steady state under consideration is known $(x^*, y^*) = (1, 1)$. The stability of this steady state depends on the eigenvalues of the Jacobian. The steady state is stable if all eigenvalues have a negative real part. Consequently only two bifurcations can separate stable from unstable parameter regions: the tangent type bifurcation where a real eigenvalue crosses the imaginary axis and a Hopf bifurcation where a pair of complex conjugate eigenvalues crosses the imaginary axis.

Because all normalized state variables and the normalized processes $(l(y_s, y_i), g(x))$ are equal to one at the steady state, the Jacobian of the normalized model contains in addition to the scale parameters only the derivatives of the

normalized processes in the steady state. We define

$$
\begin{aligned}
g_x &:= \left.\frac{\partial g(x)}{\partial x}\right|_{x^*}, \\
l_s &:= \left.\frac{\partial l(y_s, y_i)}{\partial y_s}\right|_{y_s^*, y_i^*}, \\
l_i &:= \left.\frac{\partial l(y_s, y_i)}{\partial y_i}\right|_{y_s^*, y_i^*}
\end{aligned}
\tag{4.5}
$$

as the generalized parameters. These parameters can be interpreted as non-linearity measures of the corresponding functions with respect to the variable of the derivative. If the function $G(X)$ is linear in X the derivative of the normalized function g_x is equal to one. It is zero for a constant function and two for a quadratic function. To be consistent with previous publications we let g_x be the *predator sensitivity to prey* Gross et al. (2004, 2005); Gross and Feudel (2006). In the same sense we denote by l_s and l_i the incidence sensitivity to susceptibles and to infected respectively.

In summary the Jacobian consists of 10 scaling parameters and 3 generalized parameters. How to obtain the test functions for the above mentioned bifurcations from the Jacobian is described in detail in Gross and Feudel (2004). These test functions enable us to draw three-dimensional bifurcation diagrams as described in detail in Stiefs et al. (2008).

Since we are essentially interested in the influence of different mathematical expressions for the functional response and for the incidence function, we focus our bifurcation analysis on the generalized parameters g_x, l_s and l_i. We chose the other scale parameters according to biological reasoning. It is known that in many cases the timescale for the lifetime of species belonging to different trophic levels slows down with each higher trophic levels Hendriks (1999). Hence, we could assume that the inverse timescale of the susceptible predators is less than half the timescale of the prey, i.e. $a_s = 0.4a_x$. By renormalizing the timescale we can say that $a_x = 1$ and $a_s = 0.4$. It is further reasonable to expect that the timescale of the infected predators is slightly larger than the timescale of the susceptible predators since we suppose that their overall lifetime is shorter. Let us assume $a_i = 0.5$. Clearly, this intuitive way is much more appropriate than guessing some abstract parameters. If we would analyze a specific real system at the steady state we could, in principle, also gain an appropriate value for each scale parameter by measuring the corresponding rates. Approximating all other scale parameters, we end up with three parameters which we consider as the most interesting bifurcation parameters. These are the sensitivity of the predator with respect to prey g_x and the sensitivity of the incidence function with respect to susceptibles l_s and infected l_i. The computation of three-dimensional bifurcation diagrams allows us to discuss the stability properties of the eco-epidemic model depending on

the mathematical form of the functional response $G(X)$ and the incidence function $\lambda(Y_S, Y_I)$.

4.4 Stability of the steady state: from local to global bifurcations

4.4.1 Absence of diseases

Before we analyze the effect of an infection on the predator-prey interactions, we take a look at the generalized predator-prey model in the absence of infected individuals. It is known that the predator-prey system Eq.(4.1) can exhibit self-sustained oscillations if the functional response $G(X)$ is nonlinear in X for instance a Holling type II function Holling (1959). A typical example would be the Rosenzweig-MacArthur model Rosenzweig and MacArthur (1963). These oscillations appear due to a supercritical Hopf bifurcation. Figure 4.1 shows the bifurcation diagram of the generalized predator-prey model given by Eq. (4.1). As mentioned above a_x is set to be one so that a_y corresponds to the relative inverse timescale. We see two tangent type bifurcation surfaces (blue) and one Hopf bifurcation surface (red). The steady state is stable in the top volume of the diagram. If one of the bifurcation surfaces is crossed due to a parameter variation the steady state becomes unstable. The only biologically sound parameter range for the scale parameters a_y and m_x lies between [0,1] since both parameters express some kind of weight factor measured in relation to other scale factors.

Firstly note, that such a destabilization never occurs for a variation of a_y. The timescale has therefore no influence on the stability of the steady state in this model class.

Secondly, the Hopf bifurcation surface exceeds the biologically relevant parameter range for $g_x \geq 1$. For this reason, Hopf bifurcations cannot be found in this model class if $g(x)$ and therefore $G(X)$ are linear functions ($g_x = 1$). This situation corresponds to the Lotka-Volterra model coupled with logistic growth. However, from a biological perspective, models should allow lower values of the sensitivity to prey, i.e. $g_x < 1$. Due to a limited consumption of prey the functional response $G(X)$ should saturate at high amounts of prey. Since saturation is related to low values of g_x, Hopf bifurcations should likely occur in biological realistic models.

Even, lower values of the sensitivity to prey, i.e. $g_x \leq 0$, are rather unlikely and occur only in systems with non monotonic functional responses. Biologically this region where the predation decreases with increasing prey can be related to inhibition effects or group defense techniques of the prey Andrews (1968); Freedman and Wolkowicz (1986). At $g_x = 0$ we find that the
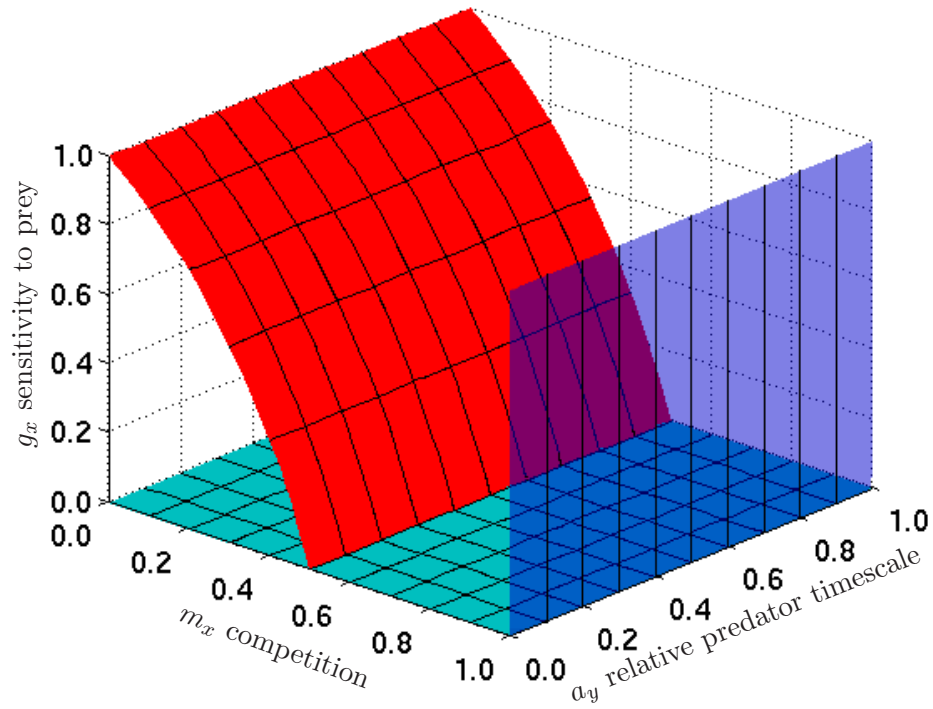
Figure 4.1: Bifurcation diagram of a generalized predator-prey model. A surface of Hopf bifurcations (red) and two surfaces of tangent type bifurcations (transparent blue) are shown. The bifurcation parameters are the prey sensitivity g_x, the timescale of the predator a_y and the competition m_x (intraspecific competition of the prey).

Hopf bifurcation ends at the lower tangent type bifurcation surface at $g_x = 0$ in a codimension-2 Takens-Bogdanov line. On this line the Jacobian has a double zero eigenvalue. In addition to the tangent type bifurcation and the Hopf bifurcation a homoclinic bifurcation emerges from the Takens-Bogdanov bifurcation line. This bifurcation is in general difficult to detect and can ecologically be related to sudden population bursts. In the model class under consideration a Takens-Bogdanov bifurcation can only be observed in systems with non monotonic functional response $G(X)$. This property is necessary to enable negative values of g_x and therefore it is also necessary to cross the Takens-Bogdanov bifurcation at $g_x = 0$.

Another way to achieve a destabilization of the steady state due to a Hopf bifurcation is to decrease the competition parameter m_x. This effect is rather counterintuitive since decreasing the competition means ecologically to improve the food conditions for the predators. Such behavior of the model can be strongly related to the paradox of enrichment Rosenzweig (1971).

4.4.2 Disease in the predator population

We now investigate the impact of a disease in this two trophic food chain as described by Eq. (4.3). In contrast to the normalized predator-prey model the normalized eco-epidemic model has not 3 but 13 parameters that may all more or less influence the stability of the steady state. Thoroughly analyzing and discussing these parameter variations is beyond the scope of this work. Instead we focus only on bifurcations that give evidence for more complex dynamics. Such complex behavior like quasiperiodic or chaotic dynamics occur usually in the neighborhood of global bifurcations or bifurcations of higher codimension, which can be found for a lot of different parameter sets in the model class under consideration. It is important to note that though the whole bifurcation analysis presented is based on local stability properties of the steady state, we are able to detect easily higher codimension bifurcations since they correspond to intersections of different bifurcation surfaces like the Takens-Bogdanov line discussed in the previous subsection.

For our analysis we chose g_x, l_s and l_i as the most important bifurcation parameters. For most of the common incidence functions (cf. Table 4.1) $l_i \leq 1$ due to saturation effects with respect to the number of infected. The sensitivity to prey g_x is for the same reason also confined to this range $g_x \leq 1$.

For the the scaling parameters we assume now that 90 percent of the losses of prey are caused by predation, which means a relative competition $m_x = 0.1$. We assume further that 95 percent of the predation is caused by healthy predators, i.e. susceptibles plus recovered, ($\tilde{f}_\alpha = 1 - f_\alpha = 0.95$) and that half of the healthy predators are susceptible ($b = 0.5$). The gain of susceptible predators results for 95 percent from biomass conversion ($e_s = 0.95$) and only

5 percent from the recovering ($\tilde{e}_s = 1 - e_s = 0.05$). The natural mortality of the healthy predators is assumed to be relatively low compared to losses due to infection ($m_y = 0.1$).

Using the parameter settings mentioned above we compute the stability of the steady state as shown in Fig. 4.2. We find as in the model without disease a surface of tangent type bifurcations (transparent blue) and a surface of Hopf bifurcations (red). But now the Hopf bifurcation surface possesses a rather complicated shape. This shape corresponds to a Whitney umbrella, a bifurcation situation which is rarely found in applications. Other examples of a Whitney umbrella are presented in Gross (2004b); Stiefs et al. (2008). In this bifurcation scenario the Hopf bifurcation surface is twisted around a codimension-3 1:1 resonant double-Hopf point characterized by two identical pairs of complex conjugate eigenvalues. As Fig. 4.2 shows, a line of codimension-2 double-Hopf bifurcations emerges from this point. At this line where the Hopf bifurcation surface intersects itself two pairs of purely imaginary complex conjugate eigenvalues can be found.

Additionally we observe two intersection lines of the Hopf bifurcation surface with the tangent type bifurcation surface. One is again a Takens-Bogdanov bifurcation and the other one is a Gavrilov-Guckenheimer bifurcation line that emerges from a so-called triple point bifurcation on the Takens-Bogdanov bifurcation line Kuznetsov (2004). On this Gavrilov-Guckenheimer line the Jacobian has a zero eigenvalue in addition to a pair of purely imaginary complex conjugate eigenvalues. In contrast to the Takens-Bogdanov bifurcation the Hopf bifurcation surface does not end on the Gavrilov-Guckenheimer bifurcation. The existence of the Gavrilov-Guckenheimer bifurcation indicates that quasiperiodic and chaotic dynamics are likely to occur in the neighborhood of this bifurcation. The double-Hopf bifurcation line instead is a clear evidence for the existence of chaotic parameter regions Kuznetsov (2004). Therefore we can conclude that the consideration of the vulnerability of the predator population to a disease can lead in general to complex dynamics in eco-epidemiological systems.

Unfortunately we have no information about the size of the chaotic parameter region since our analysis is based on mathematical theorems. In the following section we investigate a specific model that allows to translate the generalized parameters to specific system parameters and vice versa. This specific example allows not only to explicitly compute the chaotic parameter regions but also gives insights into the route to chaos.
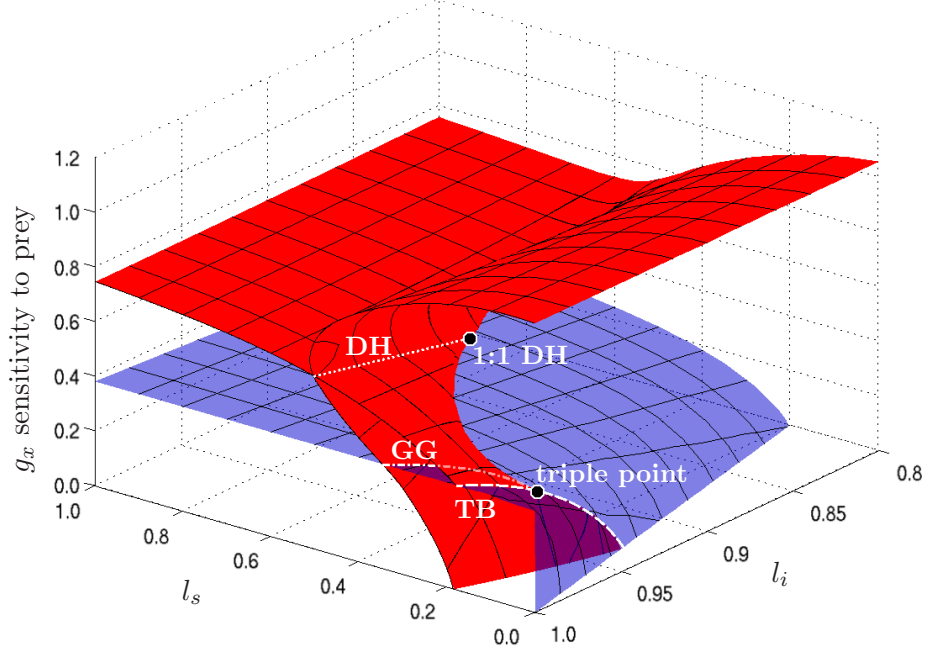
Figure 4.2: Bifurcation diagram of the generalized eco-epidemic model. A surface of Hopf bifurcations (red) and a surface of tangent type bifurcations (transparent blue) are shown. The intersection lines are a Takens-Bogdanov bifurcation line (TB), a Gavrilov-Guckenheimer bifurcation line (GG) and a double-Hopf bifurcation line (DH). The double-Hopf bifurcation line ends in a 1:1 resonant double-Hopf bifurcation point (1:1 DH) and the Gavrilov-Guckenheimer bifurcation line ends in a triple point bifurcation at the Takens-Bogdanov line. The bifurcation parameters are the generalized parameters g_x, l_s and l_i which are strongly related to the functional form of the underlying processes, namely the per capita functional response $g(x)$ and the incidence function $l(y_s, y_i)$ respectively. The fixed parameters are scale parameters $a_x = 1, a_s = 0.4, a_i = 0.9, a_r = 0.25, f_\alpha = 0.05, \ b = 0.5, \ e_s = 0.98, \ m_x = 0.1$ and $m_y = 0.1$.

4.5   Chaos in a specific eco-epidemiological system

To demonstrate the theoretical implications of the existence of a Whitney umbrella bifurcation situation in a specific model, we need to choose specific mathematical functions for the generalized processes. This means that we construct an example of a specific model that compares to the generalized parameter set of the bifurcation diagram shown in Fig. 4.2.

Since the generalized parameters represent the derivatives of the generalized processes we need to choose functions according to the parameter range of the higher codimension bifurcations. As stated above in ecology and epidemiology a large pool of proposed functional responses $G(X)$ and incidence functions $\lambda(Y_S, Y_I)$ exists. Since the double-Hopf bifurcation line appears for g_x lower than 1, which means a increase of $g(x)$ slower than linear in x, a functional response with saturation is necessary to obtain the double-Hopf bifurcation line.

Instead of defining a specific model and normalizing it we construct an already normalized specific model for the sake of simplicity. We choose a Holling type III function $g(x) = ax^2/(1+bx^2)$ as the functional response. Due to the normalization we need $g(1) = 1$. Therefore we define $a := (1 + b)$. The relation between b and g_x is then $g_x = 2/(1 + b)$. In a similar way we allow values of l_s and l_i lower than 1 as well. We use the asymptotic incidence function $l(y_s, y_i) = cy_s y_i/(1 + dy_s + ey_i)$ Diekmann and Kretzschmar (1991); Roberts (1996). In order to satisfy $l(1, 1) = 1$ we define $c := (1 + d + e)$. We find the relations $l_s = 1 + e/(1 + d + e)$ and $l_i = 1 + d/(1 + d + e)$.

Now we have a specific model that allows a translation of the parameter set of the generalized model into the parameters of the specific model. This enables us to analyze the dynamics of the system. As discussed in the previous section the double-Hopf bifurcation indicates the emergence of chaotic parameter regions. In order to find these parameter regions we compute the Lyapunov exponents of the specific system for a grid of points in the generalized parameter space close to the double-Hopf bifurcation.

The result is shown in Fig. 4.3. The two solid lines are Hopf bifurcation lines that intersect in a double-Hopf bifurcation. Within the white area the steady state (1,1) is stable. In the light grey area the system exhibits periodic long-term dynamics.

In addition to the two Hopf bifurcation lines we find numerically other bifurcation lines (two dashed, one dotted) using pathfollowing methods implemented in MATCONT Dhooge et al. (2003). The dashed lines are Neimark-Sacker bifurcations where a limit cycle becomes unstable and a stable quasiperiodic motion on a torus emerges. This behavior can be found in the dark grey parameter regions. In the black regions the largest Lyapunov exponent is positive and hence, the dynamics is chaotic. The dotted line is a period doubling

bifurcation. For small values of l_s we find first the transition to quasiperiodic motion on a torus with a subsequent transition to chaos. For larger values of l_s the periodic solution undergoes first a period doubling before the torus or Neimark-Sacker bifurcation occurs. While the transition to chaos involves always a transition from quasiperiodicity, the chaotic attractor looks different for small and large values of l_s since the Neimark-Sacker bifurcation and the period doubling swap places. Both routes to chaos are illustrated in Fig. 4.4.

The population dynamical system alone (Eq.(4.1)) as well as the epidemiological system alone (Eq.(4.2)) do not exhibit complex dynamics. Only if both are coupled to form an eco-epidemiological system with an infected predator, the dynamics can be quasiperiodic or chaotic. Our generalized analysis shows that chaos is generic in this class of models.

4.6 Discussion

We have studied a generalized eco-epidemic model which couples the behavior of a predator-prey system to the dynamics of a disease which can infect the predator. The advantage of investigating generalized models lies in the fact that the exact mathematical form of the interaction processes like predator-prey or infection interactions does not have to be specified. This allows for rather general conclusions about the stability of the positive steady state which will be reached in the long-term limit. Moreover, this generalized approach can give insight into the global dynamics of the system though only a local stability analysis is performed. Due to the usage of generalized models our results apply to certain classes of models.

The eco-epidemic model is based on two often used generalized models which exhibit only stationary points or periodic behavior when studied separately. Examples for specific versions of the predator-prey system (Eq. (4.1)) are the Rosenzweig-MacArthur system and related versions possessing different nonlinear functional responses Beddington (1975); DeAngelis et al. (1975); Rosenzweig and MacArthur (1963); Truscott and Brindley (1994). The epidemic model used as a basis is the well-known SIRS (susceptibles-infected-recovered-susceptibles) models (Eq. (4.2)). Specific versions of this model use different nonlinear incidence functions Anderson et al. (1986); Capasso and Serio (1978); Liu et al. (1986); May and Anderson (1987).

We have shown that the coupling of an ecological and an epidemiological model can lead to classes of systems exhibiting complex dynamics like quasiperiodic and chaotic behavior. Our result is based on the detection of higher codimension bifurcations like double-Hopf bifurcations, triple points and Gavrilov-Guckenheimer bifurcations. In the neighborhood of such bifurcations there exist parameter regions where quasiperiodic and chaotic behavior
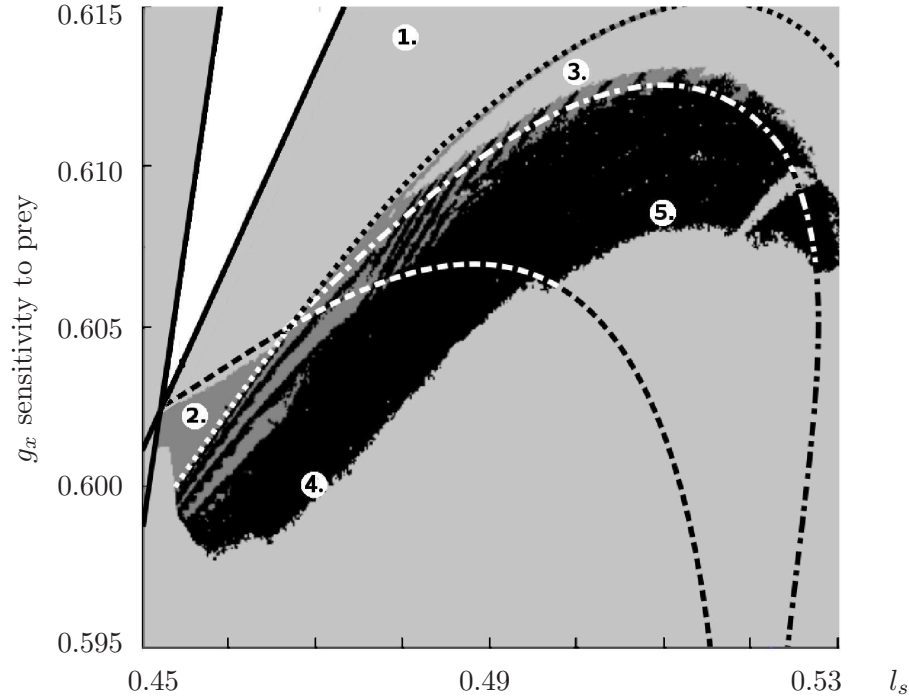
Figure 4.3: Dynamics of a specific model close to the double-Hopf bifurcation. The steady state is stable in the white area between the two Hopf bifurcation lines (solid lines). Beyond the Hopf bifurcation lines (1.) the system exhibits stable periodic dynamics (bright grey). Both Hopf bifurcation lines intersect in a codimension-2 double-Hopf bifurcation. This double-Hopf bifurcation is the starting point of a Neimark-Sacker bifurcation line (dashed). At the Neimark-Sacker bifurcation line a stable Torus emerges (2.) and the system exhibits quasiperiodic dynamics (dark grey). The dotted line is a period doubling bifurcation line. Beyond this line where the system oscillates on a period 2 orbit (3.) we find another Neimark-Sacker bifurcation (dotted-dashed line). In the black region we find chaotic dynamics (4.,5.).
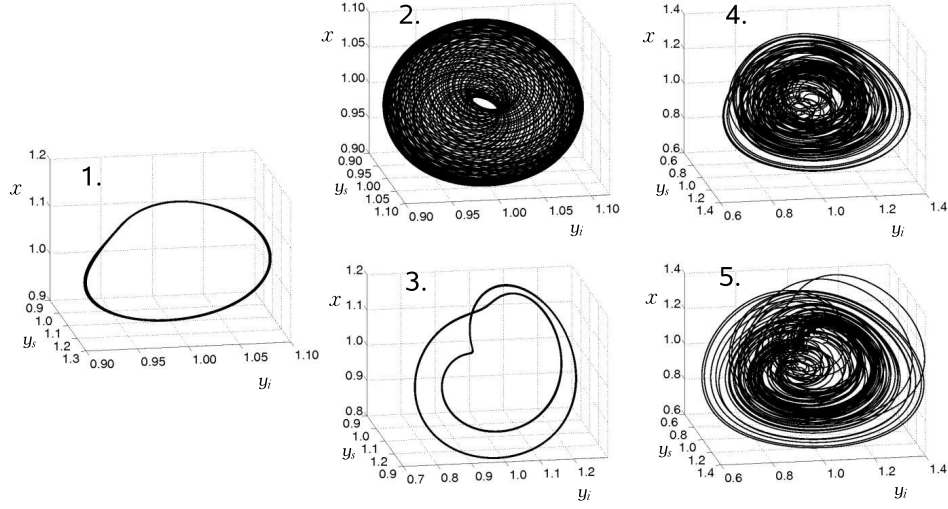
Figure 4.4: Simulations in 5 different dynamical regimes of Fig. 4.3. We see a limit cycle at $g_x = 0.614$, $l_s = 0.48$ (1.), a torus at $g_x = 0.6025$, $l_s = 0.456$ (2.), a limit cycle with doubled period at $g_x = 0.613$, $l_s = 0.5$ (3.) and two chaotic attractors at $g_x = 0.6$, $l_s = 0.47$ (4.) and $g_x = 0.608$, $l_s = 0.51$ (5.).

can be found. This mathematical finding based on bifurcation theory is illustrated with a specific model where the interaction functions are specified in order to be able to use numerical methods like path-following of bifurcations and the computation of Lyapunov exponents. As a result we can demonstrate that the chaotic parameter regions are not small and therefore not negligible, but rather large and hence, important for the dynamics of the system.

Finally we note that we were not able to find complex dynamics in the eco-epidemic model using a SIS instead of a SIRS model. Therefore it seems to be essential that we introduce the class of recovered predators for the occurrence of complex dynamics.

To our knowledge this is the first example where chaotic behavior has been found in an eco-epidemic model system with a disease in the predator population. Based on the generalized approach we can state that the emergence of chaos is generic for certain classes of eco-epidemic models and thus likely to be found.

Acknowledgements

Appendix

Normalization of the eco-epidemic model

By substitution of the normalized state variables $x := X/X^*, y_s := Y_S/Y_S^*$, $y_i := Y_I/Y_I^*$ and processes $g(x) := G(X^*x)/G(X^*), l(y_s, y_i) := \lambda(Y_S^* y_s, Y_I^* y_i)/\lambda(Y_S^*, Y_I^*)$ into Eq.(4.3) we obtain

$$
\begin{aligned}
\dot{x} &= \tfrac{1}{X^*}(SX^*x - G(X^*)g(x)(Y_S^* y_s + Y_R^* y_r + \alpha Y_I^* y_i) - M_X X^{*2} x^2), \\
\dot{y}_s &= \tfrac{1}{Y_S^*}(EG(X^*)g(x)(Y_S^* y_s + Y_R^* y_r + \alpha\beta Y_I^* y_i) - M_Y Y_S^* y_s \\
&\quad + \delta Y_R^* y_r - \lambda(Y_S^*, Y_I^*)l(y_s, y_i)), \\
\dot{y}_i &= \tfrac{1}{Y_I^*}(\lambda(Y_S^*, Y_I^*)l(y_s, y_i) - (M_Y + \mu)Y_I^* y_i - \gamma Y_I^* y_i), \\
\dot{y}_r &= \tfrac{1}{Y_R^*}(\gamma Y_I^* y_i - (M_Y + \delta)Y_R^* y_r)
\end{aligned}
\tag{4.6}
$$

Observing this ODE in the steady state yield the conditions

$$
\begin{aligned}
a_x &:= & S &= & M_X X^* + \tfrac{G(X^*)(Y_S^* + Y_R^* + \alpha Y_I^*)}{X^*}, \\
a_s &:= & M_Y + \tfrac{\lambda(Y_S^*, Y_I^*)}{Y_S^*} &= & \tfrac{1}{Y_S^*}(EG(X^*)(Y_S^* + Y_R^*) + \delta Y_R^*), \\
a_i &:= & M_Y + \mu + \gamma &= & \tfrac{\lambda(Y_S^*, Y_I^*)}{Y_I^*}, \\
a_r &:= & M_Y + \delta &= & \tfrac{\gamma Y_I^*}{Y_R^*}.
\end{aligned}
\tag{4.7}
$$

By defining the scale parameters as

$$
\begin{aligned}
f_\alpha &:= \tfrac{\alpha Y_I^*}{Y_S^* + Y_R^* + \alpha Y_I^*}, & \tilde{f}_\alpha &:= \tfrac{Y_S^* + Y_R^*}{Y_S^* + Y_R^* + \alpha Y_I^*} = 1 - f_\alpha, \\
b &:= \tfrac{Y_S^*}{Y_S^* + Y_R^*}, & \tilde{b} &:= \tfrac{Y_R^*}{Y_S^* + Y_R^*} = 1 - b, \\
m_x &:= \tfrac{M_X X^*}{a_x}, & \tilde{m}_x &:= \tfrac{G(X^*)(Y_S^* + Y_R^* + \alpha\beta Y_I^*)}{a_x X^*} = 1 - m_x, \\
e_s &:= \tfrac{EG(X^*)(Y_S^* + Y_R^*)}{a_s Y_S^*}, & \tilde{e}_{s\delta} &:= \tfrac{\delta Y_R^*}{a_s Y_S^*} = 1 - e_s, \\
m_y &:= \tfrac{M_Y X^*}{a_s}, & \tilde{m}_y &:= \tfrac{\lambda(Y_S^*, Y_I^*)}{a_s Y_S^*} = 1 - m_y,
\end{aligned}
\tag{4.8}
$$

we can rewrite Eq.(4.6) in the normalized form Eq.(4.4).

The intra-specific competion parameter

Compared to the model formulation Eq. 3.1 in Chapter 3 the primary production in this Chapter is given by the logisitc growth $\hat{S}(X, Y) = \hat{S}(X) = SX - M_X X^2$. Note, that S denotes the specific growth rate of the prey. Per definition in Sec. 3.3.2 we have $\sigma_x := \left.\frac{\mathrm{d}s(x,y)}{\mathrm{d}x}\right|_{x=x^*, y=y^*}$ and $c_x := (1 -$

$\sigma_x)/(2 - \sigma_x)$. A differentiation of $s(x,y) = \hat{S}(X^*x)/\hat{S}(X^*)$ with respect to x yields $\sigma_x = 1 - M_X X^*/(S - M_X X^*)$. From the first Equation in Eqs. (4.7) and the definition of m_x in Eqs. 4.8 we get $m_x = M_X X^*/S$ and therefore $\sigma_x = 1 - m_x/(1 - m_x)$. Substituting the latter expression in the definition of c_x yields $c_x = m_x$. In conclusion, for the logisic growth the intra-specific competition parameter of Chapter 3 is indeed equivalent to the scale parameter m_x.

Bibliography

Agladze, K. I., Krinsky, V. I., 1982. Multi-armed vortices in an active chemical medium. Nature 296, 424 – 426.

Allen, J. C., Schaffer, W. M., Rosko, D., 1993. Chaos reduces species extinction by amplifying local-population noise. Nature 364, 229–232.

Andersen, T., Elser, J., Hessen, D., 2004. Stoichiometry and population dynamics. Ecology Letters 7, 884–900.

Anderson, R. M., May, R. M., 1979. Population biology of infectious-diseases .1. Nature 280, 361–367.

Anderson, R. M., May, R. M., Joysey, K., Mollison, D., Conway, G. R., Cartwell, R., Thompson, H. V., Dixon, B., 1986. The invasion, persistence and spread of infectious diseases within animal and plant communities [and discussion]. Philosophical Transactions of the Royal Society of London. Series B, Biological Sciences 314, 533–570.

Andrews, J. F., 1968. A mathematical model for continuous culture of microorganisms utilizing inhibitory substrates. Biotechnology and Bioengineering 10, 707–723.

Arditi, R., Ginsburg, L. R., 1989. Coupling in Predator-Prey Dynamics: Ratio-Dependence. Journal of Theoretical Biology 139, 311–326.

Arino, O., El abdllaoui, A., Mikram, J., Chattopadhyay, J., 2004. Infection in prey population may act as biological control in ratio-dependent predator-prey models. Nonlinearity 17, 1101–1116.

Barlow, N. D., 2000. Non-linear transmission and simple models for bovine tuberculosis. The Journal of Animal Ecology 69, 703–713.

Baurmann, M., Gross, T., Feudel, U., 2007. Instabilities in spatially extended predator-prey systems: Spatio-temporal patterns in the neighborhood of Turing-Hopf bifurcations. Journal of Theoretical Biology 245, 220 – 229.

Bazykin, A. D., 1998. Nonlinear dynamics of interacting populations. World Scientific, Singapore.

Beddington, J. R., 1975. Mutual interference between parasites or predators and its effect on searching efficiency. The Journal of Animal Ecology 44, 331–340.

Beltrami, E., Carroll, T. O., 1994. Modelling the role of viral disease in recurrent phytoplankton blooms. Journal of Mathematical Biology 32, 857–863.

Benincà, E., Huisman, J., Heerkloss, R., Jöhnk, K. D., Branco, P., Nes, E. H. V., Scheffer, M., Ellner, S. P., 2008. Chaos in a long-term experiment with a plankton community. Nature 451, 822–825.

Berryman, A. A., 1996. What causes population cycles of forest lepidoptera? Trends in Ecology & Evolution 11, 28 – 32.

Berryman, A. A., Millstein, J. A., 1989. Are ecological-systems chaotic - and if not, why not. Trends in Ecology & Evolution 4, 26–28.

Blasius, B., Tönjes, R., 2007. Analysis and Control of Complex Nonlinear Processes in Physics, Chemistry and Biology. World Scientific, Singapoore, Ch. Predator-prey oscillations, synchronization and pattern formation in ecological systems, pp. 397–427.

Capasso, V., Serio, G., 1978. Generalization of the kermack-mckendrick deterministic epidemic model. Mathematical Biosciences 42, 43–61.

Chatterjee, S., Kundu, K., Chattopadhyay, J., 2007. Role of horizontal incidence in the occurrence and control of chaos in an eco-epidemiological system. Mathematical Medicine and Biology-A Journal of the IMA 24, 301–326.

Chattopadhyay, J., Arino, O., 1999. A predator-prey model with disease in the prey. Nonlinear Analysis-Theory Methods & Applications 36, 747–766.

Cunningham, A., Nisbet, R. M., 1983. Mathematics in Microbiology. Academic Press, Ch. Transients and oscillations in continous culture, pp. 77–103.

DeAngelis, D. L., 1992. Dynamics of Nutrient Cycling and Food Webs. Population and Community Biology series. Chapman & Hall, London.

DeAngelis, D. L., Goldstein, R. A., O'Neill, R. V., 1975. A Model for Tropic Interaction. Ecology 56, 881–892.

Dhooge, A., Govaerts, W., Kuznetsov, Y., 2003. MATCONT: A MATLAB package for numerical bifurcation analysis of ODEs. ACM Transactions on Mathematical Software 29, 141–164.

Diekmann, O., Kretzschmar, M., 1991. Patterns in the effects of infectious-diseases on population-growth. Journal of Mathematical Biology 29, 539–570.

Dijkstra, H. A., 2005. Nonlinear Physical Oceanography, 2nd Edition. Vol. 28 of Atmospheric and Oceanographic Sciences Library. Springer-Verlag, Berlin, Heidelberg, New York.

Dobson, A. P., 1988. The population biology of parasite-induced changes in host behavior. Quarterly Review of Biology 63, 139–165.

Doedel, E. J., Champneys, A. R., Fairgrieve, T. F., Kuznetsov, Y. A., Sandstede, B., Wang, X., 1997. Auto 97: Continuation and bifurcation software for ordinary differential equations (with homcont). Tech. rep., Computer Science, Concordia University, Montreal, Canada.

Doedel, E. J., Oldeman, B., 2009. Auto 97: Continuation and bifurcation software for ordinary differential equations (with homcont). Tech. rep., Concordia University, Montreal, Canada.

d'Onofrio, A., Manfredi, P., 2007. Bifurcation thresholds in an sir model with information-dependent vaccination. Mathematical Modelling of Natural Phenomena 2, 26–43.

Earn, D., Rohani, P., Grenfell, B., 1998. Persistence, chaos and synchrony in ecology and epidemiology. Proceedings of The Royal Society of London Series B-Biological Sciences 265, 7–10.

Elton, C. S., 1924. Periodic fluctuations in the number of animals: their causes and effects. British Journal of Experimental Biology 2, 119–163.

Freedman, H. I., Wolkowicz, G. S. K., 1986. Predator prey systems with group defense - the paradox of enrichment revisited. Bulletin of Mathematical Biology 48, 493–508.

Fussmann, G., Ellner, S., Shertzer, K., Hairston, N., 2000. Crossing the Hopf bifurcation in a live predator-prey system. SCIENCE 290, 1358–1360.

Gause, G. F., 1934. The Struggle for Existence. Williams & Wilkins, Baltimore, USA.

Gelfand, I. M., Kaprov, M. M., Zelevinsky, A. V., 1994. Discriminants, Resultants and Multidimensional Determinants. Birkhäuser, Boston.

Gragnani, A., Gatto, M., Rinaldi, S., 1998. Acidic deposition, plant pests, and the fate of forest ecosystems. Theoretical Population Biology 54, 257–269.

Grenfell, B., Bolker, B., Kleczkowski, A., 1995. Seasonality and extinction in chaotic metapopulations. Proceedings of The Royal Society of London Series B-Biological Sciences 259, 97–103.

Gross, T., 2004a. Population dynamics: General results from local analysis. Ph.D. thesis, Carl von Ossietzky Universität Oldenburg, ICBM, Carl von Ossietzky Univerität,, PF 2503, 26111 Oldenburg, Germany.

Gross, T., 2004b. Population Dynamics: General Results from Local Analysis. Der Andere Verlag, Tönningen, Germany.

Gross, T., Ebenhöh, W., Feudel, U., 2004. Enrichment and foodchain stability: the impact of different forms of predator-prey interaction. Journal of Theoretical Biology 227, 349–358.

Gross, T., Ebenhöh, W., Feudel, U., 2005. Long food chains are in general chaotic. Oikos 109, 135–155.

Gross, T., Feudel, U., 2004. Analytical search for bifurcation surfaces in parameter space. Physica D 195, 292–302.

Gross, T., Feudel, U., 2006. Generalized models as a universal approach to nonlinear dynamical systems. Physical Review E 73 (016205), (14 pages).

Guckenheimer, J., Holmes, P., 1983. Nonlinear Oscillations, Dynamical Systems, and Bifurcations of Vector Fields, 1st Edition. Vol. 42 of Applied Mathematical Siences. Springer-Verlag, Berlin, Heidelberg, New York.

Guckenheimer, J., Holmes, P., 2002. Nonlinear Oscillations, Dynamical Systems, and Bifurcations of Vector Fields, 7th Edition. Vol. 42 of Applied Mathematical Siences. Springer-Verlag, Berlin, Heidelberg, New York.

Guckenheimer, J., Myers, M., Sturmfels, B., 1997. Computing Hopf bifurcations I. SIAM J. Numer. Anal. 34, 1.

Hadeler, K. P., Freedman, H. I., 1989. Predator-prey populations with parasitic infection. Journal of Mathematical Biology 27, 609–631.

Hall, S., 2004. Stoichiometrically explicit competition between grazers: Species replacement, coexistence, and priority effects along resource supply gradients. The American Naturalist 164, 157–172.

Haque, M., Venturino, E., 2007. An ecoepidemiological model with disease in predator: The ratio-dependent case. Mathematical Methods in The Applied Sciences 30, 1791–1809.

Hastings, A., Hom, C. L., Ellner, S., Turchin, P., Godfray, H. C. J., 1993. Chaos in ecology - is mother-nature a strange attractor. Annual Review of Ecology and Systematics 24, 1–33.

Heino, M., Kaitala, V., Ranta, E., Lindstrom, J., 1997. Synchronous dynamics and rates of extinction in spatially structured populations. Proceedings of The Royal Society of London Series B-Biological Sciences 264, 481–486.

Hendriks, A. J., 1999. Allometric scaling og rate, age and density parameters in ecological models. Oikos 86, 293–310.

Hethcote, H. W., 2000. The mathematics of infectious diseases. SIAM Review 42, 599–653.

Hethcote, H. W., Wang, W., Han, L., Ma, Z., 2004. A predator-prey model with infected prey. Theoretical Population Biology 66, 259–268.

Hilker, F. M., Schmitz, K., 2008. Disease-induced stabilization of predator-prey oscillations. Journal of Theoretical Biology 255, 299 – 306.

Hofbauer, J., Sigmund, K., 1998. Evolutionary Games and Population Dynamics. Cambridge University Press, Cambridge.

Holling, C. S., 1959. Some characteristics of simple types of predation and parasitism. The Canadian Entomologist 91, 385–389.

Holt, R. D., McPeek, M. A., 1996. Chaotic population dynamics favors the evolution of dispersal. The American Naturalist 148, 709.

Hopf, E., 1942. Abzweigung einer periodischen lösung von einer stationären lösung eines differentialgleichungssystems. Ber. Math-Phys. Sächs. Akad. Wiss. 94, 1–22.

Huxel, G., 1999. On the influence of food quality in consumer-resource interactions. Ecology Letters 2, 256–261.

Karkanis, T., Stewart, A. J., 2001. Curvature-dependent triangulation of implicit surfaces. IEEE Computer Graphics and Applications 22, 60–69.

Kelley, C. T., 2003. Solving Nonlinear Equations with Newton's Method (Fundamentals of Algorithms). SIAM, Philadelphia.

Kermack, W. O., Mckendrick, A. G., 1927. Contributions to the mathematical - theory of epidemics - 1. Proceedings of The Royal Society 115A, 700–721.

Kooi, B. W., Boer, M. P., Kooijman, S. A. L. M., 1998. On the use of the logistic equation in food chains. Bulletin of Mathematical Biology 60, 231–246.

Kooijman, S. A. L. M., 2000. Dynamic Energy and Mass Budgets in Biological Systems. Cambridge University Press, Cambridge.

Kooijman, S. A. L. M., Andersen, T., Kooi, B. W., 2004. Dynamic Energy Budget representations of stoichiometric constraints on population dynamics. Ecology 85, 1230–1243.

Kooijman, S. A. L. M., Grasman, J., Kooi, B. W., 2007. A new class of nonlinear stochastic population models with mass conservation. Mathematical Biosciences 210, 378–394.

Koppel, J. v. d., Huisman, J., Wal, R. v. d., Olff, H., 1996. Patterns of herbivory along a prouductivity gradient: An empirical and theoretical investigation. Ecology 77, 736–745.

Kuznetsov, Y. A., 2004. Elements of Applied Bifurcation Theory, 3rd Edition. Vol. 112 of Applied Mathematical Sciences. Springer-Verlag, New York.

Kuznetsov, Y. A., Levitin, V., 1996. CONTENT: A multiplatform evnironment for analyzing dynamical systems. Tech. rep., Centrum voor Wiskunde en Informatica, Amsterdam.

Liu, R., Duvvuri, V. R. S. K., Wu, J., 2008. Spread pattern formation of h5n1-avian influenza and its implications for control strategies. Mathematical Modelling of Natural Phenomena 3, 161–179.

Liu, W., Levin, S. A., Iwasa, Y., 1986. Influence of nonlinear incidence rates upon the behavior of sirs epidemiological models. Journal of Mathematical Biology 23, 187–204.

Loladze, I., Kuang, Y., 2000. Stoichiometry in Producer-Grazer Systems: Linking Energy Flow with Element Cycling. Bulletin of Mathematical Biology 62, 1137–1162.

Lotka, A. J., 1925. Elements of physical biology. Williams & Wilkins company, Baltimore, USA.

May, R. M., Anderson, R. M., 1979. Population biology of infectious-diseases .2. Nature 280, 455–461.

May, R. M., Anderson, R. M., 1987. Transmission dynamics of HIV-infection. Nature 326, 137–142.

May, R. M., Oster, G. F., 1976. Bifurcations and dynamic complexity in simple ecological models. The American Naturalist 110, 573.

McCallum, H., Barlow, N., Hone, J., 2001. How should pathogen transmission be modelled? Trends in Ecology & Evolution 16, 295–300.

Mills, N. J., Getz, W. M., 1996. Modelling the biological control of insect pests: a review of host-parasitoid models. Ecological Modelling 92, 121 – 143, ecological Resource Modelling.

Moe, S., Stelzer, R., Forman, M., Harpole, W., Daufresne, T., Yoshida, T., 2005. Recent advances in ecological stoichiometry: Insights for population and community ecology. OIKOS 109, 29–39.

Morin, P. J., Lawler, S. P., 1995. Food web architecture and population dynamics: Theory and empirical evidence. Annual Review of Ecology and Systematics 26, 505–529.

Muller, E., Nisbet, R., Kooijman, S., Elser, J., McCauley, E., 2001. Stoichiometric food quality and herbivore dynamics. Ecology Letters 4, 519–529.

O'Neill, R., DeAngelis, D., Pastor, J., Jackson, B., Post, W., 1989. Multiple nutrient limitations in ecological models. Ecological Modelling 46, 495–510.

Pascual, M., 1993. Diffusion-Induced Chaos in a Spatial Predator–Prey System. Proceedings of The Royal Society of London Series B-Biological Sciences 251, 1–7.

Pascual, M., Caswell, H., 1997. From the cell cycle to population cycles in phytoplankton-nutrient interactions. Ecology 78, 897–912.

Perni, S., Andrew, P. W., Shama, G., 2005. Estimating the maximum growth rate from microbial growth curves: definition is everything. Food Microbiology 22, 491 – 495.

Roberts, M., 1996. The dynamics of bovine tuberculosis in possum populations, and its eradication or control by culling or vaccination. The Journal of Animal Ecology 65, 451–464.

Rosenzweig, M. L., 1971. Paradox of enrichment: Destabilization of exploitation ecosystems in ecological time. Science 171, 385–387.

Rosenzweig, M. L., MacArthur, R. H., 1963. Graphical representation and stability conditions of predator- prey interactions. Am Nat 97, 209–223.

Roy, S., Chattopadhyay, J., 2005. Disease-selective predation may lead to prey extinction. Mathematical Methods in the Applied Sciences 28, 1257–1267.

Ruxton, G. D., 1994. Low-levels of immigration between chaotic populations can reduce system extinctions by inducing asynchronous regular cycles. Proceedings of The Royal Society of London Series B-Biological Sciences 256, 189–193.

Ruxton, G. D., Rohani, P., 1998. Population floors and persistance of chaos in population models. Theoretical Population Biology 53, 75–183.

Saenz, R. A., Hethcote, H. W., 2006. Competing species models with an infectious disease. Mathematical Biosciences and Engineering 3, 219–235.

Scheffer, M., Rinaldi, S., Kuznetsov, Y., vanNes, E., 1997. Seasonal dynamics of Daphnia and algae explained as a periodically forced predator-prey system. OIKOS 80, 519–532.

Seydel, R., 1991. On detecting stationary bifurcations. International Journal of Bifurcation and Chaos 1, 335–337.

Solomon, M. E., 1949. The natural control of animal populations. Journal of Animal Ecology 18, 1–35.

Sterner, R. W., 1986. Herbivores' Direct and Indirect Effects on Algal Populations. Science 231, 605–607.

Sterner, R. W., Elser, J. J., 2002. Ecological Stoichiometry: The Biology of Elements from Molecules to the Biosphere. Princeton University Press.

Steuer, R., Gross, T., Selbig, J., Blasius, B., 2006. Structural kinetic modeling of metabolic networks. Proc Natl Acad Sci U S A 103, 11868–11873.

Steuer, R., Nesi, A. N., Fernie, A. R., Gross, T., Blasius, B., Selbig, J., 2007. From structure to dynamics of metabolic pathways: application to the plant mitochondrial TCA cycle. Bioinformatics 23, 1378–1385.

Stiefs, D., 2005. Qualitative Analyse von Effizienz und Anpassung in ökologischen Systemen. Diplomarbeit, Carl von Ossietzky Universität Oldenburg.

Stiefs, D., Gross, T., Steuer, R., Feudel, U., 2008. Computation and Visualization of Bifurcation Surfaces. International Journal of Bifurcation and Chaos 18, 2191 – 2206.

Stiefs, D., Venturino, E., Feudel, U., 2009. Evidence of chaos in eco-epidemic models. Mathematical Biosciences and Engineering 6, accepted for publication.

Sui, G., Fan, M., Loladze, I., Kuang, Y., 2007. The dynamics of a stoichiometric plant-herbivore model and its discrete analog. Mathematical Biosciences and Engineering 4, 29–46.

Swinney, H. L., Busse, F. H., 1981. Hydrodynamic instabilities and the transition to turbulence. Springer-Verlag, Berlin, Heidelberg, New York.

Titz, S., Kuhlbrodt, T., Feudel, U., 2002. Homoclinic bifurcation in an ocean circulation box model. International Journal of Bifurcation and Chaos 12, 869–875.

Truscott, J. E., Brindley, J., 1994. Ocean plankton populations as excitable media. Bulletin of Mathematical Biology 56, 981–998.

Turchin, P., Ellner, S., 2000. Living on the edge of chaos: Population dynamics of Fennoscandian voles. Ecology 81, 3099–3116.

Upadhyay, R. K., Kumari, N., Rai, V., 2008. Wave of chaos and pattern formation in spatial predator-prey systems with holling type iv predator response. Mathematical Modelling of Natural Phenomena 3, 71–95.

Van Voorn, G. A. K., Stiefs, D., Gross, T., Kooi, B. W., Feudel, U., Kooijman, S. A. L. M., 2008. Stabilization due to predator interference: comparison of different analysis approaches. Mathematical Biosciences and Engineering 5, 567–583.

Venturino, E., 1994. The influence of diseases on Lotka-Volterra systems. Rocky Mountain J. of Mathematics 24, 381–402.

Venturino, E., 1995. Mathematical Population Dynamics: Analysis of Heterogeneity, Vol. one: Theory of Epidemics. Wuertz Publishing Ltd, Winnipeg, Canada, Ch. Epidemics in predator-prey models: disease among the prey, pp. 381–393.

Venturino, E., 2001. The effect of diseases on competing species. Mathematical Biosciences 174, 111–131.

Venturino, E., 2002a. Epidemics in predator-prey models: disease in the predators. IMA Journal of Mathematics Applied in Medicine and Biology 19, 185–205.

Venturino, E., 2002b. Epidemics in predator-prey models: disease in the predators. IMA J. Math. Appl. Med. Biol. 19, 185–205.

Volterra, V., 1928. Variations and Fluctuations of the Number of Individuals in Animal Species living together. ICES J. Mar. Sci. 3, 3–51.

Wang, H., Kuang, Y., Loladze, I., 2008. Dynamics of a mechanistically derived stoichiometric producer-grazer model. Journal of Biological Dynamics 2, 286–296.

Wilmers, C., Post, E., Peterson, R., Vucetich, J., 2006. Predator disease outbreak modulates top-down, bottom-up and climatic effects on herbivore population dynamics. Ecology Letters 9, 383–389.

Wolkowicz, G. S. K., Zhu, H., Campbell, S. A., 2003. Bifurcation analysis of a predator-prey system with nonmonotonic functional response. SIAM Journal of Applied Mathematics 63, 636–682.

Xiao, D., Ruan, S., 2007. Global analysis of an epidemic model with nonmonotone incidence rate. Mathematical Biosciences 208, 419 – 429.

Xiao, Y., Bosch, F. V. D., 2003. The dynamics of an eco-epidemic model with biological control. Ecological Modelling 168, 203 – 214.

Yorke, J. A., London, W. P., 1973. Recurrent outbreaks of measles, chickenpox and mumps .2. Systematic differences in contact rates and stochastic effects. American Journal of Epidemiology 98, 469–482.

Zaikin, A. N., Zhabotinsky, A. M., 1970. Concentration wave propagation in two-dimensional liquid-phase self-oscillating system. Nature 225, 535 – 537.

Summary

Population dynamics are often investigated under the usage of simple mathematical models. The model properties of these models can be very sensitive to the mathematical formulation of the considered processes. A detailed derivation of these functional forms from field or lab experiments is in general difficult. However, in generalized modeling a further specification of the processes under consideration is avoided. Consequently, the analysis of these models allows to gain very generic system properties.

Generalized and specific modeling approaches require different computation techniques to locate bifurcations in parameter space. In Chapter 2 an innovative technique to locate bifurcations in generalized models is introduced, that allows for an efficient computation of three dimensional bifurcation diagrams. This technique is applied on two rarely investigated types of predator-prey models. One model focuses on stoichiometric constraints on the primary production and the conversion efficiency. These constraints cause dependencies that are not considered in classical predator-prey models. The other model describes how a disease spreads upon a predator population and how these dynamics influence the population interactions. The predator population is thereby structured in susceptible, infected and recovered predators. To find generic effects we use the approach of generalized modelling. The resulting bifurcation diagrams are partly combined with bifurcation diagrams of specific modeling approaches to demonstrate the interplay of generalized and specific modelling.

Although probably all natural interacting populations are influenced by limitation of nutrients and diseases, the related dependencies and the distinction between infected and uninfected are rarely considered in theoretical predator-prey models. The generalized analysis shows that these aspects of ecology qualitatively change predator-prey dynamics. In the following we briethly discuss the main results and give suggestions of further investications.

We begin with the investagtion of the generalized stoichiometric predator-prey model in Chapter 3. First, it turns out that for the classical assumption of constant efficiency the stability of equilibria depends only on two generalized parameters, the intra-specific competition and the predator sensitivity to prey.

The technique for the computation of bifurcation surfaces introduced in Chapter 2 is used to show how this two-dimensional bifurcation diagram evolves when the conversion efficiency becomes variable. The additional dimension is spanned by the food quality parameter that is related to the variability of the conversion efficiency.

The analysis shows that a variable conversion efficiency has major effects on the stability and dynamics of the system. In addition to the Hopf bifurcation, a surface of tangent bifurcations and a line of codimension-2 Takens-Bogdanov bifurcation appear. One the one hand, the latter indicates that homoclinic bifurcations are also generic in stoichiometric models. On the other hand, the Takens-Bogdanov bifurcation marks the end of the Hopf bifurcation surface. Therefore, it leads to the disappearance of the paradox of enrichment for low food quality.

The computation of three-dimensional bifurcation diagrams allows for a fast overview to get a qualitative understanding of the (de)stabilizing properties of the six system parameters. By contrast to the strong influence of the variable efficiency, it shows that stoichiometric constraints on the primary production have qualitatively rather low effects. They cause only shift of the observed bifurcation scenario. In this way we identify the variable efficiency as a key process that remarkably changes the dynamics of classical predator-prey systems.

These general properties are used to understand and predict the differences of specific stoichiometric models. First, we considered in Sec. 3.5 a variable and a simplified constant conversion efficiency model by Kooijman et al. (2004). The observation that a homoclinic and a tangent bifurcation appear in the variable efficiency model but not in the constant effiency model is in agreement with the results from the generalized analysis. Also a stoichiometric model proposed by Loladze and Kuang (2000) with unsmooth processes considering two limiting nutrients shows the appearance of tangent and homoclinic bifurcations. Further, the generalized analysis coincides with the disappearance of the paradox of enrichment in the model by Loladze and Kuang (2000). From the generalized point of view this corresponds to the fact that the unsmooth conversion process in this model allows only two discrete values for a parameter of the generalized model. For one parameter value a Hopf bifurcation exist and for the other no Hopf bifurcation can occure. In order to provide an example that allows to analyze the transition between both extreme parameter values we construct a smooth analogon model. This model shows that a Takens-Bogdanov bifurcation is responsible for the disappearance of the Hopf bifurcation, as predicted by the generalized analysis. Further, the results of the generalized analysis correctly predict a shift of the bifurcation scenario when additionally mass conservation is assumed in Sec. 3.5.4. These examples show that the generalized modeling can be used in combination to

specific models with identify properties that are generic for the model class.

The comparison to specific examples is done qualitatively but also quantitatively. We show that it is possible to translate specific bifurcation diagrams into generalized parameters and combine these projections with a generalized bifurcation diagram. This is done by fitting the specific coupling of certain generalized parameters. These combined bifurcation diagrams show in an exemplified way how specific and generalized parameters are connected. Further, it illustrates how multiple intersecting steady states that require different normalizations share one generalized diagram.

We show a counterintuitive stabilizing effect of intra-specific competition appearing likewise in constant and variable efficiency models. Instead of the related paradox of enrichment, this effect does not depend on the specific functional response under consideration. Further, a comparison to the observed paradox of nutrient enrichment in (Loladze and Kuang, 2000) shows that both, the paradox of enrichment and the paradox of nutrient enrichment, are combined in the paradox of competition observed in the generalized model. This illustrates the generic nature of the observed paradox of competition.

In the generalized eco-epidemic model in Chapter 4 where we consider a disease in the predator population, the visualization technique is used to locate bifurcations of higher codimension that give information about the appearance of complex dynamics. By the localization of a double-Hopf bifurcation in the generalized eco-epidemic model in Sec. 4.4.2, we show that chaotic parameter regions generally exist when the predator is infected by a disease.

This generalized analysis is used in Sec. 4.5 to construct a specific eco-epidemic model which is investigated to study the dynamics close to the double-Hopf bifurcation. Thereby, we find additional period-doubling and Neimark-Sacker bifurcations. We identify two routes into chaos, both involve a transition from quasiperiodicity. Most importantly, we demonstrate that the chaotic parameter regions are extended. In this way our analysis shows that, in the class of eco-epidemic models under consideration, chaos is generic and likely to occur. In other words, we show that diseases in predator populations can generally lead to chaotic dynamics.

More generally, the analysis in Chapter 4 shows that the localization of organizing centers by three-dimensional bifurcation diagrams reveals the regions of most interesting dynamics. Moreover, it provides plenty of examples for these situations since the generalized model represents a whole classes of models. From a technical perspective, the faithful representation of the Takens-Bogdanov bifurcation, the intersection with the Gavrilov-Guckenheimer bifurcation and most importantly, the complicated Whitney-umbrella structure of the Hopf bifurcation in Sec.4.5 (Fig.4.2) represents a masterpiece of the adaptive triangulation algorithm presented in this thesis.

In principle, the formulations of the models could be much more gen-

eral than in Chapter 3 and Chapter 4. The most general formulation of a predator-prey system is $\dot{X}_i = F_i(X_1, X_2)$, $i = 1, 2$. Obviously, this formulation hardly allows any conclusions about the involved processes. Instead, the models proposed in this thesis adopt some processes from conventional modeling approaches like the logistic growth in the eco-epidemic model or the linear death terms in the predator populations. This clearly reduces the degree of generality of the model but likewise focuses the analysis on the considered processes. Another advantage of this *semi general* formulation is that the results are, as it shows in the presented thesis, directly transferable to specific model examples.

In summary, the presented thesis has contributed to our understanding of stoichiometric influences on predator-prey interactions and how diseases in predator populations can influence predator-prey dynamics. On one hand, the models under consideration can be further generalized in order to see how these effects act jointly with other model modifications like nonlinear death terms. On the other hand, one could further specify and modify the eco-epidemic model to account for a specific problem. For example, one could adapt the model to analyse the dynamics of a specific disease of cats and the interaction with the rabbit population on an island (cf. Introduction). Also the method for the computation of bifurcations in generalized models could be extended in several ways. As an outlook, three possible extensions are discussed more in detail.

First, the computation of the bifurcation surfaces can potentially be extended in order to compute hypersurfaces. The proposed method for the computation of bifurcation surfaces provides a fast and efficient computation of three-dimensional bifurcation diagrams. The resolution of computed bifurcation points is locally adapted to the complexity of the surface. Once such a representation of the bifurcation surfaces is found, it is possible to trace these points while varying a fourth parameter. If necessary, additional bifurcation points can be computed in order to maintain or adapt the local resolution. In this way, one would obtain four-dimensional hypersurfaces that can be visualized in a three-dimensional diagram where the fourth parameter can be changed interactively. This technique would allow to investigate the evolution of the bifurcation landscape. Moreover, it is possible to iterate this step for additional parameters. In this way, one can explore step by step the whole bifurcation manifold. This information could be used to evaluate the (de)stabilizing effect of a parameter variation in terms of how the variation changes distance to the bifurcation surfaces in the direction of all parameters under consideration.

Second, the generalized stoichiometric predator prey model in Chapter 3 can be used as a building block in a generalized stoichiometric food web. We have shown that the variable food quality greatly affects the dynamics of

simple predator prey models. In larger population models, the variable food quality applies mainly to the autotrophs at the bottom of the food chains or webs. However, as we have discussed in Sec. 3.2, the resulting variable efficiency function depends in general on all other populations. Therefore, a specific modeling approach would become very complicated with the number of considered species. A generalized modeling approach could instead be used to overcome this difficulty. In generalized food webs, the large number of parameters makes a stability analysis in terms of three-dimensional bifurcation diagrams inappropriate. Instead, a simple numerical correlation between parameter values and the stability of the steady state can reveal how the parameter influence the stability of the steady state statistically as it has been done in (Steuer et al., 2006, 2007). In this way, the influence of a variable food quality on the stability of complex food webs could be studied from a very general perspective.

Third, the specific model in Chapter 4, Sec. 4.5, could be used to study stabilizing effects of diseases in conjunction with chaotic dynamics. In Sec. 4.2 we discussed that chaotic dynamics can prevent synchronization effects in patchy populations and therefore reduce the possibility of global extinction events. An interesting theoretical investigation beyond the scope of this work is to model population patches using the example model in Sec. 4.5 and adding a weak coupling due to migration between the patches. Theoretically it should be possible to observe predator-prey oscillations when the disease has no influence on the vital dynamics ($\alpha = \beta = 1, \mu = 0$) since the predator prey interactions are not affected by the disease. An adequate coupling should cause synchronization between the patches. Such an experiment is less artificial than it might sound. For example, the snowhare-lynx cycles from different regions in Canada show synchronization over millions of square kilometers (Blasius and Tönjes, 2007). An onset of chaotic dynamics in the model due to an increase of the influence of the vital dynamics could perturb the synchronization (Allen et al., 1993; Ruxton, 1994; Earn et al., 1998). In this way, a disease that reduces the vitality of the predator population could prevent both the prey and the predator population from global extinction.

To this end, whenever a system is too complex for an comprehensive description like our environment, simple specific and generalized models help to understand the system properties from an elementary perspective. As the presented thesis shows, both modeling approaches can fruitfully act in concert.

Samenvatting

De dynamica van ecosystemen bestaande uit populaties en hun natuurlijke voedselbronnen, kan onderzocht worden met behulp van wiskundige modellen. Met deze modellen wordt de verandering in de tijd van het aantal individuen waaruit de populaties bestaan, bestudeerd. Wetmatigheden (behoud van massa bijvoorbeeld) waaraan biologische en fysiologische processen moeten voldoen, worden gebruikt om de wiskundige vergelijkingen af te leiden. Afhankelijk van de gemaakte aannamen een veelheid aan modellen op: van de klassieke Lotka-Volterra tot de op de Dynamische Energie Budget (DEB) theorie (Kooijman 2000) gebaseerde modellen. Snelheden waarmee de biologische processen verlopen zijn voorbeelden van parameters in deze modellen. De eigenschappen van deze modellen, hier *specifieke* modellen genoemd, kunnen gevoelig afhangen van de wiskundige formulering van de beschouwde processen en de gebruikte parameter waarden. Een gedetailleerde afleiding van de vergelijkingen uit veld of laboratorium experimenten is vaak moeilijk.

Bij het gebruik van *gegeneraliseerde* modellen (Gross 2004a) wordt verdere specificatie van de beschouwde processen omzeild. Uitgangspunt hierbij is dat processen zoals toe- en afname (geboorte, groei, sterfte) met eenvoudige wiskundige formules worden beschreven. Via een normalisatie techniek worden parameters verkregen die kenmerkend zijn voor het dynamisch gedrag dat we willen bestuderen, maar ook een biologische interpretatie toestaan. Als gevolg daarvan levert de analyse eigenschappen op van klassen van modellen. Het is echter ook mogelijk de processen specifieker te omschrijven waardoor (zoals in dit proefschrift gedaan wordt) de twee type modellen met elkaar vergeleken en verbonden kunnen worden.

In dit proefschrift wordt het dynamische gedrag van de modellen bestudeerd met behulp van bifurcatie-analyses. Daarbij wordt het lange termijn gedrag bestudeerd. Parameters, die bijvoorbeeld de snelheden van de biologische processen beschrijven, worden onderscheiden van toestandsvariabelen, zoals aantal individuen, die in de tijd kunnen veranderen. De meest eenvoudige situatie is dat beide populaties van een predator-prooi systeem na lange tijd naar een evenwicht gaan waarbij beide populatiegrootes nagenoeg constant worden. Een belangrijke eigenschap van een dergelijk evenwicht is haar

stabiliteit. Indien het systeem na een verstoring weer terug keert naar het oor-
spronkelijk evenwicht wordt deze *stabiel* genoemd; indien niet dan *instabiel*.
Voorbeelden van ander lange termijn gedrag zijn: aanhoudende slingeringen
van de populatiesgroottes en chaotisch gedrag waarbij de toestand van het
systeem gevoelig af hangt van de beginsituatie en waarbij kleine verstoringen
grote gevolgen kunnen hebben.

In een bifurcatie analyse wordt de afhankelijkheid van het dynamisch ge-
drag van parameters bestudeerd. Wanneer bij het variëren van een parameter
het gedrag kwalitatief verandert wordt gezegd dat er een *bifurcatie* optreedt.
Bij een zogenaamde tangent bifurcatie treedt een plotselinge verandering op
waarbij het systeem naar een andere stationaire oplossing gaat. In een Hopf
bifurcatie verandert een evenwicht in slingerend gedrag, vaak rondom het in-
stabiele evenwicht.

De resultaten worden weergegeven in diagrammen waarbij de parameters
langs de assen staan en de bifurcaties gebieden met een zelfde gedrag be-
grenzen. Voor het berekenen van bifurcaties van gegeneraliseerde en speci-
fieke modellen zijn verschillende methoden vereist. In hoofdstuk 2 wordt een
nieuwe techniek voor het vinden van bifurcaties in gegeneraliseerde modellen
geïntroduceerd die een efficiënte berekening van driedimensionale bifurcatie
diagrammen mogelijk maakt. Driedimensionale diagrammen geven snel in-
zicht in kwalitatieve veranderingen van (de)stabilisatie eigenschappen. Deze
techniek wordt gebruikt voor het analyseren van twee predator-prooi modellen.

Het éne model is een uitbreiding van het klassieke predator-prooi systeem
waarbij rekening gehouden wordt met de beperkingen die de stoichiometrie
oplegt aan de omzetting van voedsel in biomassa. De prooi consumeert nu-
triënten (in dit geval een koolstof- en een fosforbron terwijl andere bouwstoffen
in overvloed beschikbaar zijn) en bestaat zelf uit twee componenten (weer kool-
stof en fosforhoudend). De prooi wordt opgegeten door een predator waardoor
zijn voedsel ook uit twee hoofdbestanddelen bestaat die zijn groei vastleggen.

De consumptie en verwerking van twee voedselbronnen tot nieuwe bio-
massa wordt beschouwd als één chemische reactie. Stoichiometrie is dan de
verhouding waarin de twee voedselbronnen met elkaar "reageren" en de ver-
houding tussen deze voedselbronnen en de geproduceerde nieuwe biomassa.
Met de stoichiometrie wordt naast het belang van voedselhoeveelheid ook de
kwaliteit (samenstelling) van het voedsel belangrijk. Als gevoldg hiervan is de
efficiëntie van de omzetting van prooi-biomassa naar predator-biomassa niet
meer constant, maar varieert met de voedsel samenstelling. Een ander hierbij
belangrijk aspect is de mineralisatie van afbraakproducten en dode biomassa
waarbij volledige recycling van de nutriënten wordt verondersteld.

De beperkingen opgelegd door de voedselsamenstelling brengen afhanke-
lijkheden met zich mee die in de klassieke predator-prooi modellen niet be-
schouwd worden. Als deze wel beschouwd worden dan wordt in het algemeen

in de wiskundige beschrijving een switch gebruikt waarbij beneden een drempelwaarde het ene nutriënt de groei beperkt en boven de drempel-waarde de andere. Dit is bijvoorbeeld het geval in Loladze et al. (2000). Van een systeem met een switch een gegeneraliseerde model maken is echter onmogelijk. Mede daarom wordt in dit proefschrift het switch-model vervangen door een model waarin de groei geleidelijk met de samenstelling van het voedsel verandert. Deze beschrijving wordt verkregen door toepassing van de wachttijd theorie op het verwerkingsproces van random beschikbaar komende bouwstenen voor nieuwe biomassa. Dit specifieke model kan wel rechtstreeks met een het gegeneraliseerde model vergeleken worden.

Het andere model beschrijft hoe een ziekte zich over een predatorpopulatie verspreid en hoe dit de interactie tussen de populaties beïnvloedt en daarmee het dynamisch gedrag. In de predator populatie wordt daarbij onderscheid gemaakt tussen drie klassen individuen, namelijk het aantal vatbare (S van susceptibles), besmettelijke, I (infectious), en immune R (recovered) predatoren. In het klassieke model wordt genegeerd dat individuen sterven en geboren worden. Dit kan alleen maar een redelijke aanname zijn als een epidemie op een korte tijdschaal plaatsvindt.

Om het verwantschap tussen de gegeneraliseerde en de specifieke modelformulering te demonstreren worden diagrammen verkregen met beide modellen gecombineerd. Daartoe worden een aantal parameters in het gegeneraliseerde model voor dat doel gekozen. In wat volgt behandelen we kort de belangrijkste resultaten.

We beginnen met het onderzoek van het gegeneraliseerd stoichiometrische predator-prooi model in hoofdstuk 3.

De analyse toont aan dat een variabele efficiëntie van de omzetting van prooi-biomassa naar predator-biomassa, grote invloed heeft op de stabiliteit en het dynamische gedrag van het systeem. Naast de "Hopf bifurcatie vlak", is er een vlak van "tangent bifurcaties" en ontstaat er een kromme lijn van zogenaamde codimensie-2 "Takens-Bogdanov bifurcaties". Dit toont aan dat er homocline bifurcaties zijn. Daarnaast markeert de Takens-Bogdanov het einde van de Hopf bifurcatie-vlak. Daarom verdwijnt de "paradox van de verrijking". De paradox van de verrijking is het effect dat als het nutriëntaanbod verhoogd wordt het systeem boven een bepaalde drempel (aangegeven door de Hopf bifurcatie) gaat slingeren, en bij nog verder ophogen de minimumwaarden tijdens een periode zo klein wordt dat uitsterven van de populaties waarschijnlijk is.

In tegenstelling tot de sterke invloed van een variabele efficiëntie, blijken de stoichiometrische beperkingen opgelegd aan de prooi kwalitatief weinig effect te hebben. De beperkingen veroorzaken enkel een verschuiving van het waargenomen bifurcatiescenario. Op deze manier kan men de variabele efficiëntie als sleutelproces identificeren dat het dynamisch gedrag van de klassieke

predator-prooi verandert.

De eigenschappen van het gegeneraliseerde model worden ook gebruikt om verschillen tussen specifieke modellen te begrijpen en te voorspellen. In hoofdstuk 3 worden daarom naast een gesimplificeerd model met constante conversie efficiëntie, meedere modellen met een variabele efficiëntie bestudeerd. Het feit dat een homocline en een tangent bifurcatie in het variabele efficiëntie model wel voorkomen maar niet in het constante efficiëntie model is in overeenstemming met de resultaten van de gegeneraliseerde analyse. Ook het stoichiometrische model met een switch procesbeschrijvingen, heeft een tangent en een homocline bifurcatie. Met de resultaten van het gegeneraliseerde model kan beschreven worden hoe de "paradox van de verrijking" in het Loladze et al. (2000) model verdwijnt. Ook voorspelt de gegeneraliseerde analyse correct het opschuiven van het bifurcatie scenario als rekening gehouden wordt met de wet van behoud van massa.

In het gegeneraliseerde eco-epidemisch model in hoofdstuk 4 waarin we een ziekte in de predatorpopulatie bestuderen, wordt de visualisatie techniek gebruikt om de hogere co-dimensie bifurcaties te lokaliseren. Die geven informatie over het eventuele bestaan van complex dynamisch gedrag. De gegeneraliseerde analyse wordt gebruikt voor de constructie van een specifiek eco-epidemisch model waarvan het gedrag onderzocht wordt in de buurt van de dubbele-Hopf bifurcatie. Belangrijk is dat het gebied waarin chaos optreed groot is. Op deze manier laat de analyse zien dat in een klasse van eco-epidemisch modellen chaos generiek is en dat het waarschijnlijk vaak voorkomt dat ziektes in predatorpopulaties leiden tot chaotisch gedrag.

Meer in het algemeen kunnen we stellen dat de analyse in hoofdstuk 4 aantoont dat de lokalisatie van een centrum waaruit alles afgeleid kan worden, door middel van driedimensionale diagrammen, situaties opleveren met interessant dynamisch gedrag. Bovendien geeft het meerdere voorbeelden van deze situaties omdat het gegeneraliseerde model een hele klasse van modellen representeert. De berekende gecompliceerde Whitney-paraplu structuur van de Hopf-bifurcatie in fig.4.2 toont de mogelijkheden van de toepassing van het in hoofdstuk 2 ontwikkelde adaptieve algoritme.

Deze voorbeelden laten zien dat de gegeneraliseerd modellen gebruikt kunnen worden in combinatie met specifieke modellen en waarbij algemene eigenschappen worden geïdentificeerd voor de klasse van modellen. Wanneer een natuurlijk systeem een zeer gecompliceerd beschrijving vereist, kunnen eenvoudige specifieke en gegeneraliseerde modellen helpen de eigenschappen van het systeem te begrijpen vanuit de onderliggende basis principes. Dit proefschrift toont de meerwaarde van een gecombineerde analyse van beide modellen.

Dankwoord

Hiermit möchte ich mich bei allen bedanken, die wesentlich zum Gelingen dieser Arbeit beigetragen haben. In erster Linie gebührt mein Dank meiner Doktormutter Ulrike Feudel für die hervorragende Betreuung. Ulrike hat trotz ihrer zahlreichen Verpflichtungen es immer geschafft mich inhaltlich, organisatorisch, finanziell und moralisch Unterstützung zu leisten. Sie hat mir internationale Zusammenarbeiten ermöglicht und mich oft auf den Reisen begleitet und unterstützt. Ohne sie, wäre diese Arbeit nicht möglich gewesen.

Further I have to thank Bob Kooi, my co-promoter and George van Voorn for a wonderfull collaboration and for giving me the opportunity of a double-promotion. Thank you for the fiddly but also fruitful co-work in front of the whiteboard on the connection of generalized and specific modeling. Thank you for the experience that science can be thrilling like a murder mystery. Also many thanks to Bas Kooijman and the whole group. I always enjoyed my visits at the Vrije Universiteit in Amsterdam and the friendly atmosphere.

Auch möchte ich mich bei Thilo Gross bedanken, der die entscheidenden Weichen in meinem bisherigen wissenschaftlichen Werdegang gestellt hat und mich noch immer begleitet. Ich bin immer wieder von Thilos Abstraktionsverögen und seinem didaktischen Geschick, komplizierte Zusammenhänge auf einfacher Art und Weise zu vermitteln, begeistert. Diese Arbeit baut zu großen Teilen auf seinen Leistungen auf.

I thank Ezio Venturino for collaboration and the unresting search for complex dynamics. Finally we succeeded (and found it in biological dynamical system where it was intended). Also many thanks to Anna for always welcome me in Torino. Thanks both of you for the kind hospitality.

Ich möchte mich bei meinen Bürokollegen Martin Baurmann, Yvonne Schmitz und Alexandra Kroll für die heitere Arbeitsatmosphäre bedanken. Klemens Buhmann für die technische Betreuung, die unzähligen Geschenke und und vieles mehr. Besonders seine Kaffe-Pad-Maschine hat wesentlich zum gelingen dieser Arbeit beigetragen. Jöran März danke ich für die unzähligen Spaziergänge zur Mensa, gute Gespräche und die moralische und technische Unterstützung für den Abschluss der Arbeit. Insgesamt möchte ich mich bei allen Kollegen aus Oldenburg für das schöne Zeit in der Arbeitsgruppe beanken. Mit

ihnen verging sie wie im Fluge.

Auch möchte ich mich bei meinen neuen Kollegen im MPI bedanken, die mich freundlich aufgenommen und mir bei dem Abschluss der Arbeit geholfen haben. Insbesondere danke ich Elke Zimmer, Lars Rudolf, Martin Zumsande und Ly Do für die nützlichen Hinweise bei der Fertigstellung der Arbeit.

Von ganzem Herzen danke ich meinen Eltern und meinen Brüdern für die imense moralische und finanzielle Unterstützung. Ohne euch wäre ich nicht so weit gekommen.

Zum Schluss möchte ich mich liebevoll bei meiner Frau Birgit und meiner Tochter Josta Berenike bedanken, die ich mehr als alles andere in der Welt schätze. Sie sind gemeinsam mit mir diesen Weg gegangen und ohne sie hätte ich ihn nicht eingeschlagen.

Curriculum Vitae

Name: Dirk Stiefs
Date of Birth: 1979-08-06
Place of Birth: Wilhelmshaven, Germany
Nationality: German

Education and Qualifications

since Mar. 2009   Guest scientist position in the group BioND - Dynamics of Biological Networks at the Max Planck Institute for the Physics of Complex Systems, Dresden, Germany

June 2006 - Nov. 2008   Qualification in higher education (Hochschuldidaktische Qualifizierung)

Nov. 2005 - Feb. 2009   Graduate student in the group Theoretical Physics / Complex Systems at the Institute of Chemistry and Biology of the Marine Environment (ICBM), Carl von Ossietzky University, Oldenburg, Germany.

Oct. 2001 - Nov. 2005   Diplom (MSc equivalent) in physics, Carl von Ossietzky University, Oldenburg, Germany. Thesis: *Qualitative Analysis of Yield and Adaption in Ecological Systems* Grade: *sehr gut (excellent)*

Oct. 1999 - Sep. 2001   Vordiplom (pre-Diploma), Carl von Ossietzky University, Oldenburg, Germany. Grade: *sehr gut (excellent)*

Aug. 1996 - July 1999   Abitur (A-level equivalent), Gymnasiale Oberstufe der IGS, Wilhelmshaven, Germany. Grade: *sehr gut (1.4) (excellent)*

International Work Experience

Sep. - Oct 2002   Praktical training in pico second spectroscopy, Institute of Biochemical Physics, Moscow

List of Publications

Stiefs, D., Gross, T., Steuer, R., Feudel, U., 2008. Computation and Visualization of Bifurcation Surfaces. International Journal of Bifurcation and Chaos 18 (8), 2191 – 2206.

Stiefs, D., van Voorn, G. A. K., Kooi, B. W., Gross, T., Feudel, U., 2009. Stoichiometric producer-grazer systems, submitted to The American Naturalist

Stiefs, D., Venturino, E., Feudel, U., 2009. Evidence of Chaos in Eco-epidemic Models. Mathematical Biosciences and Engineering 6 (4), accepted

Stiefs, D., Venturino, E., Gross, T., Feudel, U., 2008. Computing 3D Bifurcation Diagrams. American Institute of Physics Conference Proceedings, 1048, 958 – 961,

van Voorn, G. A. K., **Stiefs, D.**, Gross, T., Kooi, B. W., Feudel, U., Kooijman, S. A. L. M., 2008. Stabilization due to predator interference: comparison of different analysis approaches. Mathematical Biosciences and Engineering 5 (3), 567 – 583.